Development of a Tsunami Forecast Model for Monterey, CA

Yong Wei

Abstract

As part of NOAA's tsunami forecast system, this study addresses the development, validation, and stability tests of the tsunami forcast model for Monterey, California. Based on the Method of Splitting Tsunami (MOST), the tsunami forecast model is constructed at a spatial resolution of 1 arcsec (~ 30 m) in the finest grid to accomplish a 4-hour simulation of wave inundation onto dry land within 10 minutes of CPU time. A referenced inundation model is developed in parallel using grids of higher resolution up to 1/3 arcsec (~ 8.3 m) to provide a modeling reference for the forecast model. The model validations using historical tsunami events show good agreement between the model computation and observations, and provide quantitative estimation of the inundation, tsunami runup and computed maximum values for these events. The stability of the forecast model is evaluated based on 51 hypothetical scenarios generated in all subduction zones of the Pacific Rim at magnitudes ranging from M_w 7.5 to M_w 9.3. A micro tsunami test provides further model stability test under no-wave condition. Model computation shows that an M_w 9.3 event from central Alaska-Aleutian Subduction Zone may potentially generate tsunami runup as high as 7.3 m at the coastline of Monterey City, where the common land level is about 8 m.

1. Background and Objectives

The National Oceanic and Atmospheric Administration (NOAA) Center for Tsunami, Research (NCTR) at the NOAA Pacific Marine Environmental Laboratory (PMEL) has developed a tsunami forecasting capability for operational use by NOAA's two Tsunami Warning Centers located in Hawaii and Alaska (Titov *et al.*, 2005). The system is designed to efficiently provide basin-wide warning of approaching tsunami waves accurately and quickly. The system, termed Short-term Inundation Forecast of Tsunamis (SIFT), combines real-time tsunami event data with numerical models to produce estimates of tsunami wave arrival times and amplitudes at a coastal community of interest. The SIFT system integrates several key components: deep-ocean observations of tsunamis in real time, a basin-wide pre-computed propagation database of water level and flow velocities based on potential seismic unit sources, an inversion algorithm to refine the tsunami source based on deep-ocean observations during an event, and high-resolution tsunami forecast models termed Standby Inundation Models (SIMs).

Monterey, CA is a coastal community located in northern California, 115 miles south of San Francisco and 350 miles north of Los Angeles (Figure 1), with a population of

30,641 in City of Monterey and 408,238 in Monterey County as of July 2008. Figure 2 shows the coast of Monterey Bay has highest population density in the county, about 325-1832 people per square mile. Most of the residents are living in a low-lying area prone to tsunami inundation with elevation less than 8 m. Monterey harbor is part of the Monterey Bay National Marine Sanctuary. Monterey Harbor is an attraction for residents and visitor by providing access to many recreational and commercial opportunities. The entire coastal area of Monterey County is susceptible to tsunamis, especially the low-lying areas and riverine valleys to the north. In the past 100 years, Monterey county has experienced 8 tsunamis and been impacted significantly by the 1960 Chile tsunami. In response to natural hazards, the county of Monterey developed a Multi-Jurisdictional Hazard Mitigation Plan in 2007 that is to be updated every five years (http://www.co.monterey.ca.us/oes/hazard-mitigation.asp). For tsunami, this plan included a tsunami hazard map implementing the USC tsunami inundation limit (Barberopoulou et al., 2009), as well as the "potential tsunami hazard elevations". The latter is to accommodate in Monterey County the typical tsunami runup, 6.4 to 15 m (21 to 50 feet), from large tsunamis in the Pacific Ocean over the last 80 years. The objective of the present study, then, is to develop an operational forecast model for Monterey, California, for the purpose of minimizing false alarms that disrupt port activities and to provide the region with accurate and timely information necessary to make decisions in the event of tsunami generation,

2. Forecast Methodology

A high-resolution inundation model was used as the basis for development of a tsunami forecast model to operationally provide an estimate of wave arrival time, wave height, and inundation at Monterey, CA following tsunami generation. All tsunami forecast models are run in real time while a tsunami is propagating across the open ocean. The Monterey model was designed and tested to perform under stringent time constraints given that time is generally the single limiting factor in saving lives and property. The goal of this work is to maximize the length of time that the community of Monterey has to react to a tsunami threat by providing accurate information quickly to emergency managers and other officials responsible for the community and infrastructure.

The general tsunami forecast model, based on the Method of Splitting Tsunami (MOST), is used in the tsunami inundation and forecasting system to provide real-time tsunami forecasts at selected coastal communities. The model runs in minutes while employing high-resolution grids constructed by the National Geophysical Data Center. The Method of Splitting Tsunami (MOST) is a suite of numerical simulation codes

capable of simulating three processes of tsunami evolution: earthquake, transoceanic propagation, and inundation of dry land. The MOST model has been extensively tested against a number of laboratory experiments and benchmarks (Synolakis *et al.*, 2008) and was successfully used for simulations of many historical tsunami events. The main objective of a forecast model is to provide an accurate, yet rapid, estimate of wave arrival time, wave height, and inundation in the minutes following a tsunami event. Titov and González (1997) describe the technical aspects of forecast model development, stability, testing, and robustness, and Tang *et al*., 2009 provide detailed forecast methodology

A basin-wide database of pre-computed water elevations and flow velocities for unit sources covering worldwide subduction zones has been generated to expedite forecasts (Gica *et al.*, 2008). As the tsunami wave propagates across the ocean and successively reaches tsunameter observation sites, recorded sea level is ingested into the tsunami forecast application in near real-time and incorporated into an inversion algorithm to produce an improved estimate of the tsunami source. A linear combination of the pre-computed database is then performed based on this tsunami source, now reflecting the transfer of energy to the fluid body, to produce synthetic boundary conditions of water elevation and flow velocities to initiate the forecast model computation.

Accurate forecasting of the tsunami impact on a coastal community largely relies on the accuracies of bathymetry and topography and the numerical computation. The high spatial and temporal grid resolution necessary for modeling accuracy poses a challenge in the run-time requirement for real-time forecasts. Each forecast model consists of three telescoped grids with increasing spatial resolution in the finest grid, and temporal resolution for simulation of wave inundation onto dry land. The forecast model utilizes the most recent bathymetry and topography available to reproduce the correct wave dynamics during the inundation computation. Forecast models, including the Monterey model, are constructed for at-risk populous coastal communities in the Pacific and Atlantic Oceans. Previous and present development of forecast models in the Pacific (Titov *et al*., 2005; Titov, 2009; Tang *et al*., 2008; Wei *et al*., 2008) have validated the accuracy and efficiency of each forecast model currently implemented in the real-time tsunami forecast system. Models are tested when the opportunity arises and are used for scientific research. Tang *et al*., 2009 provide forecast methodology details.

3.Model development

The general methodology for modeling at-risk coastal communities is to develop a set of three nested grids, referred to as A, B, and C-grids, each of which becomes successively finer in resolution as they telescope into the population and economic center

of the community of interest. The offshore area is covered by the largest and lowest resolution C-grid while the near-shore details are resolved within the finest scale A-grid to the point that tide gauge observations recorded during historical tsunamis are resolved within expected accuracy limits. The procedure is to begin development with large spatial extent merged bathymetric topographic grids at high resolution, and then optimize these grids by sub sampling to coarsen the resolution and shrink the overall grid dimensions to achieve a 4 to 10 hr simulation of modeled tsunami waves within the required time period of 10 min of wall-clock time. The basis for these grids is a high-resolution digital elevation model constructed by the National Geophysical Data Center and NCTR using all available bathymetric, topographic, and shoreline data to reproduce the wave dynamics during the inundation computation for an at-risk community. For each community, data are compiled from a variety of sources to produce a digital elevation model referenced to Mean High Water in the vertical and to the World Geodetic System 1984 in the horizontal (http://ngdc.noaa.gov/mgg/inundation/tsunami/inundation.html). From these digital elevation models, a set of three high-resolution, "reference" elevation grids are constructed for development of a high-resolution reference

3.1 Study Area and NOS Tide Station

The City of Monterey is situated on the Monterey Bay National Marine Sanctuary, a Federally protected ocean area extending 450 km along the coast, where the San Andreas Fault System traverses in a northwest-southeast direction and controls much of the overall geologic character of the region. This series of sub-parallel faults forms the boundary between the Pacific and North American tectonic plates, the former of which is sliding northwest several centimeters per year relative to the latter. In the vicinity of the sanctuary, the San Andreas Fault System is basically composed of four fault zones: the San Gregorio Fault that extends from Monterey to Half Moon Bay and is predominantly offshore; the Monterey – Tularcitos Fault zone that extends over a wide area from Monterey to Santa Cruz within Monterey Bay; The San Simeon Fault; and the infamous San Andreas Fault that is almost entirely onshore in this region. An earthquake probability study by the USGS (Working Group on California Earthquake Probabilities, 2003) determined that there is a 62 percent chance of a magnitude 6.7 or greater earthquake occurring on one of the faults in the greater San Francisco Bay Area between 2003 and 2032. In this time period, there is a 10 percent chance of a magnitude 6.7 or greater earthquake on the San Gregorio Fault and a 21 percent chance of a similar earthquake on the San Andreas Fault.

Monterey is subject to both distant and local tsunami threats. The last major tsunami to hit the coast of this area occurred in 1964, which affected the entire California coastline and the tsunami waves were particularly high from Crescent City to Monterey with heights on the open coast ranging from 2.1 – 6.4 m. The recorded wave amplitude at Monterey Bay tide gage, located on the south side on the Monterey Bay, is about 1 m, but reached as high as 3.4 m at Santa Cruz Harbor situating on the north side of the Monterey Bay. Similarly, the 1946 Unimak tsunami barely produced any noticeable waves at Monterey Harbor but reached over 3 m at Santa Cruz. Other recorded tsunami waves in the past 20 years are mostly smaller than 0.2 m in amplitude, causing no damage to the coastline. The submarine canyon offshore of Monterey Bay has been identified as a region of mass movement features. Slumps, debris flows and other submarine landslides are concentrated along canyon walls and the lower continental slope, with many additional distinct and youthful slumps at the base of the headward walls of Monterey Canyon (Greene et al., 2002). Land mass movement features in the Monterey Bay region suggest that a potential for tsunami generation exists (Greene and Ward, 2003). A small landslide occurred at the head of Monterey Canyon during the 1989 Loma Prieta Mw 6.9 earthquake with a small tsunami about 0.5 m high reported to have entered the Moss Landing Harbor and a turbidity current reported to have traveled down the canyon axis (Greene and Hicks, 1990; Schwing et al., 1990; Garfield et al., 1994). Ward (2005) showed that a 0.1 km^3 of material failure in Monterey Canyon could induce more than 7 meters of runup over 25 km of the coast, posing severe tsunami threats to the City of Monterey.

The NOS tide station at Monterey Harbor is located at with a MSL water depth of about 2.5 m on wharf #2 north of the main boat harbor (Figure 4). The tide station was established in November of 1973, and the present installation was installed in September of 1988. The mean tide range at Monterey Harbor is about 1 m, and the mean sea level is increasing at the rate of 1.34 +/- 1.35 mm per year. Out of more than 25 historical events, eight of them have produced useful tsunami wave records at the Monterey Harbor tide station that can be used to validate the present forecast model. The eight tsunami events include the 26 March 1964 Alaska, 4 October 1994 Kuril, 10 June 1996 Andreanov, 23 June 2001 Peru, 3 May 2007 Tonga, 15 November 2006 Kuril, 13 January 2007 Kuril and 15 August 2007 Peru.

2.2 Digital Elevation Model (DEM) of Monterey, CA

Accurate bathymetry and topography in offshore and coastal regions play the key role, globally and locally, in tsunami generation, propagation and inundation. Currently,

the global bathymetric and topographic datasets are available for public-domain research. Marks and Smith (2006) conducted an evaluation on 6 publicly available global bathymetry grids: DBDB2 (Digital Bathymetric Data Base by Naval Research Laboratory), ETOPO2 (Earth Topography by National geophysical Data Center), GEBCO (Genercal Bathymetric Charts of the Oceans by British Oceanographic Data Center), GINA (Geographic Information Network of Alaska), Smith and Sandwell (1997) and S2004. They concluded the original Smith and Sandwell grid might be the best source among these global bathymetric grids. Subsequently they developed a new 1-min global topography grid S2004 that combines the Smith and Sandwell below 1000m depth and equatorward of 72° and GEBCO grids in shallow water and polar region. NOAA Center for Tsunami Research (NCTR) developed a Pacific-Basin 30sec grid, derived primarily the Smith and Sandwell grid and the SRTM30_PLUS grid, with amendments in areas where NCTR has better bathymetry. This comprehensive dataset covers the entire Pacific Ocean and part of the Arctic Ocean from E120° to W68°, and S80° to N80°.

While developing bathymetric and topographic grids for specific coastal communities, NCTR has been collaborating with National Geographic Data Center (NGDC) in the Tsunami Inundation Gridding Project since 2005 to build high-resolution digital elevation models (DEMs) for more U.S. coastal regions, and satisfy the needs of tsunami forecast model development in the near future. Currently, The finished datasets are downloadable, along with the associated documentation, in ESRI ArcGIS ASCII grid format at http://www.ngdc.noaa.gov/dem/.

The Monterey DEM was delivered to PMEL by NGDC in January of 2008 at a 1/3-arc-sec grid resolution with a coverage area of 122.52°W to 121.52°W, 36.09°N to 37.11°N (Taylor et al., 2008). The data sources of the Monterey DEM include NOAA's National Ocean Service (NOS), Office of Coastal Survey (OCS) and Coastal Services Center (CSC), California State University Seafloor Mapping Laboratory, the U.S. Geological Survey (USGS), and the California Department of Fish and Game Marine Region GIS unit (CDFG). The horizontal and vertical datum of the dataset are the World Geodetic System 1984 (WGS 84) and the mean high water, respectively. The spatial resolution ranges from 1 m to 1 km for the bathymetric datasets, and 2.5 m to ~ 8.3 m (1/3 arc second) for the topographic datasets (Taylor et al., 2008).

2.3 Model Setup

Figures 5 to 10 show the computational grids, derived from aforementioned Monterey DEMs, of reference inundation model and the optimized forecast model. Figure 5 and 6 shows the computational domain of outmost grid A covers the main California coastlines

with a grid resolution of 36 arc seconds for the reference inundation model and 2 arc minutes for the forecast model, respectively. The western boundary in both grids is extended to > 4,000 m water depth allowing natural transition of boundary conditions from the pre-computed propagation database (Gica et al., 2008). The study area of Monterey City is positioned in the middle of the outmost grid A and away from the boundaries to minimize the influence of boundary forcing. For same reason, the outmost grid A is extended to 30°N to avoid settling the south boundary on the shelf when adapting the tsunami dynamics from the propagation database. The intermediate grid B covers the entire Monterey Bay and the western boundary is extended to a water depth of 3,000 m. The submarine canyon offshore of Monterey Bay is included in this grid to represent accurate wave transformation from deep water to the shallow shelf, where the nonlinearity of tsunami waves is amplified the most. The inmost grid C covers the south part of Monterey bay and most of the Monterey City coastline, including the entire Monterey Harbor. Figure 9 and 10 show the coastline of Monterey is mostly linear with gradually changing water depth offshore. The contours of the water depth are nearly parallel to the shoreline indicating less tsunami energy directionality except for the headland at northwest of Monterey Harbor, which make it more convincing to use a small grid C coverage for the forecast model (Figure 10) compared to that of the RIM (Figure 9) when the computing time is a major concern. Table 1 provides the details of model setup and input parameters for all grids of both models.

3. Results and Discussions

3.1 Model Validation

The DART arrays have played critical roles in defining the tsunami source and provided accurate real-time tsunami forecast for U.S. coastlines since they became tested in the 1990s and modernized in 2001. Previous studies have shown successful applications of NOAA's experimental tsunami forecast system that constrains the tsunami source from the real-time DART measurements, which is subsequently used to provide real-time propagation and coastal inundation forecast (Titov et al., 2003; Wei et al., 2008; Tang et al., 2008; and Titov, 2008). These real-time inversions of the tsunami source have shown a forecast accuracy up to 90% of the tsunami waveforms at distant coastlines (Wei et al., 2008; Tang et al., 2008). Six of such validated events were used to validate the Monterey forecast model, including the 10 June 1996 Andreanov, 3 May 2006 Tonga, 15 November 2006 Kuril, 13 January 2007 Kuril, 1 April 2007 Solomon, and 15 August 2007 Peru. As aforementioned, the great 1964 Alaksa tsunami has produced notable wave amplitude up to 1 m. The distinct tsunami waves registered by

Monterey tide station are valuable to validate the Monterey forecast model due to its high signal-to-noise ratio compared to other events. This study also computed the destructive tsunamis of 1946 Unimak, to demonstrate the wave dynamics at the coast of Monterey. Comparisons between computation and observation for these events are shown in Figure 6.

Figure 11 to 18 show favorable agreement between the modeling results and observations for most of the historical events in spite of the background noise. The modeled time series of 1964 tsunami computed by the forecast model is excellent compared to the observations up to 16 hours after the initial generation of the tsunami, except for some phase shift and lightly larger wave amplitude due to the uncertainty of the tsunami source. The time series computed from the reference inundation model showed larger amplitude with a maximum of 2.3 m compared to that obtained forecast model and observations. Figure 11 (b) and (d) show that the modeled tsunami amplitudes in RIM are about 40% larger than in the forecast model along the coastline of Monterey City. According to the historical accounts at Monterey during the 1964 tsunami, there were no noticeable damages at the coastline of Monterey, which confirms the no-inundation scenario computed by the forecast model. It should be noted here that the model discrepancy between the reference model and forecast model is minimum for all other historical events validated in this study, meaning it is an event-dependent, instead of a systematic, modeling issue. This issue is currently under investigation and will be addressed in future report. Tsunami-driven wave current has been a real concern for most harbors.

The real-time DART measurements were used to derive valid tsunami sources during the events of 3 May 2006 Tonga, 15 November 2006 Kuril Islands, 13 January 2007 Kuril Islands and 15 August 2007 Peru. The computed time series at Monterey tide station for these events show excellent agreement with the first 3 to 4 hours of measurements (Figures 15a, 17a, and 18a), except the tide gage was not functioning properly during the 15 November 2006 tsunami (Figure 16a). The modeling results from RIM and forecast model showed minor discrepancies for the first 4 to 5 waves, and then started to show small offsets in amplitude and phase, which are expected between models using different spatial and temporal resolutions. Compared to the forecast model, the Monterey RIM employs three times higher grid resolution adequately representing the local bathymetric and topographic features, which results in enhanced modeling capability in capturing the late waves. RIM provides model reference for the computational accuracy of its optimized version, the tsunami forecast model. Despite the differences in the late waves six hours after the first tsunami arrival, one can see that the

main tsunami wave characteristics such as the maximum wave amplitude and the wave period have been accurately computed in Monterey forecast model. A main advantage of using an optimized model for tsunami forecast is its real-time computational efficiency, which achieves 90% or higher modeling accuracy (Wei et al., 2008) while saving the CPU time by 150 times (Table 1).

The maximum computed current speed at Monterey is generally small in the offshore area due to the sloping ocean bottom. In spite of the flow speed at the headland northwest of Monterey Harbor, the computed results show larger current speed at the entrance of Monterey Harbor as well as inside the boat harbor indicating potential harbor damages due to strong current, which was the main reason responsible for the significant damages in the boat harbor of Crescent City during the 15 November 2006 Kuril Islands tsunami (Kelly et al., 2006; Uslu et al., 2007). For the 1964 Alaska tsunami, the computed wave current speed by forecast model is about 0.8 – 1.0 m/s (1.6 – 2.0 knots) near the entrance of Monterey harbor and inside the boat harbor (Figure 11(e)), whereas the current speed induced by the 1946 Unimak tsunami is about half of that (Figure 19(e)).

3.2 Model stability tests using artificial tsunamis

Model stability of the forecast model is evaluated using 51 hypothetical events, 40 mega scenarios of M_w 9.3, 10 small scenarios of M_w 7.5 and one "no-wave" scenario, generated in each source zone around the Pacific Rim (Table 2). With an averaged 28.4 m slip on a combination of 20 unit sources covering a rupture area of 1000 km by 100 km, each M_w 9.3 scenario imitates an equivalent or greater event of the 2004 Indian tsunami, which caused severe devastation along the coastline of Indian Ocean and accounted for hundreds of thousands of deaths. Modeling experiences have shown that the singularities in the bathymetry and topography may cause model instabilities not only when the waves are large, but also when they are small enough to be taken over by accumulated numerical errors induced by those singularities. For such reason, the present study also evaluates the model stabilities using small artificial tsunami scenarios of M_w 7.5, which represents a unit tsunami scenario, one-meter slip on one unit source, developed in the propagation database (Gica et al., 2008). Another key test is the "no wave" scenario, 0.0001 m slip on one unit source in the present study, to examine the model stability under extremely small (close to null) wave forcing at the boundary. A successful no-wave test expects only wave activities in the same order of the boundary forcing without unreasonable amplification.

Figures 20 to 59 show the computational results, including the maximum computed wave amplitude and current speed, of all M_w 9.3 mega scenarios in all three telescoped

grids, as well as the time series at the warning point that best represents the location of the tide station. No model instabilities were observed in all these model runs, with or without tsunami inundation occurring. The mega scenario ACSZ 4 from central Aleutian-Alaska Subduction Zone strikes Monterey coastline most severely, while an M_w 9.3 event generated in the northern of South America has almost no influence at Monterey. Among all the mega scenarios, the computed maximum positive wave amplitude at the warning point ranges from 0.19 m in scenario CSSZ 5 to 5.2 m in scenario ACSZ 4. Similarly, the computed maximum negative wave amplitude at the warning point ranges from -0.23 m in CSSZ 5 to -7.6 m in scenario ACSZ 4. The computed maximum tsunami runup height reaches 7.3 m above mean high water (~ 7.8 m above mean sea level) in Monterey for scenario 4. Considering most of the Monterey City area has an land elevation of 8 m, a potential M_w 9.3 mega tsunami from central Aleutian-Alaska Subduction Zone may be catastrophic for this area. The fault area of ACSZ 4 roughly corresponds to the rupture area of an M_w 9.0 earthquake that triggered the destructive 1964 Alaska tsunami, which however did not cause much damages in Monterey. The mega tsunami testing also gives rise to another two noticeable phenomena:

(a) The grid B, covering the entire Monterey Bay, clearly shows that the tsunamis from all directions in the Pacific will tend to hit north end of the Monterey Bay, where the City of Santa Cruz is located, much harder than the south end where situates the City of Monterey. This has been confirmed by the historical destructive tsunamis of 1946 and 1964.

(b) The modeling results also show that the tsunamis from NTSZ, NVSZ, MOSZ and KISZ may cause larger late waves arriving 8 to 12 hours after the first tsunami arrival, and even 20 hours later if from CSSZ. Most of these late waves are possibly due to the reflected waves by the ocean ridges or islands in the Pacific.

The small artificial scenarios generated ignorable waves less than 1 cm at the warning point, and show no modeling instabilities (Figures 60 to 69). With little boundary forcing, the no-wave scenario produced tiny ripples at the order of 10-5 cm throughout the entire computational domain, meaning the present forecast model is robust enough to produce results without numerical amplification.

4. Summary and Conclusions

This study developed the tsunami forecast model for the community of Monterey, California. The developed model is being implemented into NOAA's Short-term Inundation Forecast of Tsunami (SIFT) to provide real-time modeling forecast of the water elevation, runup and inundation for the coastal community at Monterey and its

vicinity. This study has discussed the details of each individual component of the tsunami forecast model, including the bathymetry and topography, the basic model setup and model parameters. The forecast model employs grids as fine as 30 m and can accomplish 4-hour simulation after tsunami arrival in 10 minutes of CPU time. Using grids as fine as 8 m, a referenced inundation model is developed in parallel to provide reference of the model accuracy for the forecast model.

Model validations have been carried out for the Monterey forecast model and RIM using eight historical tsunami events by comparing the modeling results and the observation at the tide station. The computed time series at Monterey tide station showed excellent agreement with observations. The model validation using historical tsunamis shows these events did not cause serious damages or inundation to the coastline of Monterey. This study created a total of 51 artificial M_w 9.3, M_w 7.5 and no-wave tsunami scenarios at the level of from all the source zones in the Pacific to ensure the stability of the developed forecast model under the strike of the highest wave amplitude of 7.3 m at the coastlines of Monterey.

All model validation and stability tests demonstrated that the developed tsunami forecast model and RIM for Monterey are accurate, robust and efficient for their implementation in short-term real-time tsunami forecast and long-term tsunami inundation study.

5. Acknowledgments

The author wishes to thank Edison Gica and Jean Newman for their propagation database work. The author would like to Dr. Hongqiang Zhou for reviewing this report. The author would also like to especially acknowledge and thank Sandra Bigley for editorial review of this report. Collaborative contributions of the National Weather Service, the National Geophysical Data Center, and the National Data Buoy Center were invaluable. Funding for this publication and all work leading to development of a tsunami forecast model for Monterey, California was provided by the National Oceanic and Atmospheric Administration. This publication is also partially funded by the Joint Institute for the Study of the Atmosphere and Ocean (JISAO) under NOAA Cooperative Agreement No. NA17RJ1232, JISAO Contribution No. ****. This is PMEL Contribution No. ****.

6. References

Barberopoulou, A., J.C. Borrero, B. Uslu, N. Kalligeris, J.D. Goltz, R.I. Wilson, and C.E. Synolakis (2009): New maps of California to improve tsunami preparedness. Eos Trans. AGU, 90(16), 137–144.

Gica, E., M. Spillane, V.V. Titov, C. Chamberlin, and J.C. Newman (2008): Development of the forecast propagation database for NOAA's Short-term Inundation Forecast for Tsunamis (SIFT). NOAA Tech. Memo. OAR PMEL-139, 89 pp.

Greene, H.G., N.M. Maher and C.K. Paull (2002), Physiography of the Monterey Bay National Marine Sanctuary and implications about continental margin development, Marine Geology, 181, 55-82.

Greene, H.G. and S.N. Ward (2003), Mass movement features along the central California margin and their modeled consequences for tsunami generation, Submarine Mass Movements and Their Consequences, edited by Locat, L. and Mienert J., Kluwer Academic Publishers, Netherlands.

Kelly, A., L. Dengler, B. Uslu, A. Barberopoulou, S. Yim, and K.J. Bergen (2006), Recent tsunami highlights need for awareness of tsunami duration*, Eos Trans.* AGU, 87, 566-567.

Marks, K.M., and Smith, W.H.F. (2006): An evaluation of publicly available global bathymetry grids. Marine Geophysical Researches, 27, 19-34.

Suleimani, E.N., Combellick, R.A., Hansen, R.A. and Carver, G.A. (2002). Tsunami hazard mapping of Alaska coastal communities. *Alaska GeoSurvery News*, 6(2), 5p.

Synolakis, C.E., E.N. Bernard, V.V. Titov, U. Kanoglu and F.I. Gonzalez (2008), Validation and verification of tsunami numerical models, Pure and Applied Geophysics, 165(11-12), 2197-2228.

Tang, L.J., Chamberline, C., Titov, V.V. (2008): A Stand-by Inundation Model of Kahului, Hawaii for NOAA Short-term Inundation Forecasting For Tsunamis (SIFT). NOAA Tech. Memo. OAR PMEL-XXX, 56p.

Tang, L., V.V. Titov, Y. Wei, H.O. Mofjeld, M. Spillane, D. Arcas, E.N. Bernard, C. Chamberlin, E. Gica and J. Newman (2008), Tsunami forecast analysis for the May 2006 Tonga tsunami, *Journal of Geophysical Research*, 113, C12015, doi: 10.1029/2008JC004922.

Taylor, L.A., B.W. Eakins, K.S. Carignan, R.R. Warnken, T. Sazonova, and D.C. Schoolcraft (2008), Digital elevation model for Monterey, California: procedures, data sources and analysis, prepared for the Pacific Marine Environmental Laboratory (PMEL) NOAA Center for Tsunami Research by the NOAA National Geophysical Data Center, 33p.

Titov, V.V. (2008), Tsunami forecasting, in *the Sea*, vol. 15, edited by E. Bernard, and A. Robinson, Chap. 12, pp. 367-396, Harvard Univ. Press, Cambridge, Mass.

Titov, V.V., Gonzalez, F.I., Bernard, E.N., Eble, M.C., Mofjeld, H.O., Newman, J.C. and Venturato, A.J. (2005). Real-time tsunami forecasting: challenges and solutions. Natural Hazards, 35(1), 41-58.

Titov, V.V., H.O. Mofjeld, F.I. Gonzalez and J.C. Newman (1999): Offshore forecasting of Alaska-Aleutian subduction zone tsunamis in Hawaii. NOAA Technical Memorandum. ERL PMEL-114, January 1999, 22 pp.

Uslu, B., J.C. Borrero, L.A. Dengler, and C.E. Synolakis (2007), Tsunami inundation at Crescent City, California generated by earthquake along the Cascadia Subduction Zone, *Geophy. Res. Lett.*, 34, L20601, doi:10.1029/2007GL030188.

Ward, S.N. and S. Simon (2005), Tsunami thoughts, Canadian Society of Exploration Geophysicists Recorder, 30(10), 38-44.

Wei, Y, E. N. Bernard, L. Tang, R. Weiss, V.V. Titov, C. Moore, M. Spillane, M. Hopkins and U. Kanoglu (2007): Real-time experimental forecast of the Peruvian tsunami of August 2007 for U.S. coastlines. *Geophys. Res. Lett*., *35*, L04609, doi: 10.1029/2007GL032250.

Working Group on California Earthquake Probabilities (2003), Earthquake Probabilities in the San Francisco Bay Region: 2002 -2031, U.S. Geological Survey Open File Report 03-214, 235p.

Figures:

Figure 15 Model validation at Monterey for 23 June 2001 Peru tsunami. (a) Computed and observed time series at Monterey tide station; (b) Computed maximum wave amplitude in grid C of RIM; (c) Computed maximum current speed in grid C of RIM; (d) Computed maximum wave amplitude in grid C of forecast model; (e) Computed current speed in grid C of forecast model. The black rectangular in (b) and (c) indicates the computational domain of forecast model grid C in (d) and (e).

Figure 16 Model validation at Monterey for 3 May 2006 Tonga tsunami. (a) Computed and observed time series at Monterey tide station; (b) Computed maximum wave amplitude in grid C of RIM; (c) Computed maximum current speed in grid C of RIM; (d) Computed maximum wave amplitude in grid C of forecast model; (e) Computed current speed in grid C of forecast model. The black rectangular in (b) and (c) indicates the computational domain of forecast model grid C in (d) and (e)

Figure 17 Model validation at Monterey for 11 November 2006 Kuril Islands tsunami. (a) Computed and observed time series at Monterey tide station; (b) Computed maximum wave amplitude in grid C of RIM; (c) Computed maximum current speed in grid C of RIM; (d) Computed maximum wave amplitude in grid C of forecast model; (e) Computed current speed in grid C of forecast model. The black rectangular in (b) and (c) indicates the computational domain of forecast model grid C in (d) and (e).

Figure 18. Model validation at Monterey for 13 January 2007 Kuril Islands tsunami. (a) Computed and observed time series at Monterey tide station; (b) Computed maximum wave amplitude in grid C of RIM; (c) Computed maximum current speed in grid C of RIM; (d) Computed maximum wave amplitude in grid C of forecast model; (e) Computed current speed in grid C of forecast model. The black rectangular in (b) and (c) indicates the computational domain of forecast model grid C in (d) and (e).

Figure 19. Model validation at Monterey for 15 August 2007 Peru tsunami. (a) Computed (+12 min) and observed time series at Monterey tide station; (b) Computed maximum wave amplitude in grid C of RIM; (c) Computed maximum current speed in grid C of RIM; (d) Computed maximum wave amplitude in grid C of forecast model; (e) Computed current speed in grid C of forecast model. The black rectangular in (b) and (c) indicates the computational domain of forecast model grid C in (d) and (e).

Figure 20. Model results at Monterey for 1 April 1946 Alaska tsunami. (a) Computed time series at Monterey tide station; (b) Computed maximum wave amplitude in grid C of RIM; (c) Computed maximum current speed in grid C of RIM; (d) Computed maximum wave amplitude in grid C of forecast model; (e) Computed current speed in grid C of forecast model. The black rectangular in (b) and (c) indicates the computational domain of forecast model grid C in (d) and (e).

Figure 21. Model stability testing results at Monterey for artificial mega tsunami scenario ACSZ 1. (a) Computed time series at Monterey warning point; (b) Computed maximum wave amplitude in grid A of the forecast model; (c) Computed maximum current speed in grid B of the forecast model; (d) Computed maximum wave amplitude in grid C of the forecast model; (e) Computed current speed in grid C of the forecast model.

Figure 22. Model stability testing results at Monterey for artificial mega tsunami scenario ACSZ 2. (a) Computed time series at Monterey warning point; (b) Computed maximum

wave amplitude in grid A of the forecast model; (c) Computed maximum current speed in grid B of the forecast model; (d) Computed maximum wave amplitude in grid C of the forecast model; (e) Computed current speed in grid C of the forecast model.

Figure 23. Model stability testing results at Monterey for artificial mega tsunami scenario ACSZ 3. (a) Computed time series at Monterey warning point; (b) Computed maximum wave amplitude in grid A of the forecast model; (c) Computed maximum current speed in grid B of the forecast model; (d) Computed maximum wave amplitude in grid C of the forecast model; (e) Computed current speed in grid C of the forecast model.

Figure 24. Model stability testing results at Monterey for artificial mega tsunami scenario ACSZ 4. (a) Computed time series at Monterey warning point; (b) Computed maximum wave amplitude in grid A of the forecast model; (c) Computed maximum current speed in grid B of the forecast model; (d) Computed maximum wave amplitude in grid C of the forecast model; (e) Computed current speed in grid C of the forecast model.

Figure 25. Model stability testing results at Monterey for artificial mega tsunami scenario ACSZ 5. (a) Computed time series at Monterey warning point; (b) Computed maximum wave amplitude in grid A of the forecast model; (c) Computed maximum current speed in grid B of the forecast model; (d) Computed maximum wave amplitude in grid C of the forecast model; (e) Computed current speed in grid C of the forecast model.

Figure 26. Model stability testing results at Monterey for artificial mega tsunami scenario ACSZ 6. (a) Computed time series at Monterey warning point; (b) Computed maximum wave amplitude in grid A of the forecast model; (c) Computed maximum current speed in grid B of the forecast model; (d) Computed maximum wave amplitude in grid C of the forecast model; (e) Computed current speed in grid C of the forecast model.

Figure 27. Model stability testing results at Monterey for artificial mega tsunami scenario ACSZ 7. (a) Computed time series at Monterey warning point; (b) Computed maximum wave amplitude in grid A of the forecast model; (c) Computed maximum current speed in grid B of the forecast model; (d) Computed maximum wave amplitude in grid C of the forecast model; (e) Computed current speed in grid C of the forecast model.

Figure 28. Model stability testing results at Monterey for artificial mega tsunami scenario CSSZ 1. (a) Computed time series at Monterey warning point; (b) Computed maximum wave amplitude in grid A of the forecast model; (c) Computed maximum current speed in grid B of the forecast model; (d) Computed maximum wave amplitude in grid C of the forecast model; (e) Computed current speed in grid C of the forecast model.

Figure 29. Model stability testing results at Monterey for artificial mega tsunami scenario CSSZ 2. (a) Computed time series at Monterey warning point; (b) Computed maximum wave amplitude in grid A of the forecast model; (c) Computed maximum current speed in grid B of the forecast model; (d) Computed maximum wave amplitude in grid C of the forecast model; (e) Computed current speed in grid C of the forecast model.

Figure 30. Model stability testing results at Monterey for artificial mega tsunami scenario CSSZ 3. (a) Computed time series at Monterey warning point; (b) Computed maximum wave amplitude in grid A of the forecast model; (c) Computed maximum current speed in grid B of the forecast model; (d) Computed maximum wave amplitude in grid C of the forecast model; (e) Computed current speed in grid C of the forecast model.

Figure 31. Model stability testing results at Monterey for artificial mega tsunami scenario CSSZ 4. (a) Computed time series at Monterey warning point; (b) Computed maximum wave amplitude in grid A of the forecast model; (c) Computed maximum current speed in grid B of the forecast model; (d) Computed maximum wave amplitude in grid C of the forecast model; (e) Computed current speed in grid C of the forecast model.

Figure 32. Model stability testing results at Monterey for artificial mega tsunami scenario CSSZ 5. (a) Computed time series at Monterey warning point; (b) Computed maximum wave amplitude in grid A of the forecast model; (c) Computed maximum current speed in grid B of the forecast model; (d) Computed maximum wave amplitude in grid C of the forecast model; (e) Computed current speed in grid C of the forecast model.

Figure 33. Model stability testing results at Monterey for artificial mega tsunami scenario CSSZ 6. (a) Computed time series at Monterey warning point; (b) Computed maximum wave amplitude in grid A of the forecast model; (c) Computed maximum current speed in grid B of the forecast model; (d) Computed maximum wave amplitude in grid C of the forecast model; (e) Computed current speed in grid C of the forecast model.

Figure 34. Model stability testing results at Monterey for artificial mega tsunami scenario CSSZ 7. (a) Computed time series at Monterey warning point; (b) Computed maximum wave amplitude in grid A of the forecast model; (c) Computed maximum current speed in grid B of the forecast model; (d) Computed maximum wave amplitude in grid C of the forecast model; (e) Computed current speed in grid C of the forecast model.

Figure 35. Model stability testing results at Monterey for artificial mega tsunami scenario CSSZ 8. (a) Computed time series at Monterey warning point; (b) Computed maximum wave amplitude in grid A of the forecast model; (c) Computed maximum current speed in grid B of the forecast model; (d) Computed maximum wave amplitude in grid C of the forecast model; (e) Computed current speed in grid C of the forecast model.

Figure 36. Model stability testing results at Monterey for artificial mega tsunami scenario CSSZ 9. (a) Computed time series at Monterey warning point; (b) Computed maximum wave amplitude in grid A of the forecast model; (c) Computed maximum current speed in grid B of the forecast model; (d) Computed maximum wave amplitude in grid C of the forecast model; (e) Computed current speed in grid C of the forecast model.

Figure 37. Model stability testing results at Monterey for artificial mega tsunami scenario NTSZ 1. (a) Computed time series at Monterey warning point; (b) Computed maximum wave amplitude in grid A of the forecast model; (c) Computed maximum current speed in grid B of the forecast model; (d) Computed maximum wave amplitude in grid C of the forecast model; (e) Computed current speed in grid C of the forecast model.

Figure 38. Model stability testing results at Monterey for artificial mega tsunami scenario NTSZ 2. (a) Computed time series at Monterey warning point; (b) Computed maximum wave amplitude in grid A of the forecast model; (c) Computed maximum current speed in grid B of the forecast model; (d) Computed maximum wave amplitude in grid C of the forecast model; (e) Computed current speed in grid C of the forecast model.

Figure 39. Model stability testing results at Monterey for artificial mega tsunami scenario NTSZ 3. (a) Computed time series at Monterey warning point; (b) Computed maximum wave amplitude in grid A of the forecast model; (c) Computed maximum current speed in

grid B of the forecast model; (d) Computed maximum wave amplitude in grid C of the forecast model; (e) Computed current speed in grid C of the forecast model.

Figure 40. Model stability testing results at Monterey for artificial mega tsunami scenario NTSZ 4. (a) Computed time series at Monterey warning point; (b) Computed maximum wave amplitude in grid A of the forecast model; (c) Computed maximum current speed in grid B of the forecast model; (d) Computed maximum wave amplitude in grid C of the forecast model; (e) Computed current speed in grid C of the forecast model.

Figure 41. Model stability testing results at Monterey for artificial mega tsunami scenario NVSZ 1. (a) Computed time series at Monterey warning point; (b) Computed maximum wave amplitude in grid A of the forecast model; (c) Computed maximum current speed in grid B of the forecast model; (d) Computed maximum wave amplitude in grid C of the forecast model; (e) Computed current speed in grid C of the forecast model.

Figure 42. Model stability testing results at Monterey for artificial mega tsunami scenario NVSZ 2. (a) Computed time series at Monterey warning point; (b) Computed maximum wave amplitude in grid A of the forecast model; (c) Computed maximum current speed in grid B of the forecast model; (d) Computed maximum wave amplitude in grid C of the forecast model; (e) Computed current speed in grid C of the forecast model.

Figure 43. Model stability testing results at Monterey for artificial mega tsunami scenario NVSZ 3. (a) Computed time series at Monterey warning point; (b) Computed maximum wave amplitude in grid A of the forecast model; (c) Computed maximum current speed in grid B of the forecast model; (d) Computed maximum wave amplitude in grid C of the forecast model; (e) Computed current speed in grid C of the forecast model.

Figure 44. Model stability testing results at Monterey for artificial mega tsunami scenario NVSZ 4. (a) Computed time series at Monterey warning point; (b) Computed maximum wave amplitude in grid A of the forecast model; (c) Computed maximum current speed in grid B of the forecast model; (d) Computed maximum wave amplitude in grid C of the forecast model; (e) Computed current speed in grid C of the forecast model.

Figure 45. Model stability testing results at Monterey for artificial mega tsunami scenario MOSZ 1. (a) Computed time series at Monterey warning point; (b) Computed maximum wave amplitude in grid A of the forecast model; (c) Computed maximum current speed in grid B of the forecast model; (d) Computed maximum wave amplitude in grid C of the forecast model; (e) Computed current speed in grid C of the forecast model.

Figure 46. Model stability testing results at Monterey for artificial mega tsunami scenario MOSZ 2. (a) Computed time series at Monterey warning point; (b) Computed maximum wave amplitude in grid A of the forecast model; (c) Computed maximum current speed in grid B of the forecast model; (d) Computed maximum wave amplitude in grid C of the forecast model; (e) Computed current speed in grid C of the forecast model.

Figure 47. Model stability testing results at Monterey for artificial mega tsunami scenario NGSZ 1. (a) Computed time series at Monterey warning point; (b) Computed maximum wave amplitude in grid A of the forecast model; (c) Computed maximum current speed in grid B of the forecast model; (d) Computed maximum wave amplitude in grid C of the forecast model; (e) Computed current speed in grid C of the forecast model.

Figure 48. Model stability testing results at Monterey for artificial mega tsunami scenario NGSZ 2. (a) Computed time series at Monterey warning point; (b) Computed maximum wave amplitude in grid A of the forecast model; (c) Computed maximum current speed in grid B of the forecast model; (d) Computed maximum wave amplitude in grid C of the forecast model; (e) Computed current speed in grid C of the forecast model.

Figure 49. Model stability testing results at Monterey for artificial mega tsunami scenario EPSZ 1. (a) Computed time series at Monterey warning point; (b) Computed maximum wave amplitude in grid A of the forecast model; (c) Computed maximum current speed in grid B of the forecast model; (d) Computed maximum wave amplitude in grid C of the forecast model; (e) Computed current speed in grid C of the forecast model.

Figure 50. Model stability testing results at Monterey for artificial mega tsunami scenario EPSZ 2. (a) Computed time series at Monterey warning point; (b) Computed maximum wave amplitude in grid A of the forecast model; (c) Computed maximum current speed in grid B of the forecast model; (d) Computed maximum wave amplitude in grid C of the forecast model; (e) Computed current speed in grid C of the forecast model.

Figure 51. Model stability testing results at Monterey for artificial mega tsunami scenario RNSZ 1. (a) Computed time series at Monterey warning point; (b) Computed maximum wave amplitude in grid A of the forecast model; (c) Computed maximum current speed in grid B of the forecast model; (d) Computed maximum wave amplitude in grid C of the forecast model; (e) Computed current speed in grid C of the forecast model.

Figure 52. Model stability testing results at Monterey for artificial mega tsunami scenario RNSZ 2. (a) Computed time series at Monterey warning point; (b) Computed maximum wave amplitude in grid A of the forecast model; (c) Computed maximum current speed in grid B of the forecast model; (d) Computed maximum wave amplitude in grid C of the forecast model; (e) Computed current speed in grid C of the forecast model.

Figure 53. Model stability testing results at Monterey for artificial mega tsunami scenario KISZ 1. (a) Computed time series at Monterey warning point; (b) Computed maximum wave amplitude in grid A of the forecast model; (c) Computed maximum current speed in grid B of the forecast model; (d) Computed maximum wave amplitude in grid C of the forecast model; (e) Computed current speed in grid C of the forecast model.

Figure 54. Model stability testing results at Monterey for artificial mega tsunami scenario KISZ 2. (a) Computed time series at Monterey warning point; (b) Computed maximum wave amplitude in grid A of the forecast model; (c) Computed maximum current speed in grid B of the forecast model; (d) Computed maximum wave amplitude in grid C of the forecast model; (e) Computed current speed in grid C of the forecast model.

Figure 55. Model stability testing results at Monterey for artificial mega tsunami scenario KISZ 3. (a) Computed time series at Monterey warning point; (b) Computed maximum wave amplitude in grid A of the forecast model; (c) Computed maximum current speed in grid B of the forecast model; (d) Computed maximum wave amplitude in grid C of the forecast model; (e) Computed current speed in grid C of the forecast model.

Figure 56. Model stability testing results at Monterey for artificial mega tsunami scenario KISZ 4. (a) Computed time series at Monterey warning point; (b) Computed maximum wave amplitude in grid A of the forecast model; (c) Computed maximum current speed in

grid B of the forecast model; (d) Computed maximum wave amplitude in grid C of the forecast model; (e) Computed current speed in grid C of the forecast model.

Figure 57. Model stability testing results at Monterey for artificial mega tsunami scenario KISZ 5. (a) Computed time series at Monterey warning point; (b) Computed maximum wave amplitude in grid A of the forecast model; (c) Computed maximum current speed in grid B of the forecast model; (d) Computed maximum wave amplitude in grid C of the forecast model; (e) Computed current speed in grid C of the forecast model.

Figure 58. Model stability testing results at Monterey for artificial mega tsunami scenario KISZ 6. (a) Computed time series at Monterey warning point; (b) Computed maximum wave amplitude in grid A of the forecast model; (c) Computed maximum current speed in grid B of the forecast model; (d) Computed maximum wave amplitude in grid C of the forecast model; (e) Computed current speed in grid C of the forecast model.

Figure 59. Model stability testing results at Monterey for artificial mega tsunami scenario KISZ 7. (a) Computed time series at Monterey warning point; (b) Computed maximum wave amplitude in grid A of the forecast model; (c) Computed maximum current speed in grid B of the forecast model; (d) Computed maximum wave amplitude in grid C of the forecast model; (e) Computed current speed in grid C of the forecast model.

Figure 60. Model stability testing results at Monterey for artificial mega tsunami scenario KISZ 8. (a) Computed time series at Monterey warning point; (b) Computed maximum wave amplitude in grid A of the forecast model; (c) Computed maximum current speed in grid B of the forecast model; (d) Computed maximum wave amplitude in grid C of the forecast model; (e) Computed current speed in grid C of the forecast model.

Figure 61. Model stability testing results at Monterey for artificial tsunami scenario ACSZ b10. (a) Computed time series at Monterey warning point; (b) Computed maximum wave amplitude in grid A of the forecast model; (c) Computed maximum current speed in grid B of the forecast model; (d) Computed maximum wave amplitude in grid C of the forecast model; (e) Computed current speed in grid C of the forecast model.

Figure 62. Model stability testing results at Monterey for artificial tsunami scenario ACSZ b60. (a) Computed time series at Monterey warning point; (b) Computed maximum wave amplitude in grid A of the forecast model; (c) Computed maximum current speed in grid B of the forecast model; (d) Computed maximum wave amplitude in grid C of the forecast model; (e) Computed current speed in grid C of the forecast model.

Figure 63. Model stability testing results at Monterey for artificial tsunami scenario CSSZ b80. (a) Computed time series at Monterey warning point; (b) Computed maximum wave amplitude in grid A of the forecast model; (c) Computed maximum current speed in grid B of the forecast model; (d) Computed maximum wave amplitude in grid C of the forecast model; (e) Computed current speed in grid C of the forecast model.

Figure 64. Model stability testing results at Monterey for artificial tsunami scenario NTSZ b22. (a) Computed time series at Monterey warning point; (b) Computed maximum wave amplitude in grid A of the forecast model; (c) Computed maximum current speed in grid B of the forecast model; (d) Computed maximum wave amplitude in grid C of the forecast model; (e) Computed current speed in grid C of the forecast model.

Figure 65. Model stability testing results at Monterey for artificial tsunami scenario NVSZ b11. (a) Computed time series at Monterey warning point; (b) Computed maximum wave amplitude in grid A of the forecast model; (c) Computed maximum current speed in grid B of the forecast model; (d) Computed maximum wave amplitude in grid C of the forecast model; (e) Computed current speed in grid C of the forecast model.

Figure 66. Model stability testing results at Monterey for artificial tsunami scenario MOSZ b9. (a) Computed time series at Monterey warning point; (b) Computed maximum wave amplitude in grid A of the forecast model; (c) Computed maximum current speed in grid B of the forecast model; (d) Computed maximum wave amplitude in grid C of the forecast model; (e) Computed current speed in grid C of the forecast model.

Figure 67. Model stability testing results at Monterey for artificial tsunami scenario NGSZ b6. (a) Computed time series at Monterey warning point; (b) Computed maximum wave amplitude in grid A of the forecast model; (c) Computed maximum current speed in grid B of the forecast model; (d) Computed maximum wave amplitude in grid C of the forecast model; (e) Computed current speed in grid C of the forecast model.

Figure 68. Model stability testing results at Monterey for artificial tsunami scenario EPSZ b9. (a) Computed time series at Monterey warning point; (b) Computed maximum wave amplitude in grid A of the forecast model; (c) Computed maximum current speed in grid B of the forecast model; (d) Computed maximum wave amplitude in grid C of the forecast model; (e) Computed current speed in grid C of the forecast model.

Figure 69. Model stability testing results at Monterey for artificial tsunami scenario KISZ b13. (a) Computed time series at Monterey warning point; (b) Computed maximum wave amplitude in grid A of the forecast model; (c) Computed maximum current speed in grid B of the forecast model; (d) Computed maximum wave amplitude in grid C of the forecast model; (e) Computed current speed in grid C of the forecast model.

Figure 70. Model stability testing results at Monterey for artificial micro tsunami scenario EPSZ b15. (a) Computed time series at Monterey warning point; (b) Computed maximum wave amplitude in grid A of the forecast model; (c) Computed maximum current speed in grid B of the forecast model; (d) Computed maximum wave amplitude in grid C of the forecast model; (e) Computed current speed in grid C of the forecast model.

Tables:

Forecast model .in file:

```
0.0001 Minimum amplitude of input offshore wave (m)
1.0    nput minimum depth for offshore (m)
0.1    nput "dry land" depth for inundation (m)
0.0009 Input friction coefficient (n**2)
1      let a and b run up
300.0  blowup limit
1.0    input time step (sec)
43200  input amount of steps
12     Compute "A" arrays every n-th time step, n=
1      Compute "B" arrays every n-th time step, n=
36     Input number of steps between snapshots
1      ...Starting from
1      ...saving grid every n-th node, n=
monterey_run2d/gridA
monterey_run2d/gridB
monterey_run2d/gridC
./
./
1 1 1 1      NetCDF output for A, B, C, SIFT
1 Timeseries locations:
3 110 199    monterey     238.110556   36.605 depth m: 5.8
MRY Monterey, CA
```

Reference model .in file:

```
0.0001 Minimum amplitude of input offshore wave (m)
1.0  Input minimum depth for offshore (m)
0.1   Input "dry land" depth for inundation (m)
0.0009 Input friction coefficient (n**2)
1     let a and b run up 300.0 blowup limit
0.25   input time step (sec)
115200 input amount of steps
15     Compute "A" arrays every n-th time step, n=
1 COmpute "B" arrays every n-th time step, n=
120   Input number of steps between snapshots
1 ...Starting from
1 ...saving grid every n-th node, n=
rim_gridA
rim_gridB
rim_gridC
./
./
1 1 1 1      NetCDF output for A, B, C, SIFT
```

Grid	Region	Reference Inundation Model (RIM)			Stand-by Inundation Model (SIM)		
		Coverage	Cell	Time	Coverage	Cell	Time
		Lat. [°N]	Size	Step	Lat. [°N]	Size	Step
		Lon. [°W]	["]	[sec]	Lon. [°W]	["]	[sec]
A	South Carolina	30-40	36	3.75	30-40	120	12.0
		127-117	(1001×1001)		127-117	(301×301)	
B	Monterey Bay	36.3 -37.1	3	0.25	36.3 -37.1	18	2.0
		122.52 –121.53	(1198×981)		122.52 – 121.53	(199×161)	
C	Monterey Harbor	33.58-36.71	1/3	0.25	36.58-36.66	2×1	2.0
		121.958-121.77	(2031×1405)		121.95-121.84	(253×289)	
Minimum offshore depth [m]			1		1		
Water depth for dry land [m]			0.1		0.1		
Friction coefficient (n^2)			0.0009		0.0009		
CPU time for a 4-hour simulation (min)			1489		10.4		
Warning point coordinates			121.88667W, 36.605N				

Table 1 Model setup and input parameters of Monterey forecast model and reference model.

Name of Scenario	Unit Source Combination	Name of Scenario	Unit Source Combination
ACSZ 1	28.4 × (a1-a10, b1-b10)	NVSZ 1	28.4 × (a1-a10, b1-b10)
ACSZ 2	28.4 × (a11-a20, a11-a20)	NVSZ 2	28.4 × (a11-a20, b11-b20)
ACSZ 3	28.4 × (a21-a30, b21-b30)	NVSZ 3	28.4 × (a21-a30, b21-b30)
ACSZ 4	28.4 × (a31-a40, b31-b40)	NVSZ 4	28.4 × (a28-a37, b28-b37)
ACSZ 5	28.4 × (a41-a50, b41-b50)	MOSZ 1	28.4 × (a1-a10, b1-b10)
ACSZ 6	28.4 × (a46-a55, b46-b55)	MOSZ 2	28.4 × (a8-a17, b8-b17)
ACSZ 7	28.4 × (a56-a65, b56-b65)	NGSZ 1	28.4 × (a1-a10, b1-b10)
CSSZ 1	28.4 × (a1-a10, b1-b10)	NGSZ 2	28.4 × (a6-a15, b6-b15)
CSSZ 2	28.4 × (a11-a20, a11-a20)	EPSZ 1	28.4 × (a11-A20, b11-b20)
CSSZ 3	28.4 × (a21-a30, b21-b30)	EPSZ 2	28.4 × (a9-A18, b9-b18)
CSSZ 4	28.4 × (a31-a40, b31-b40)	RNSZ 1	28.4 × (a1-A10, b1-b10)
CSSZ 5	28.4 × (a41-a50, b41-b50)	RNSZ 2	28.4 × (a13-A22, b13-b22)
CSSZ 6	28.4 × (a51-a60, b51-b60)	KISZ 1	28.4 × (a1-a10, b1-b10)
CSSZ 7	28.4 × (a61-a70, b61-b70)	KISZ 2	28.4 × (a11-a10, b11-b20)
CSSZ 8	28.4 × (a71-a80, b71-b80)	KISZ 3	28.4 × (a21-a30, b21-b30)
CSSZ 9	28.4 × (a81-a90, b81-b90)	KISZ 4	28.4 × (a32-a41, b32-b41)
NTSZ 1	28.4 × (a1-a10, b1-b10)	KISZ 5	28.4 × (a42-a51, b42-b51)
NTSZ 2	28.4 × (a11-a20, b11-b20)	KISZ 6	28.4 × (a52-a61, b52-b61)
NTSZ 3	28.4 × (a21-a30, b21-b30)	KISZ 7	28.4 × (a56-a65, b56-b65)
NTSZ 4	28.4 × (a30-a39, b30-b39)	KISZ 8	28.4 × (a66-a75, b66-b75)
ACSZ b10	1.0 × b10	ACSZ b60	1.0 × b60
CSSZ b80	1.0 × b80	NTSZ b22	1.0 × b22
NVSZ b11	1.0 × b11	MOSZ b9	1.0 × b19
NGSZ b9	1.0 × b9	EPSZ b9	1.0 × b9
RNSZ b9	1.0 × b9	KISZ b13	1.0 × b13
EPSZ b15	0.0001 × b15		

Table 2. Tsunami source of 51 artificial scenarios used for stability testing, where ACSZ = Alaska-Aleutian-Canada source zone, CSSZ = Central and South America source zone; NTSZ = New Zealand-Kermadec-Tonga source zone; NVSZ = New Britain-Solomons-Vanuatu source zone; MOSZ = Manus OCB source zone; NGSZ = North New Guinea source zone; EPSZ = East Philippines source zone; RNSZ = Ryukyu-Kyushu-Nankai source zone; KISZ = Kamchatka-Kuril-Japan trench source zone.

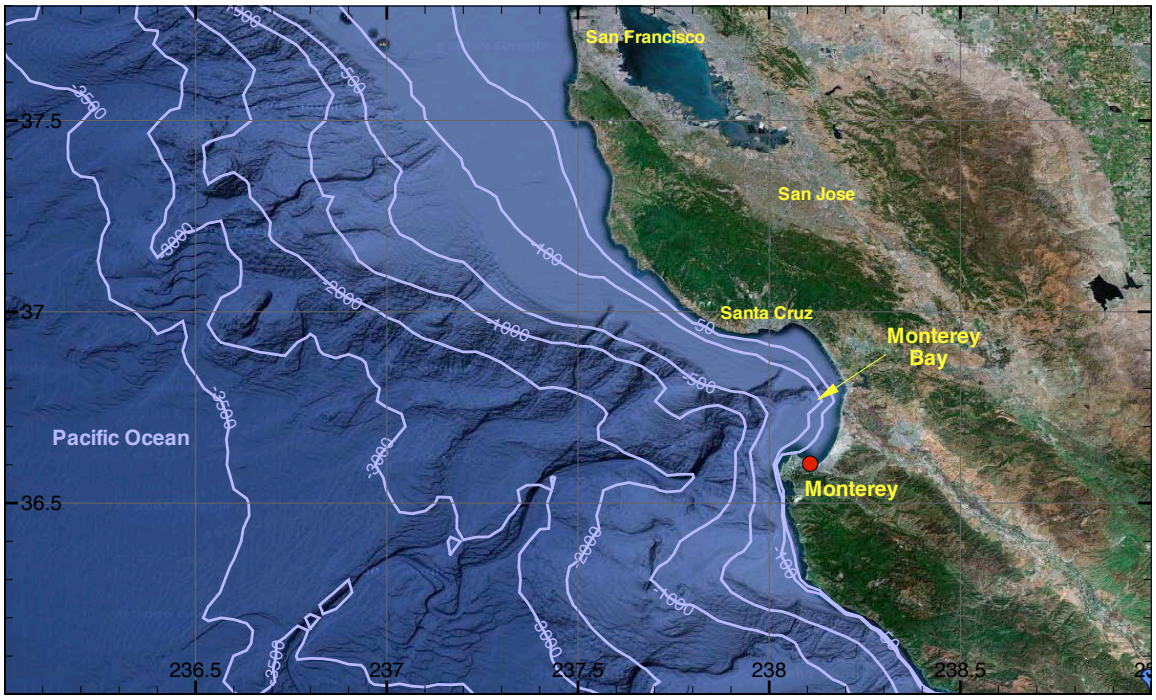

Figure 1 Location of Monterey, Canifornia.

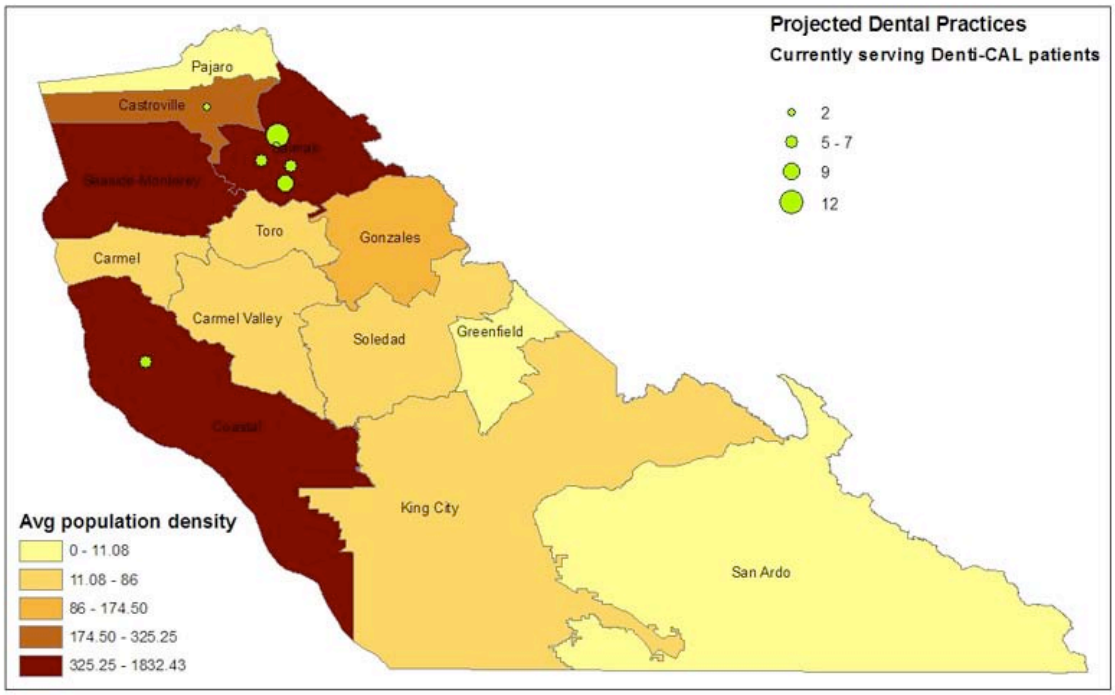

Figure 2 2007 average population density of Monterey County.

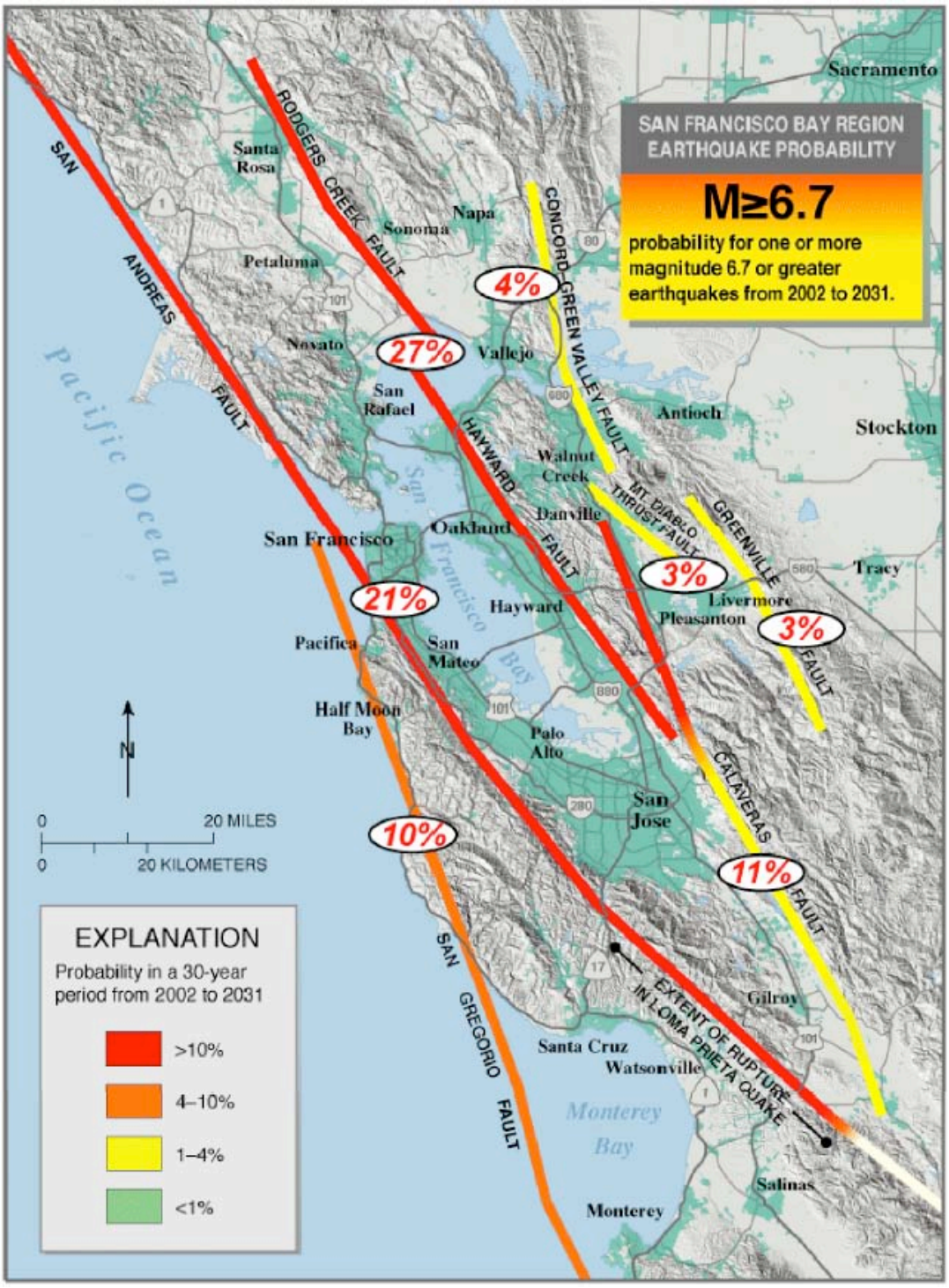

Figure 3 Probabilities of Mw 6.7 or stronger earthquakes occurring on faults in the San Francisco Bay Region during 2001-2031, where the probability of occurrence on each fault in indicated in ovals, and colors indicate the corresponding probabilities of each fault segment. Credit: Working Group on California Earthquake Probabilities (2003).

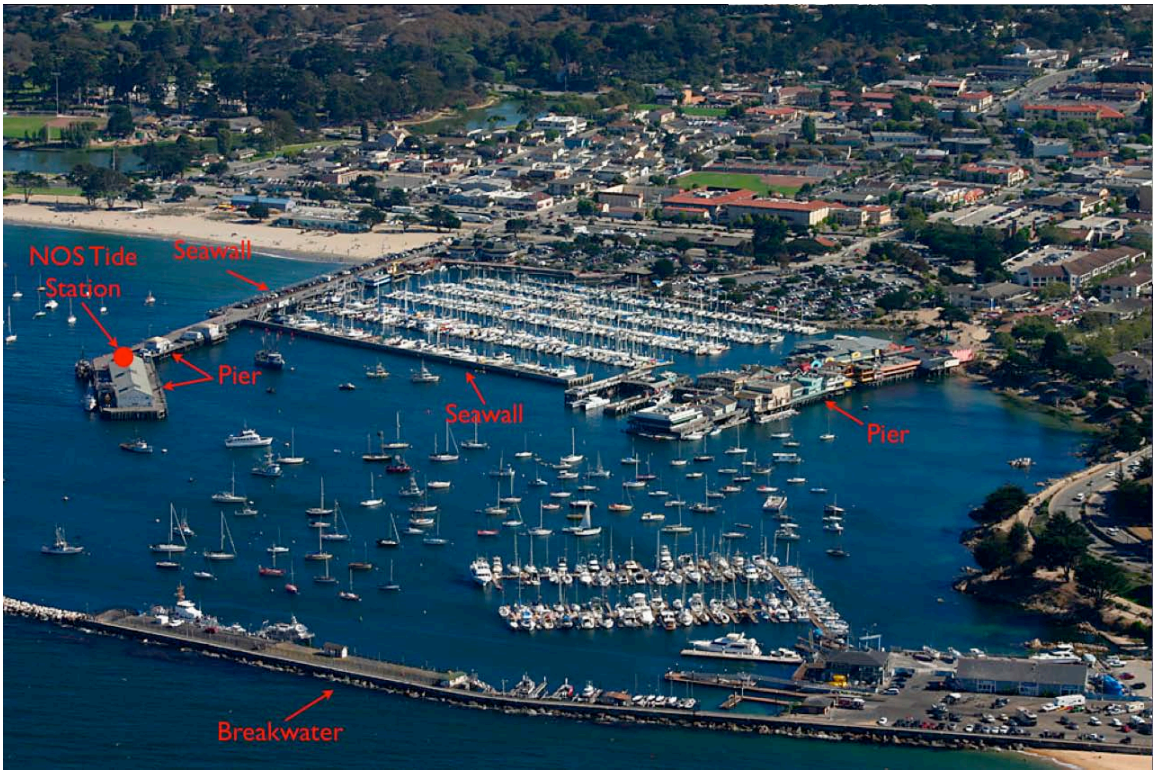

Figure 4 Aerial photo overlooking Monterey Harbor.

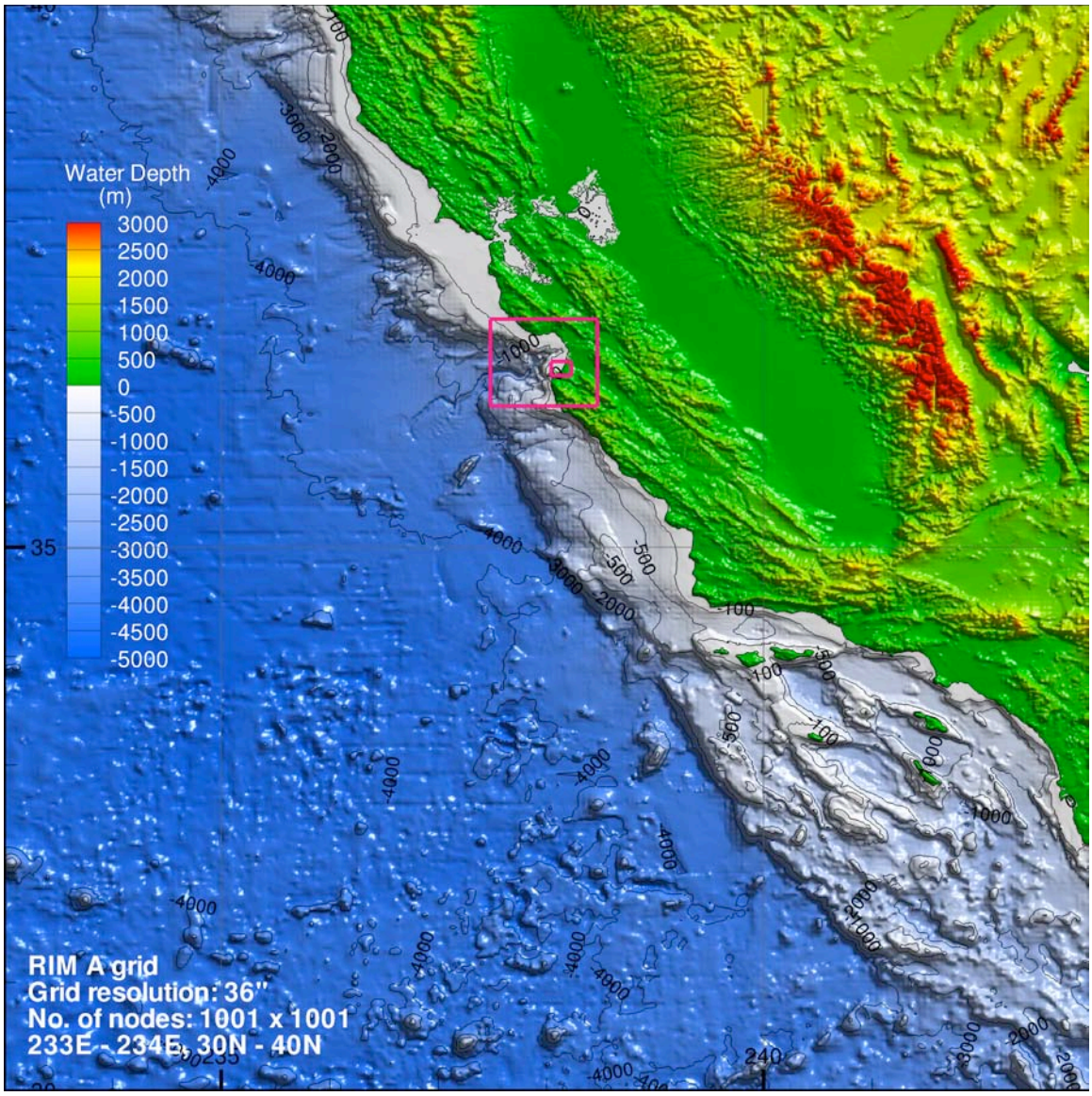

Figure 5 Bathymetry and topography of the outmost grid A for the reference model at Monterey, CA.

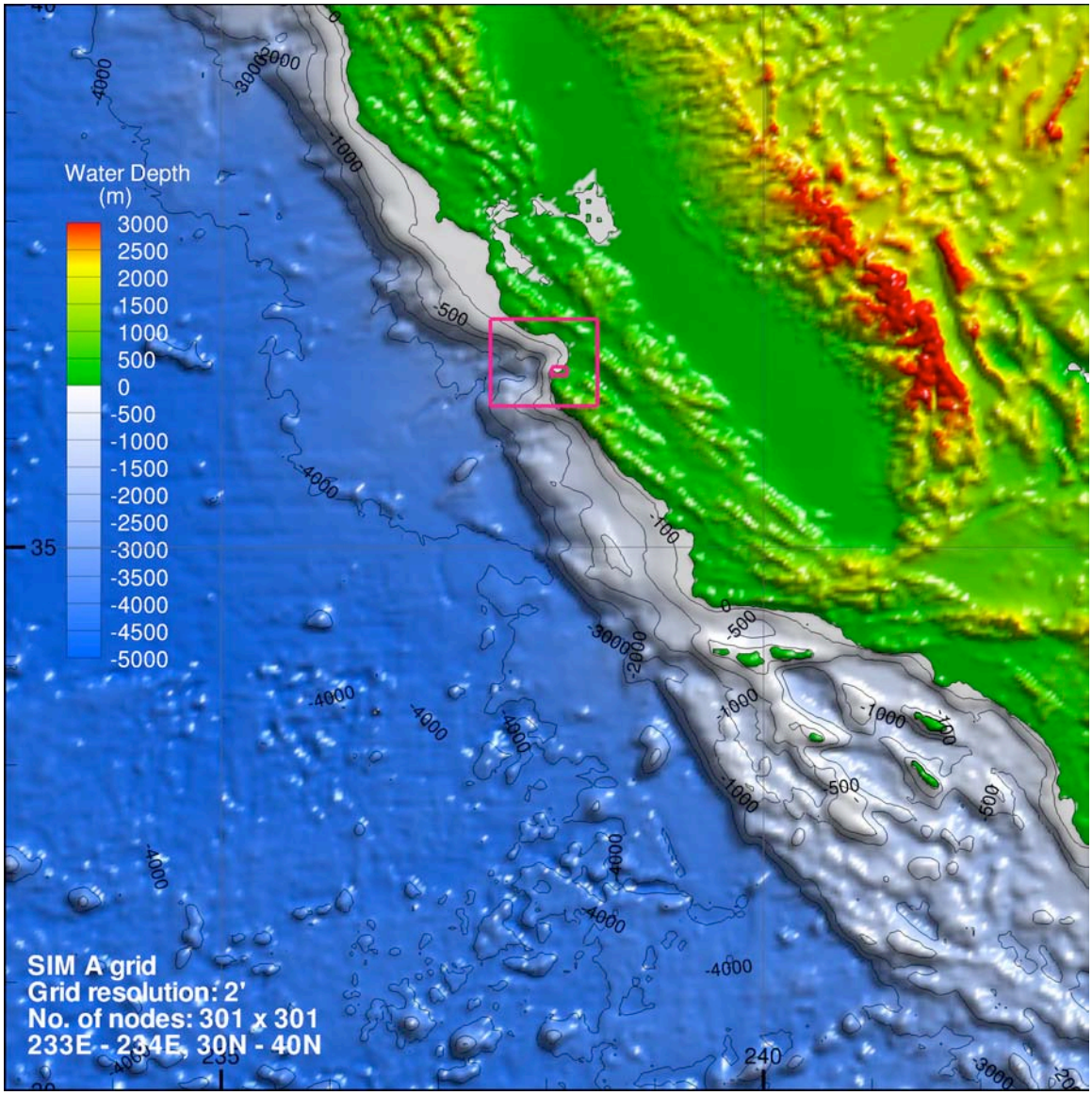

Figure 6 Bathymetry and topography of the outmost grid A for the optimized forecast model at Monterey, CA.

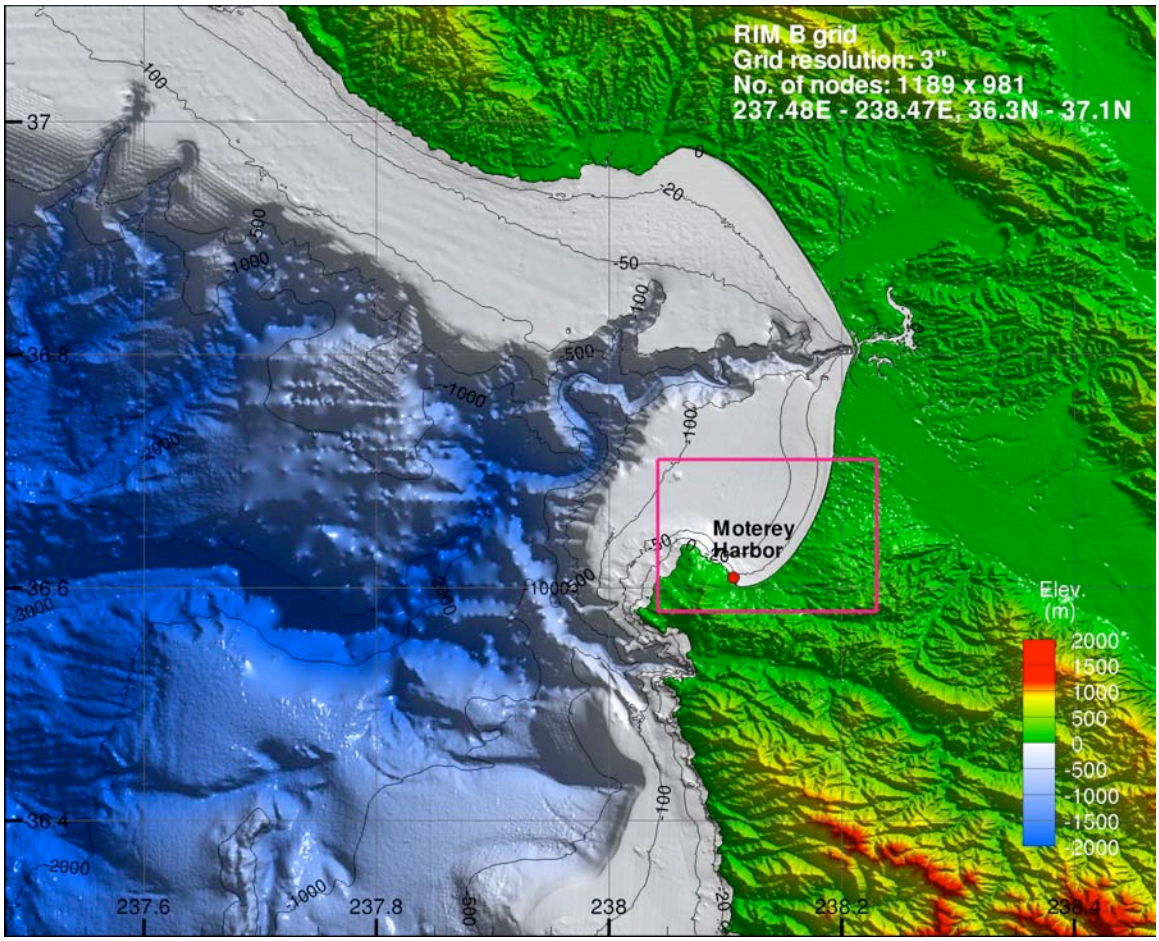

Figure 7 Bathymetry and topography of the intermediate grid B for the reference model at Monterey, CA.

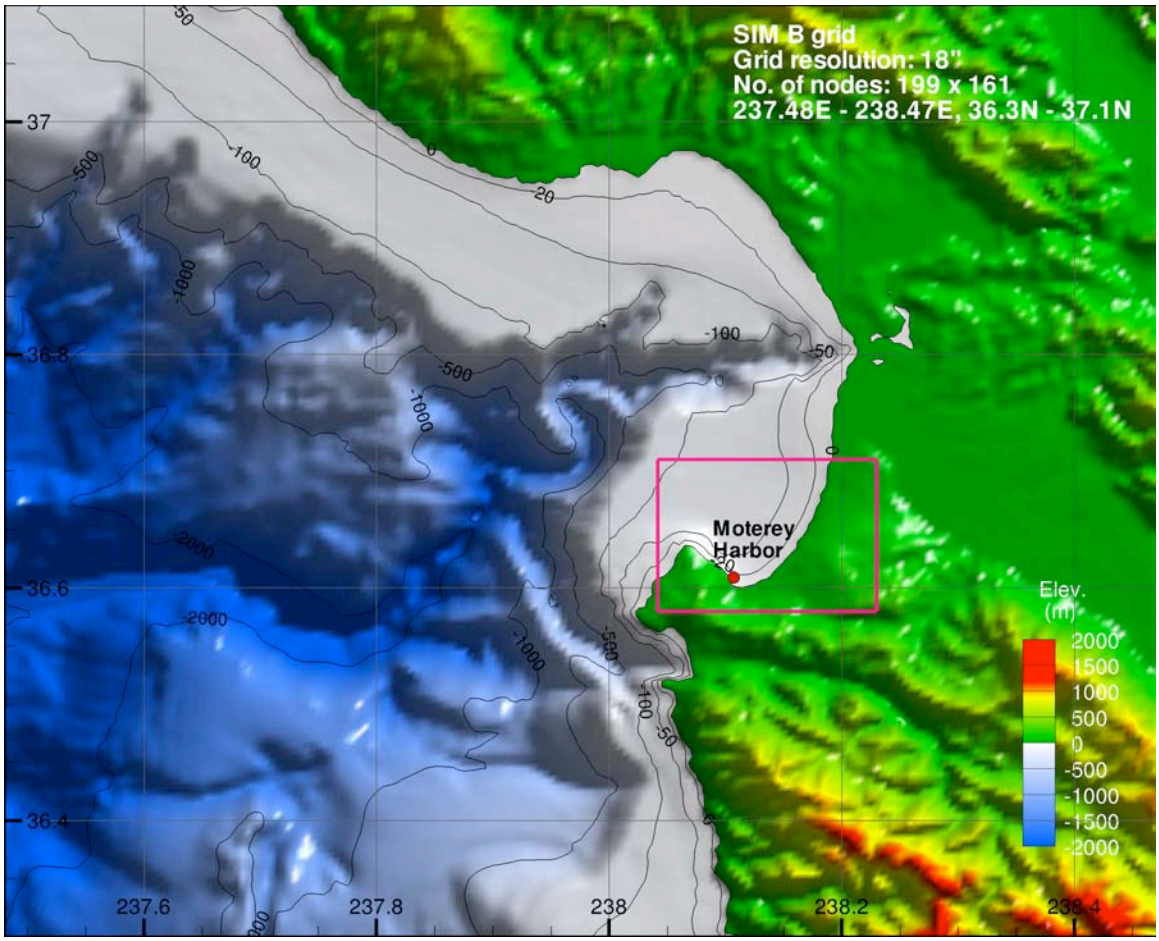

Figure 8 Bathymetry and topography of the intermediate grid B for the optimized forecast model at Monterey, CA.

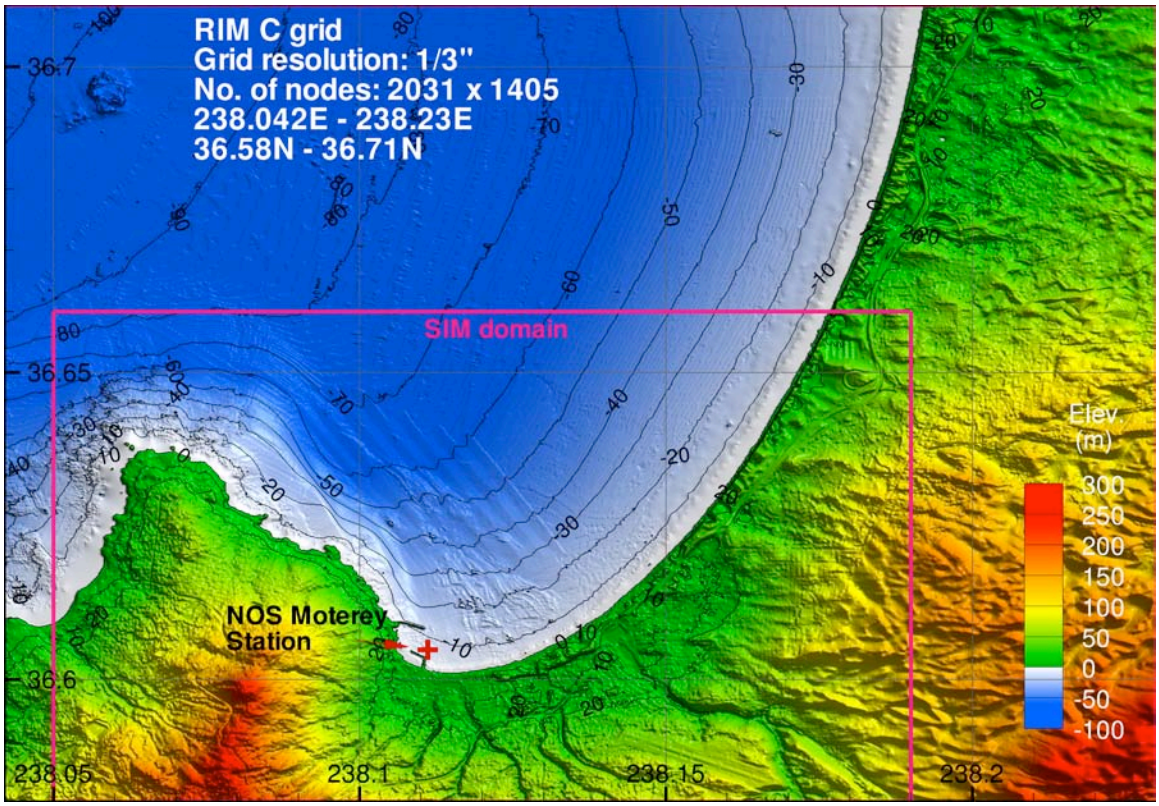

Figure 9 Bathymetry and topography of the inmost grid C for the reference model at Monterey, CA.

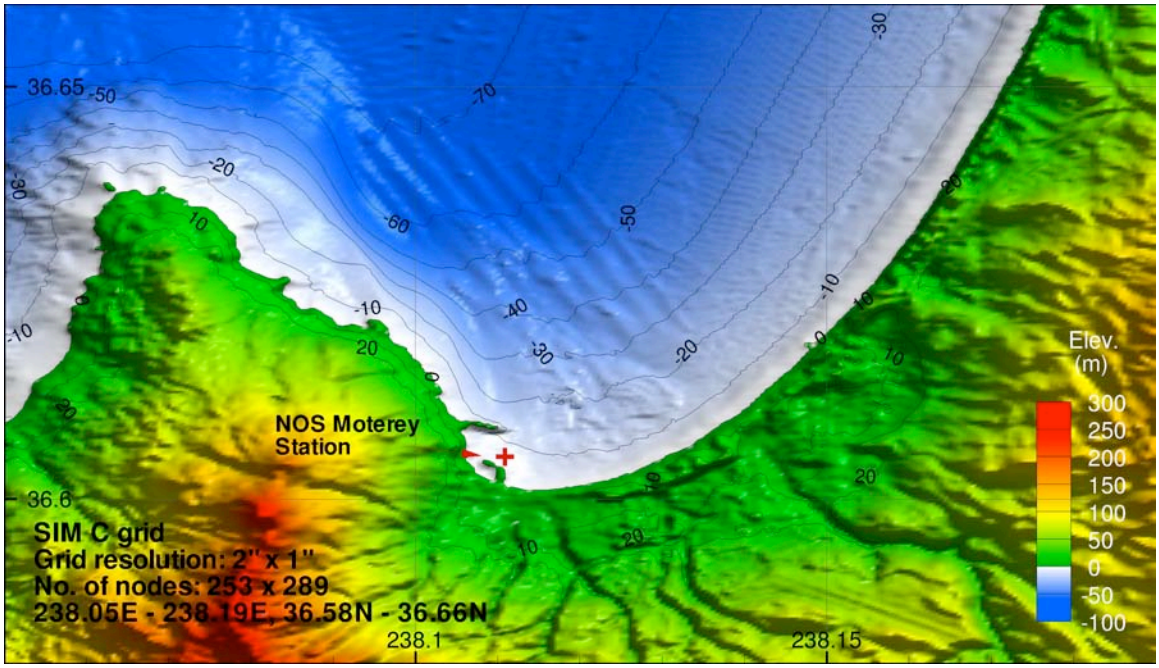

Figure 10 Bathymetry and topography of the inmost grid C for the optimized forecast model at Monterey, CA.

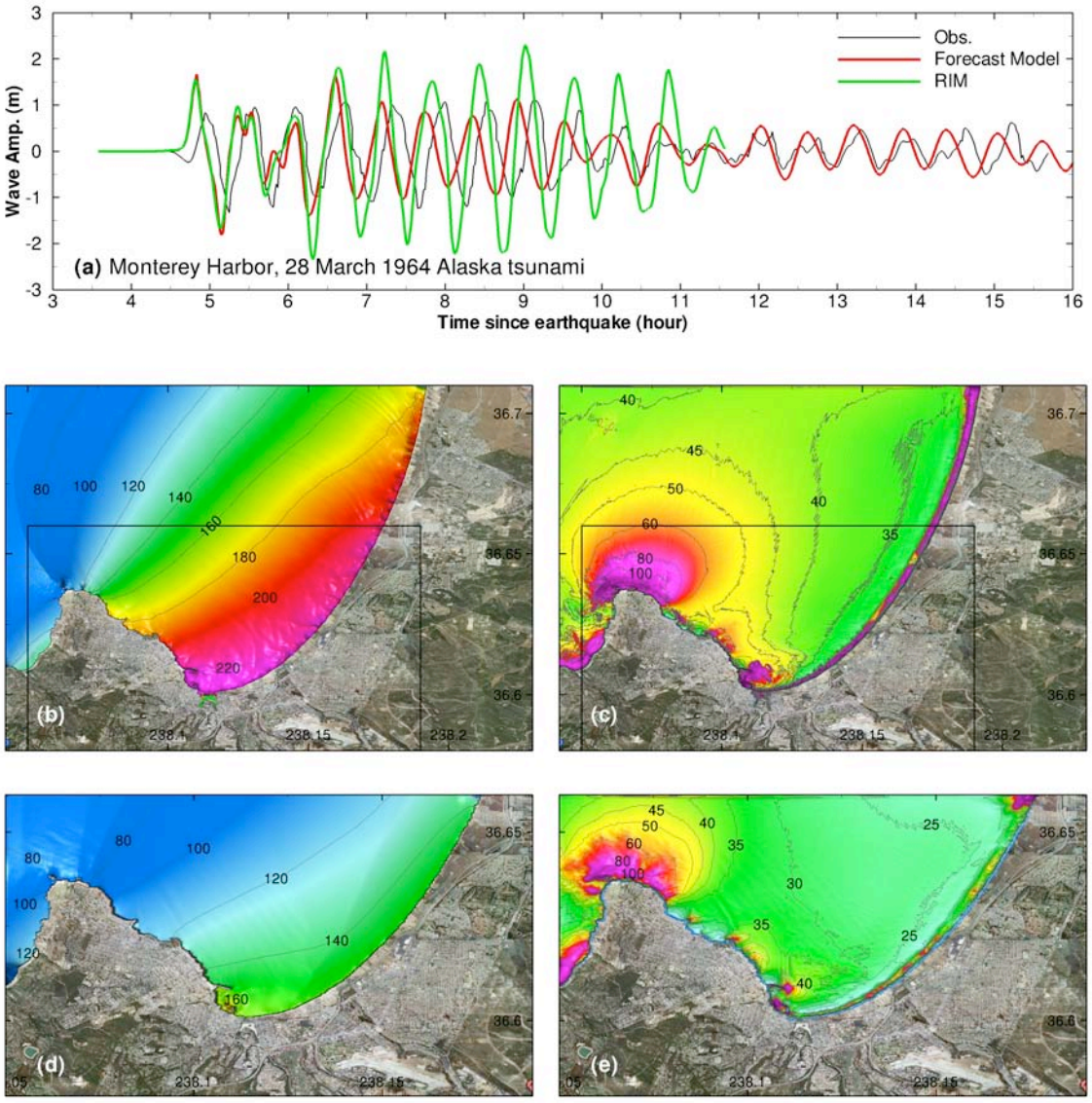

Figure 11. Model validation at Monterey for 28 March 1964 Alaska tsunami. (a) Computed and observed time series at Monterey tide station; (b) Computed maximum wave amplitude in grid C of RIM; (c) Computed maximum current speed in grid C of RIM; (d) Computed maximum wave amplitude in grid C of forecast model; (e) Computed current speed in grid C of forecast model. The black rectangular in (b) and (c) indicates the computational domain of forecast model grid C in (d) and (e).

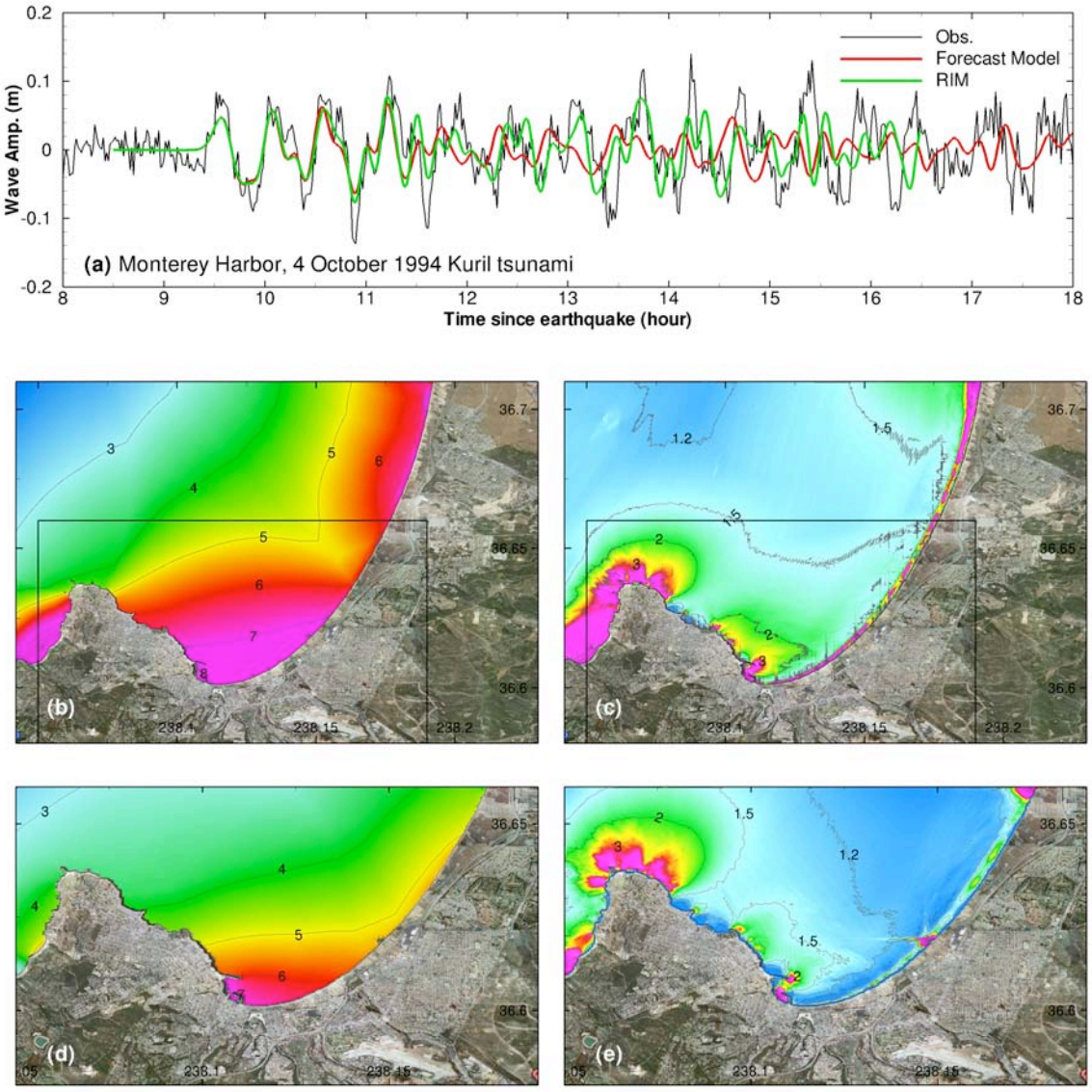

Figure 12. Model validation at Monterey for 4 October 1994 Kuril Islands tsunami. (a) Computed and observed time series at Monterey tide station; (b) Computed maximum wave amplitude in grid C of RIM; (c) Computed maximum current speed in grid C of RIM; (d) Computed maximum wave amplitude in grid C of forecast model; (e) Computed current speed in grid C of forecast model. The black rectangular in (b) and (c) indicates the computational domain of forecast model grid C in (d) and (e).

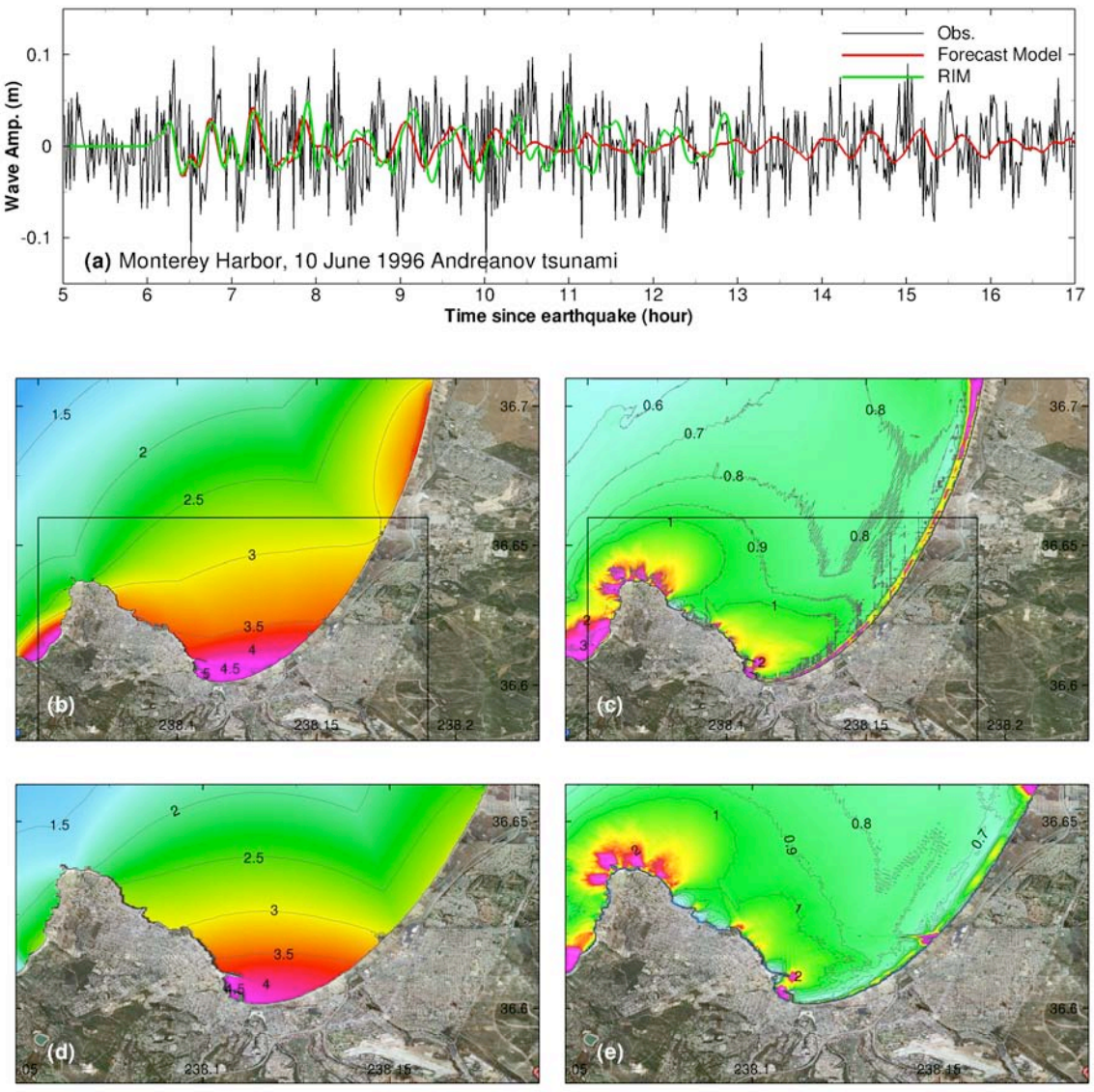

Figure 13. Model validation at Monterey for 4 October 1994 Kuril Islands tsunami. (a) Computed and observed time series at Monterey tide station; (b) Computed maximum wave amplitude in grid C of RIM; (c) Computed maximum current speed in grid C of RIM; (d) Computed maximum wave amplitude in grid C of forecast model; (e) Computed current speed in grid C of forecast model. The black rectangular in (b) and (c) indicates the computational domain of forecast model grid C in (d) and (e).

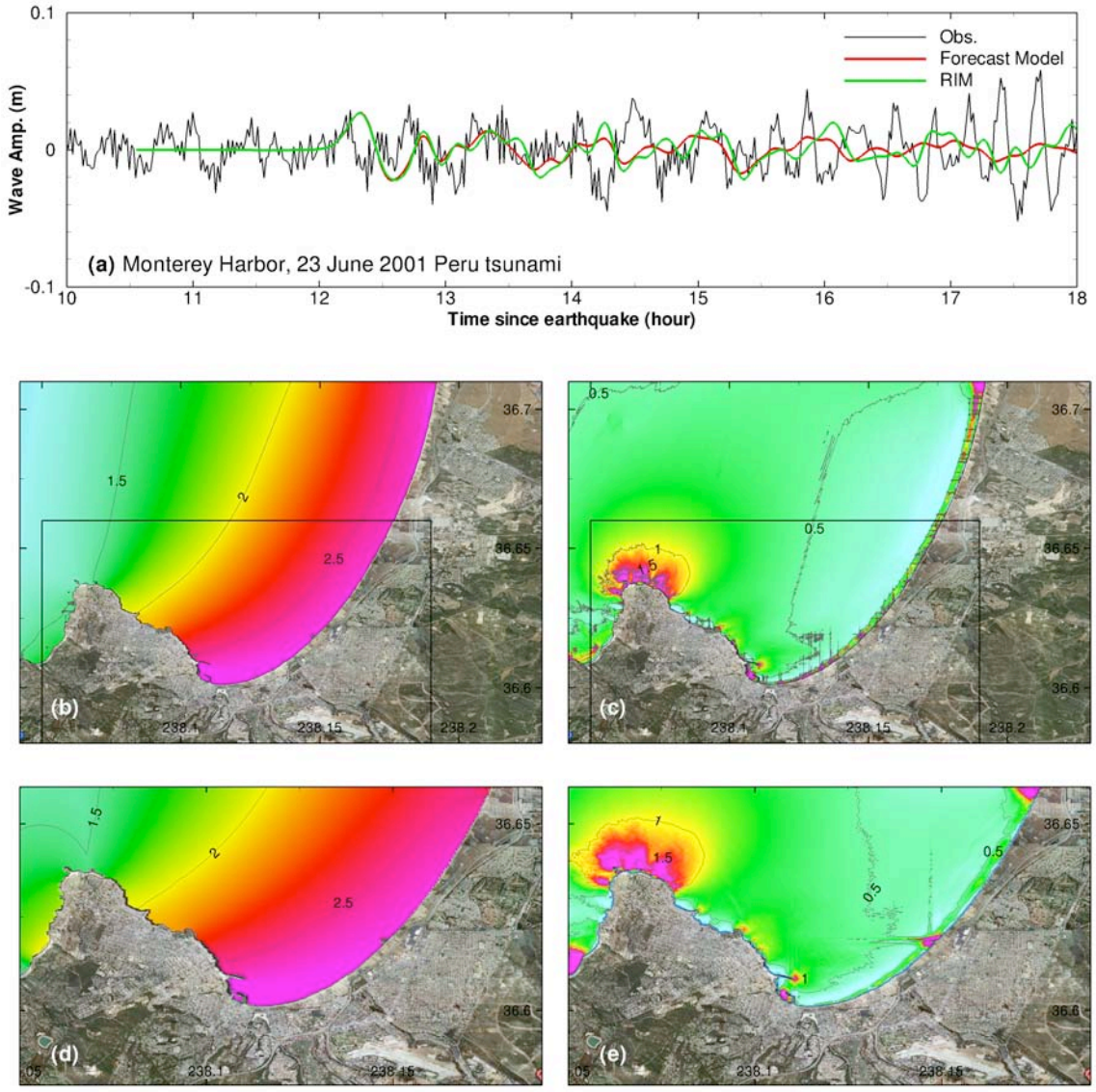

Figure 14 Model validation at Monterey for 23 June 2001 Peru tsunami. (a) Computed and observed time series at Monterey tide station; (b) Computed maximum wave amplitude in grid C of RIM; (c) Computed maximum current speed in grid C of RIM; (d) Computed maximum wave amplitude in grid C of forecast model; (e) Computed current speed in grid C of forecast model. The black rectangular in (b) and (c) indicates the computational domain of forecast model grid C in (d) and (e).

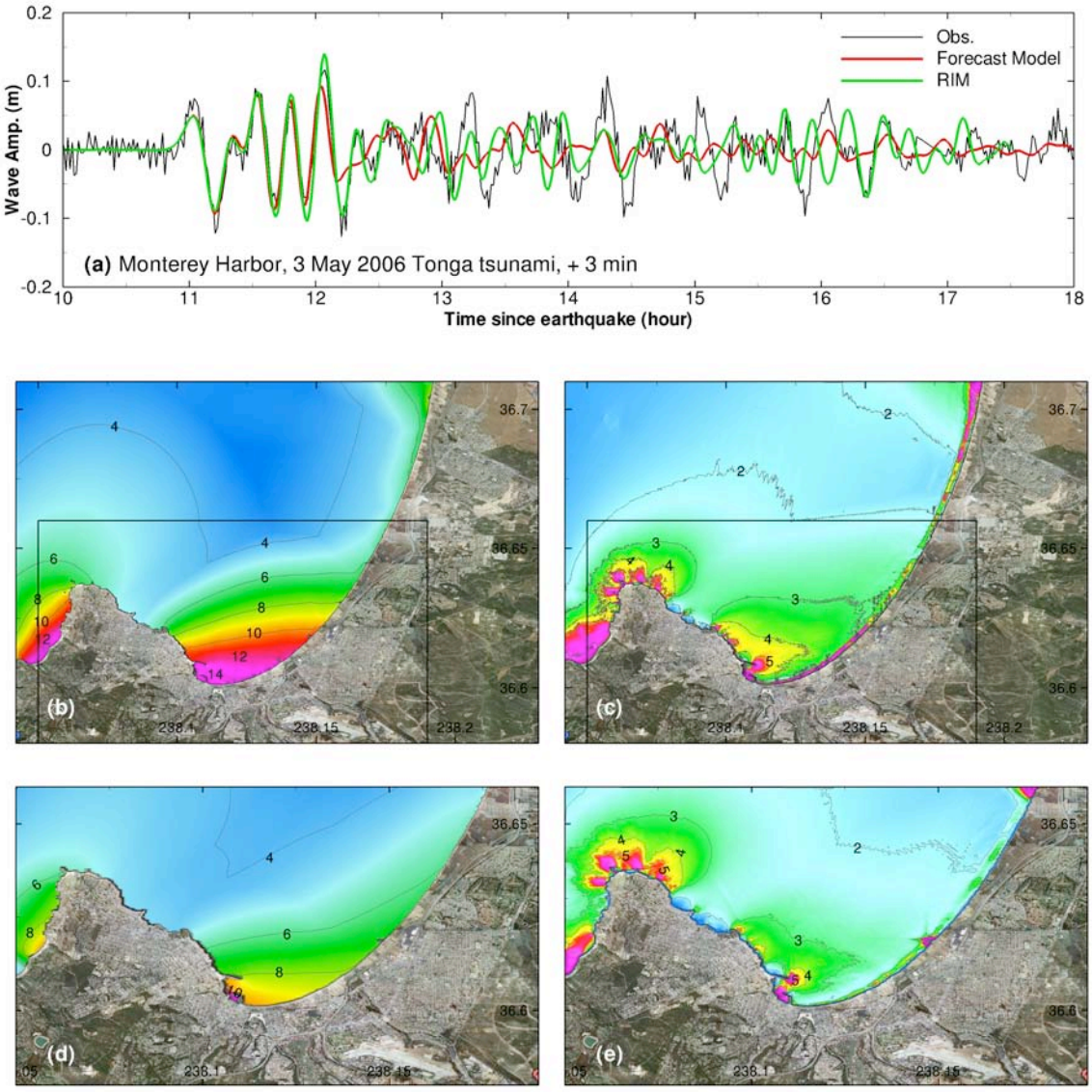

Figure 15 Model validation at Monterey for 3 May 2006 Tonga tsunami. (a) Computed and observed time series at Monterey tide station; (b) Computed maximum wave amplitude in grid C of RIM; (c) Computed maximum current speed in grid C of RIM; (d) Computed maximum wave amplitude in grid C of forecast model; (e) Computed current speed in grid C of forecast model. The black rectangular in (b) and (c) indicates the computational domain of forecast model grid C in (d) and (e).

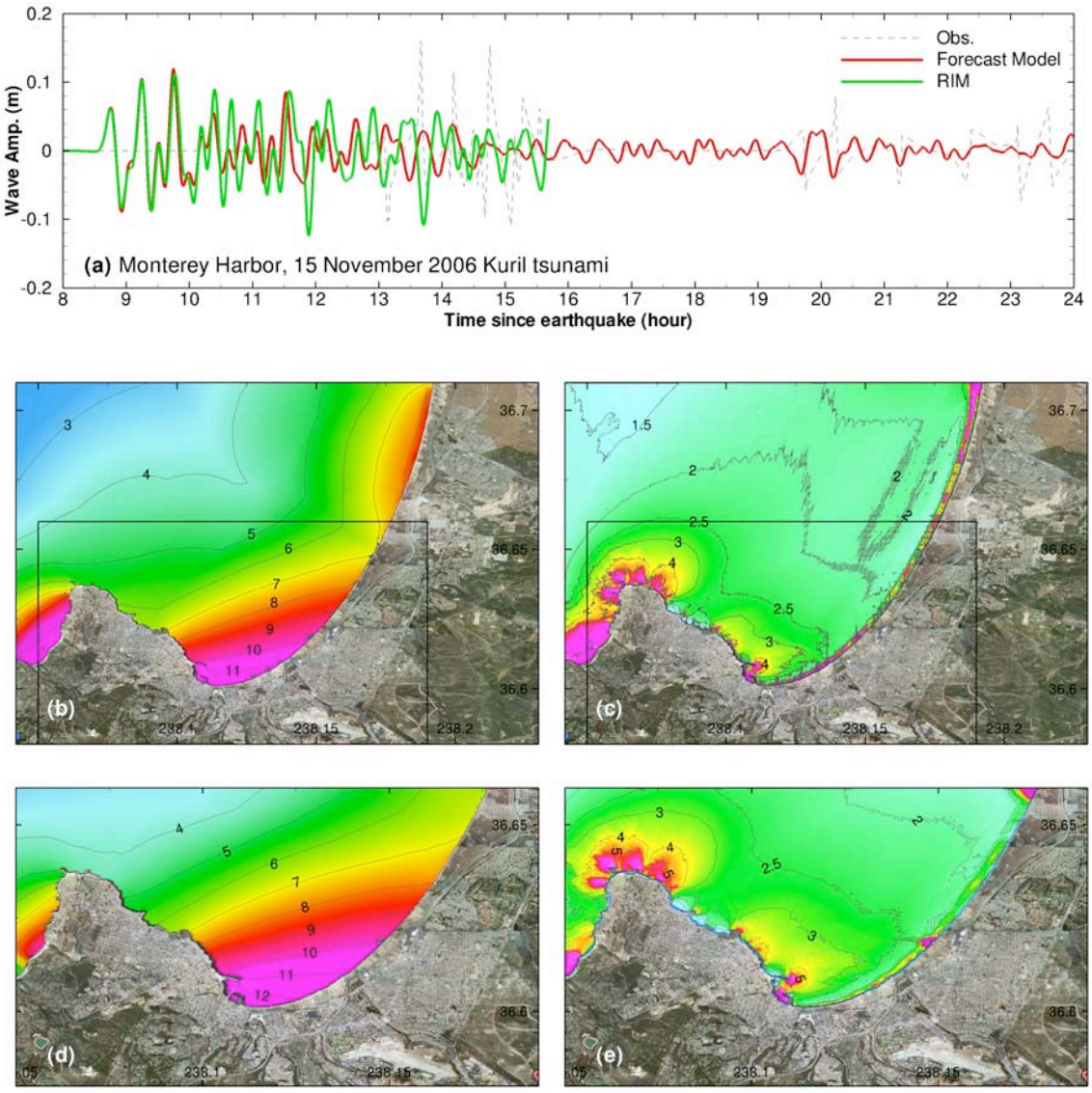

Figure 16 Model validation at Monterey for 11 November 2006 Kuril Islands tsunami. (a) Computed and observed time series at Monterey tide station; (b) Computed maximum wave amplitude in grid C of RIM; (c) Computed maximum current speed in grid C of RIM; (d) Computed maximum wave amplitude in grid C of forecast model; (e) Computed current speed in grid C of forecast model. The black rectangular in (b) and (c) indicates the computational domain of forecast model grid C in (d) and (e).

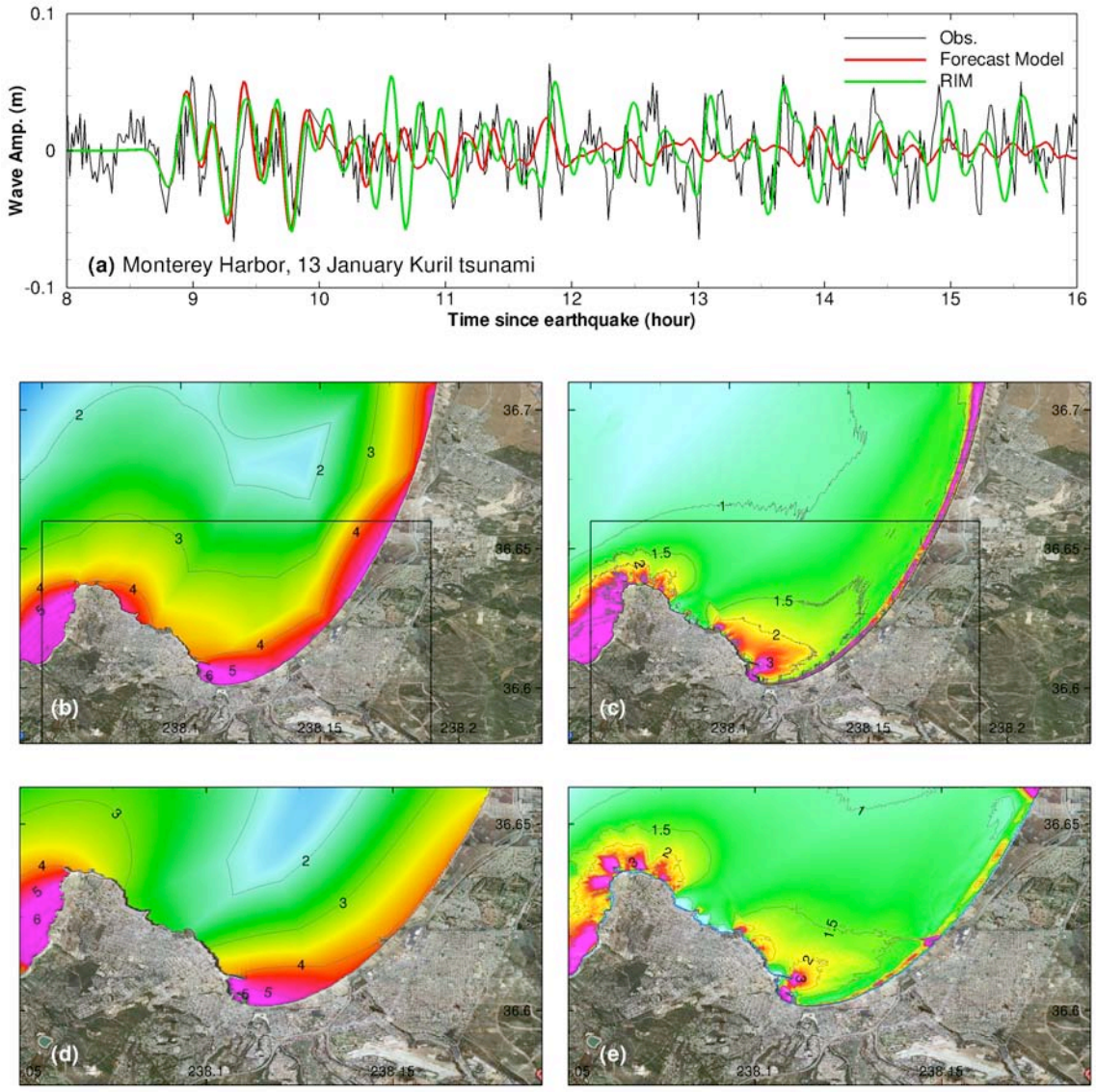

Figure 17. Model validation at Monterey for 13 January 2007 Kuril Islands tsunami. (a) Computed and observed time series at Monterey tide station; (b) Computed maximum wave amplitude in grid C of RIM; (c) Computed maximum current speed in grid C of RIM; (d) Computed maximum wave amplitude in grid C of forecast model; (e) Computed current speed in grid C of forecast model. The black rectangular in (b) and (c) indicates the computational domain of forecast model grid C in (d) and (e).

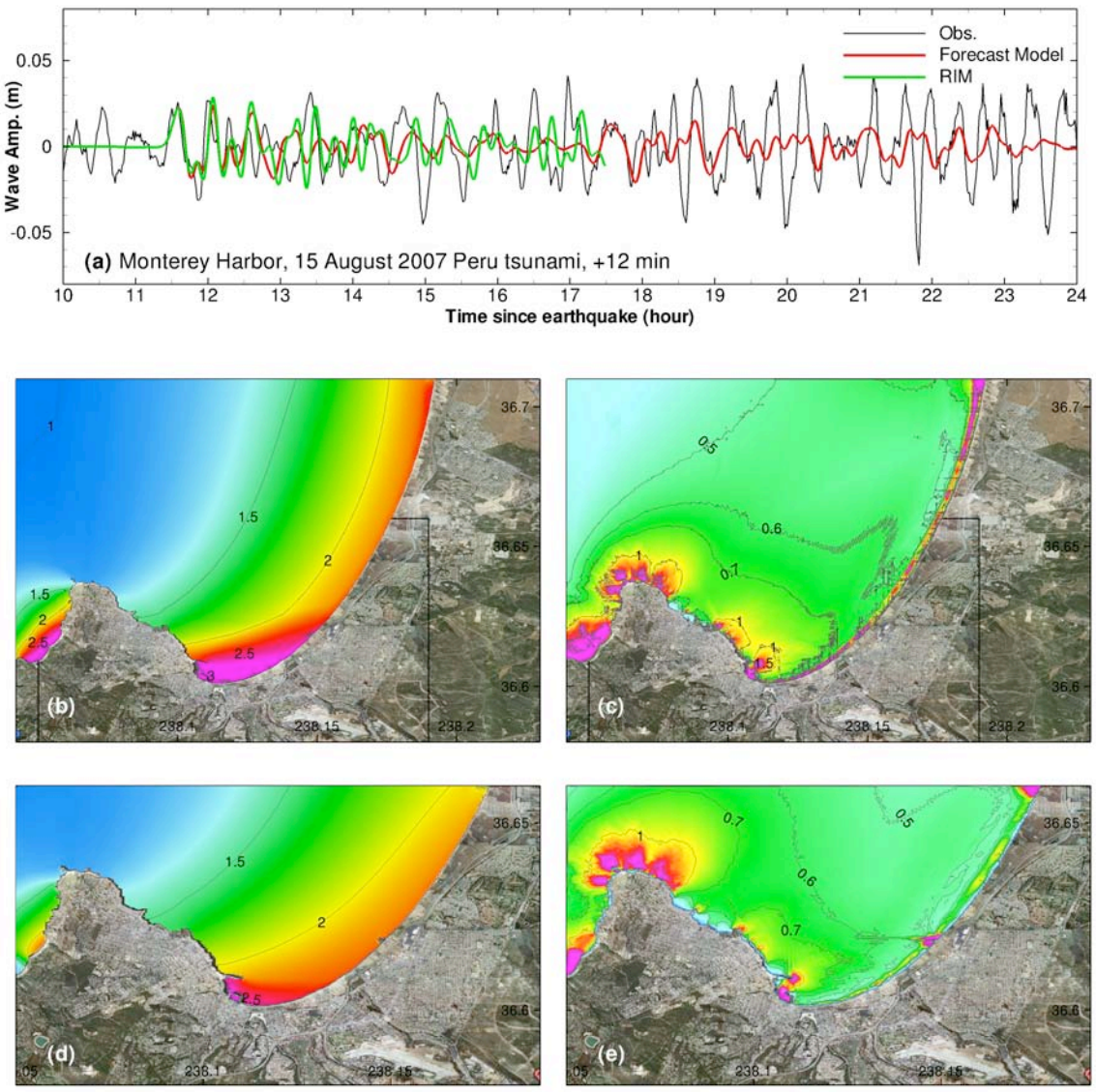

Figure 18. Model validation at Monterey for 15 August 2007 Peru tsunami. (a) Computed (+12 min) and observed time series at Monterey tide station; (b) Computed maximum wave amplitude in grid C of RIM; (c) Computed maximum current speed in grid C of RIM; (d) Computed maximum wave amplitude in grid C of forecast model; (e) Computed current speed in grid C of forecast model. The black rectangular in (b) and (c) indicates the computational domain of forecast model grid C in (d) and (e).

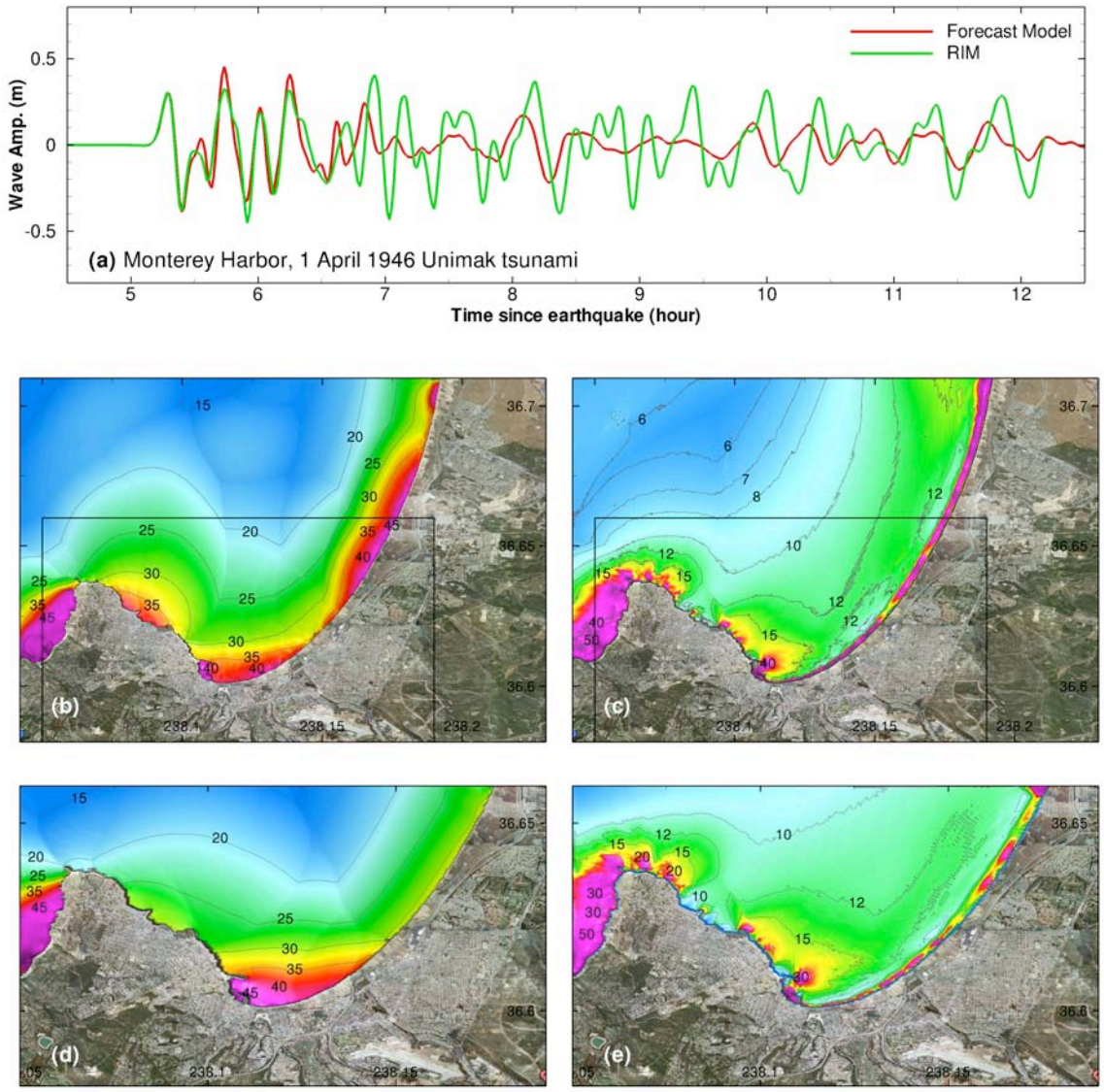

Figure 19. Model results at Monterey for 1 April 1946 Alaska tsunami. (a) Computed time series at Monterey tide station; (b) Computed maximum wave amplitude in grid C of RIM; (c) Computed maximum current speed in grid C of RIM; (d) Computed maximum wave amplitude in grid C of forecast model; (e) Computed current speed in grid C of forecast model. The black rectangular in (b) and (c) indicates the computational domain of forecast model grid C in (d) and (e).

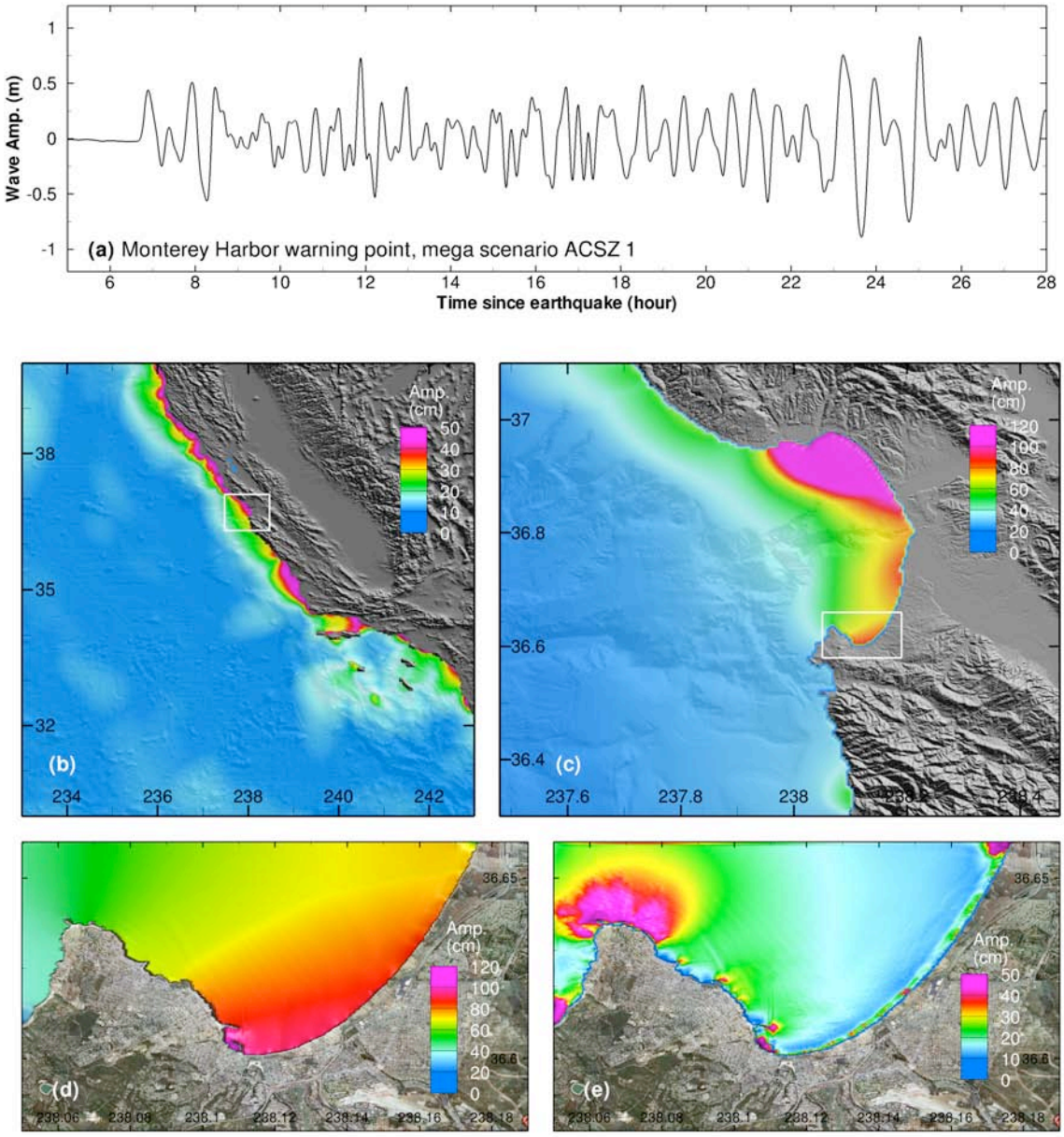

Figure 20. Model stability testing results at Monterey for artificial mega tsunami scenario ACSZ 1. (a) Computed time series at Monterey warning point; (b) Computed maximum wave amplitude in grid A of the forecast model; (c) Computed maximum current speed in grid B of the forecast model; (d) Computed maximum wave amplitude in grid C of the forecast model; (e) Computed current speed in grid C of the forecast model.

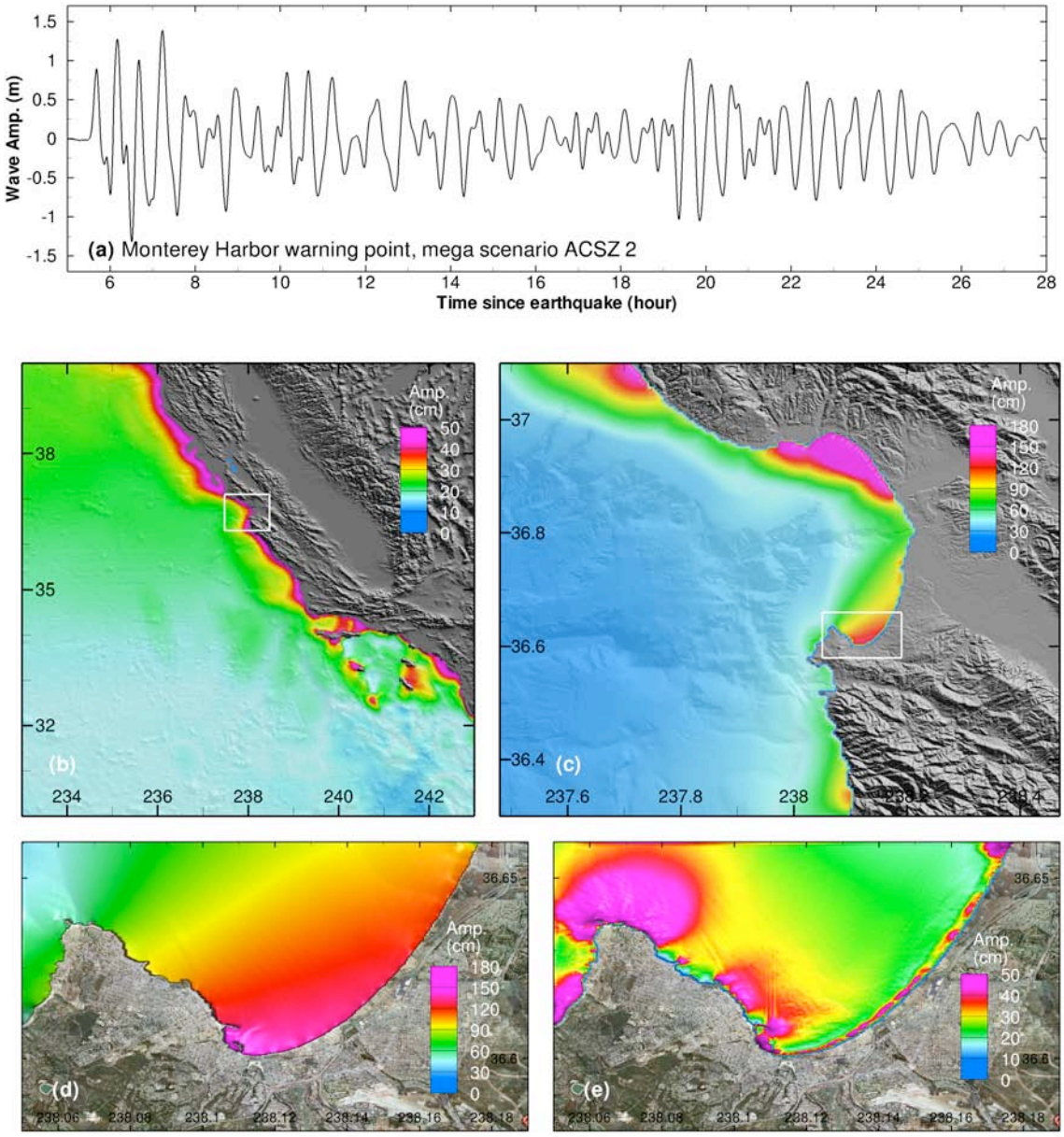

Figure 21. Model stability testing results at Monterey for artificial mega tsunami scenario ACSZ 2. (a) Computed time series at Monterey warning point; (b) Computed maximum wave amplitude in grid A of the forecast model; (c) Computed maximum current speed in grid B of the forecast model; (d) Computed maximum wave amplitude in grid C of the forecast model; (e) Computed current speed in grid C of the forecast model.

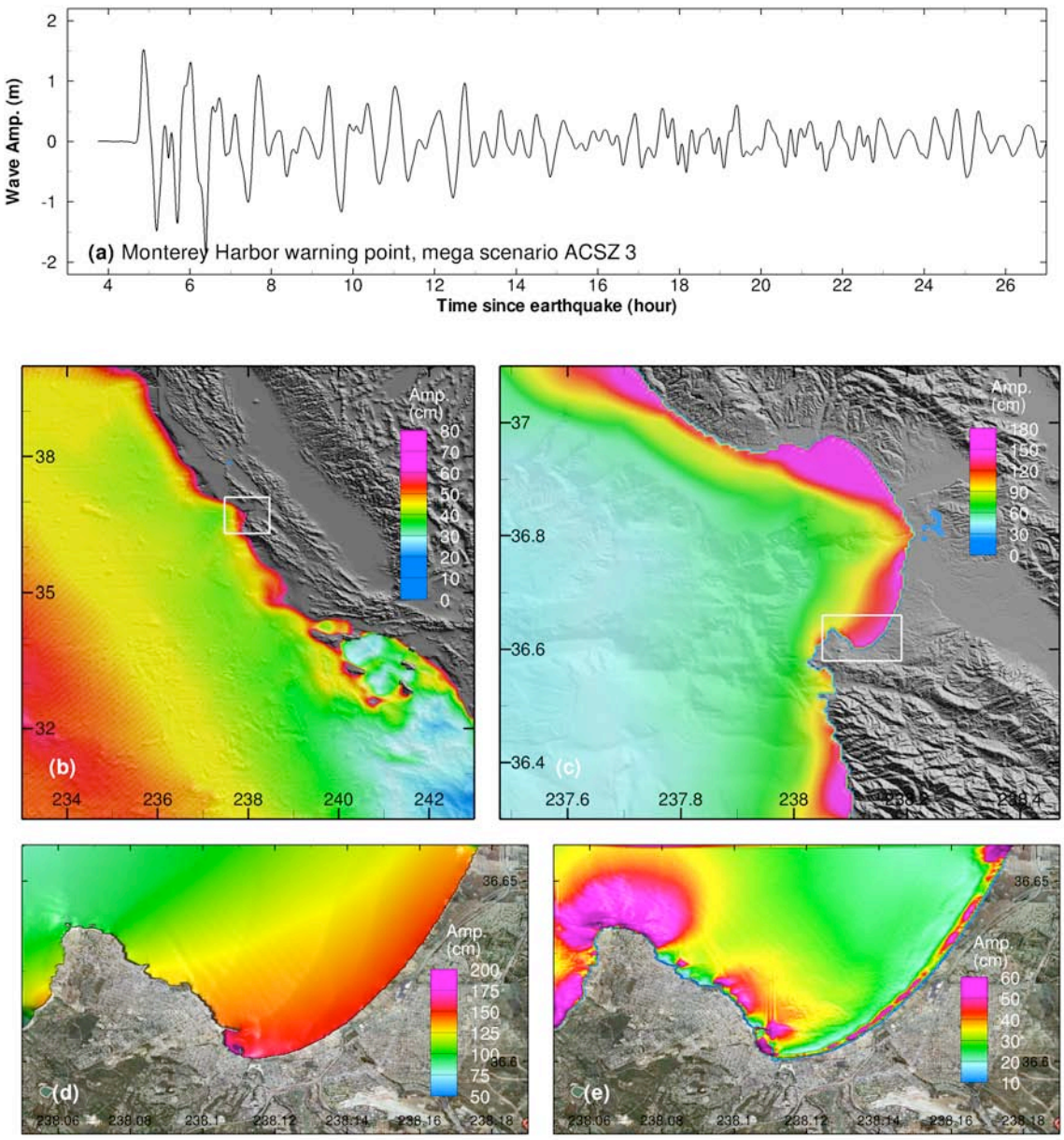

Figure 22. Model stability testing results at Monterey for artificial mega tsunami scenario ACSZ 3. (a) Computed time series at Monterey warning point; (b) Computed maximum wave amplitude in grid A of the forecast model; (c) Computed maximum current speed in grid B of the forecast model; (d) Computed maximum wave amplitude in grid C of the forecast model; (e) Computed current speed in grid C of the forecast model.

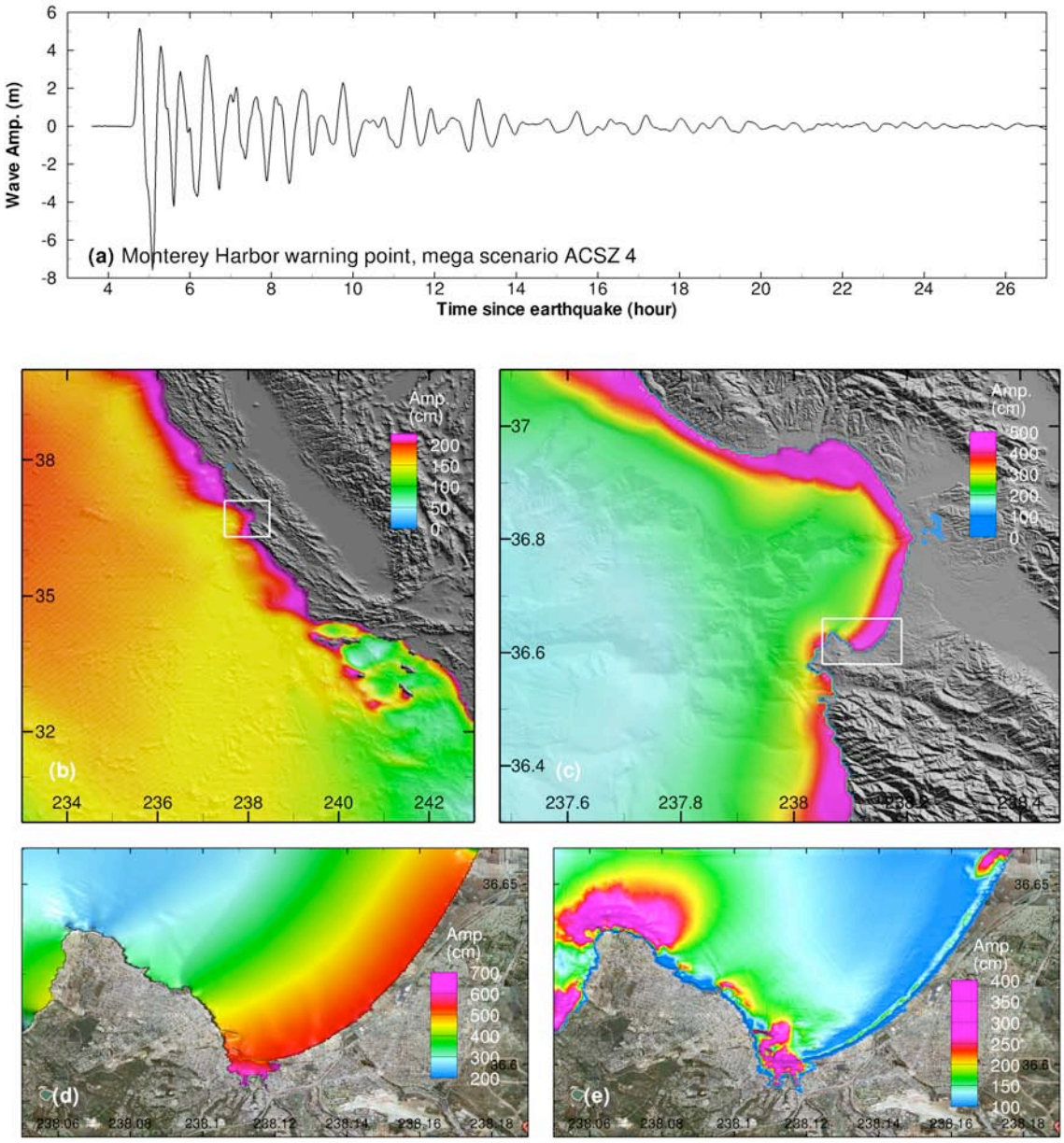

Figure 23. Model stability testing results at Monterey for artificial mega tsunami scenario ACSZ 4. (a) Computed time series at Monterey warning point; (b) Computed maximum wave amplitude in grid A of the forecast model; (c) Computed maximum current speed in grid B of the forecast model; (d) Computed maximum wave amplitude in grid C of the forecast model; (e) Computed current speed in grid C of the forecast model.

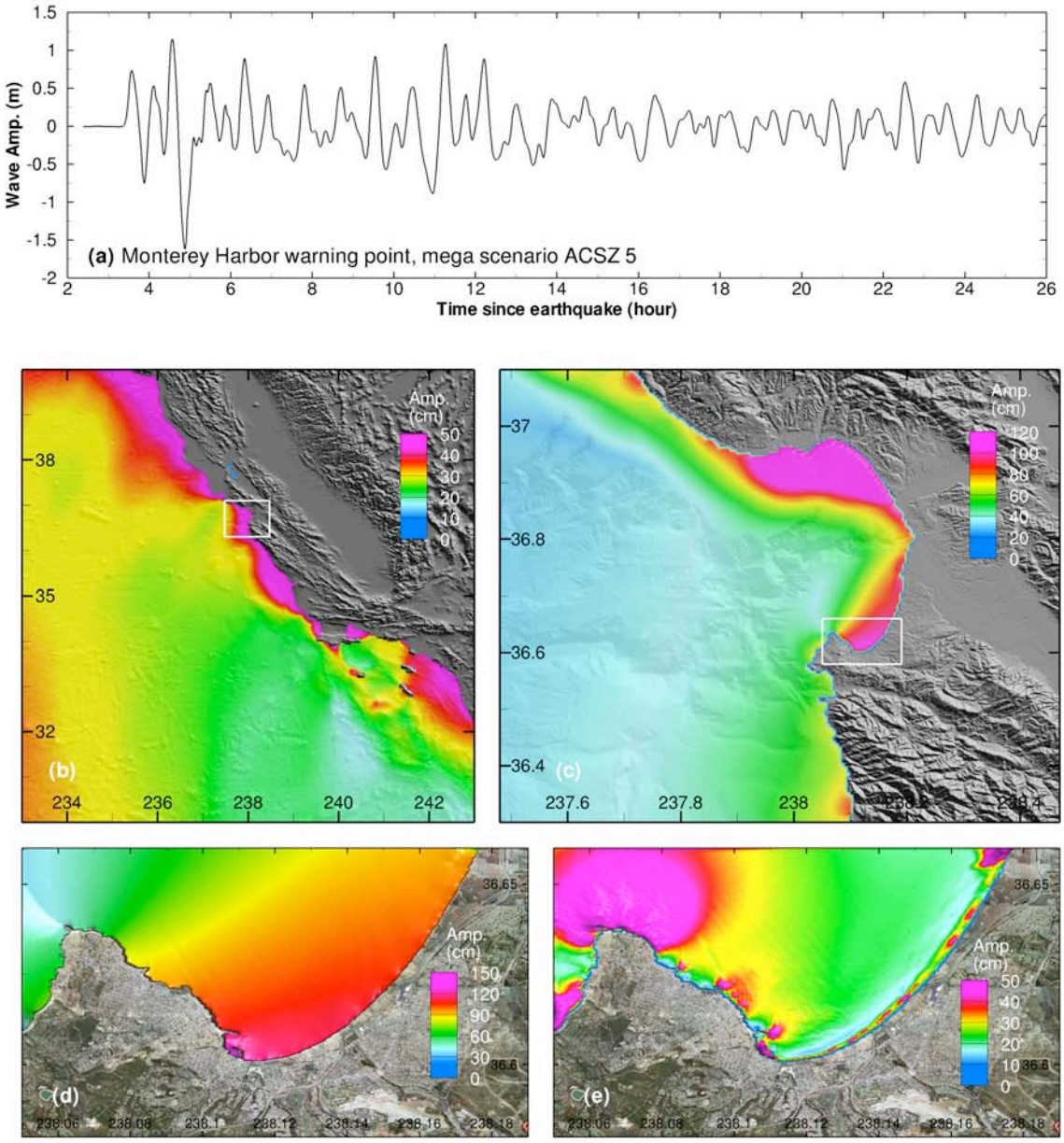

Figure 24. Model stability testing results at Monterey for artificial mega tsunami scenario ACSZ 5. (a) Computed time series at Monterey warning point; (b) Computed maximum wave amplitude in grid A of the forecast model; (c) Computed maximum current speed in grid B of the forecast model; (d) Computed maximum wave amplitude in grid C of the forecast model; (e) Computed current speed in grid C of the forecast model.

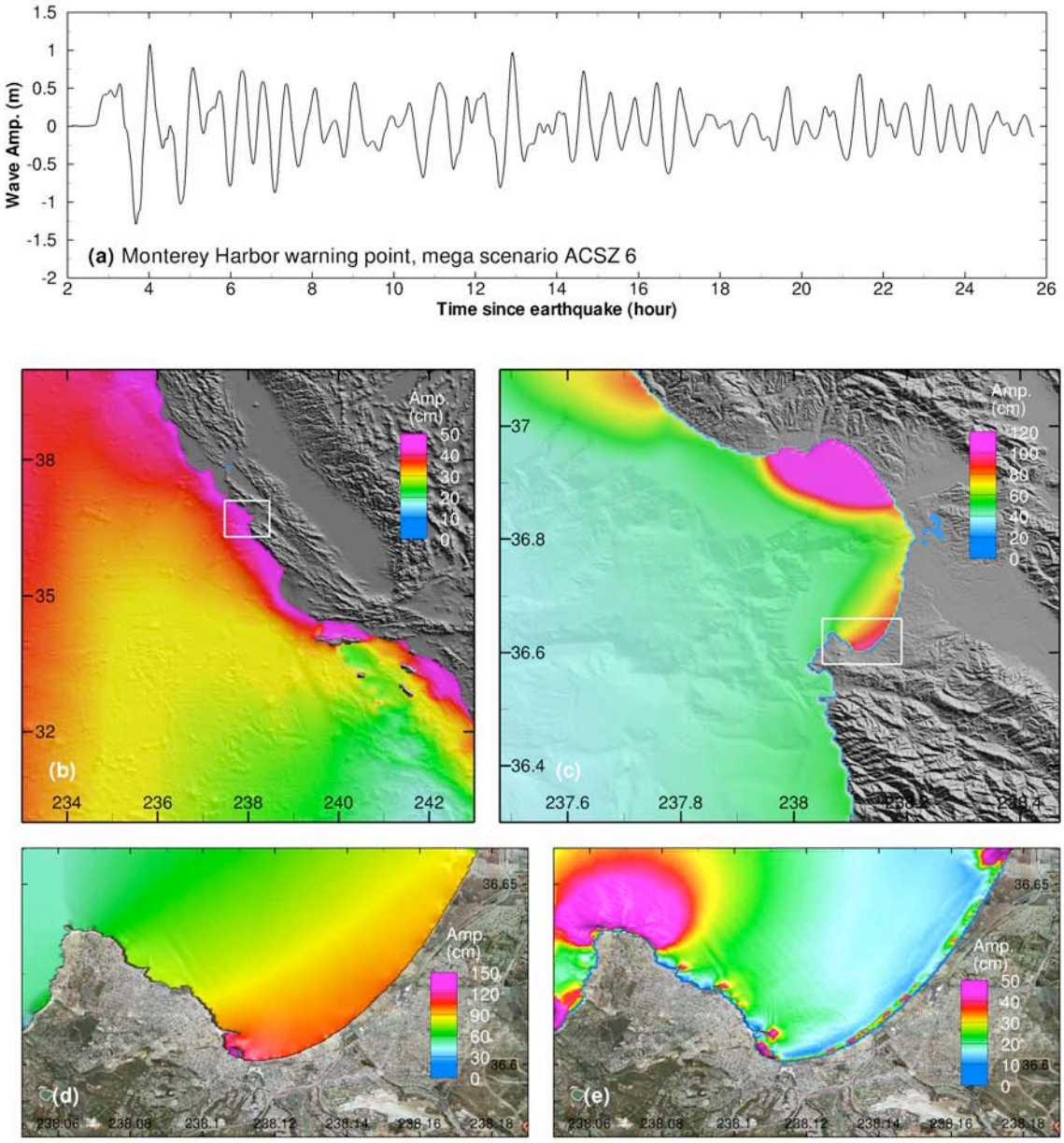

Figure 25. Model stability testing results at Monterey for artificial mega tsunami scenario ACSZ 6. (a) Computed time series at Monterey warning point; (b) Computed maximum wave amplitude in grid A of the forecast model; (c) Computed maximum current speed in grid B of the forecast model; (d) Computed maximum wave amplitude in grid C of the forecast model; (e) Computed current speed in grid C of the forecast model.

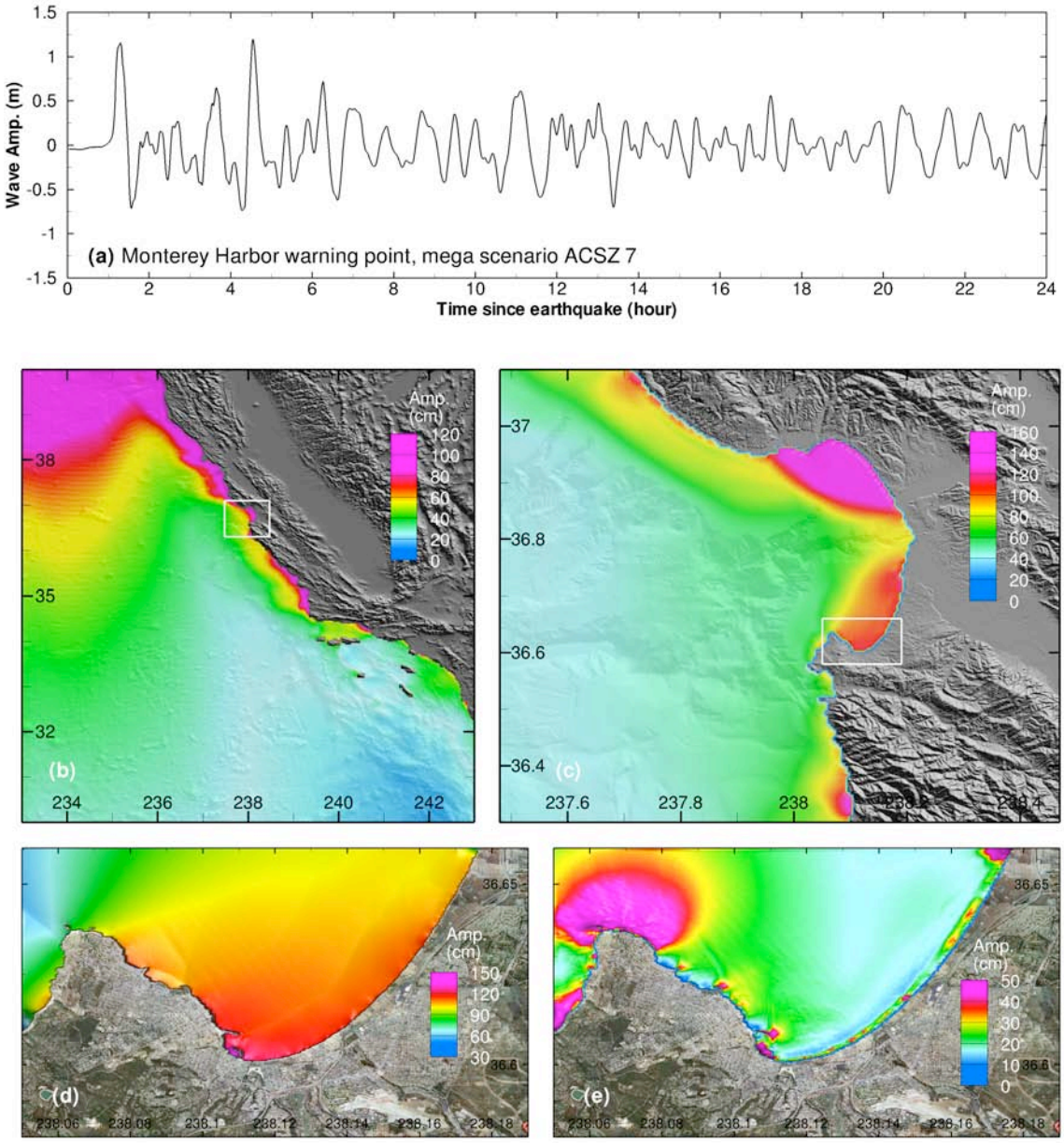

Figure 26. Model stability testing results at Monterey for artificial mega tsunami scenario ACSZ 7. (a) Computed time series at Monterey warning point; (b) Computed maximum wave amplitude in grid A of the forecast model; (c) Computed maximum current speed in grid B of the forecast model; (d) Computed maximum wave amplitude in grid C of the forecast model; (e) Computed current speed in grid C of the forecast model.

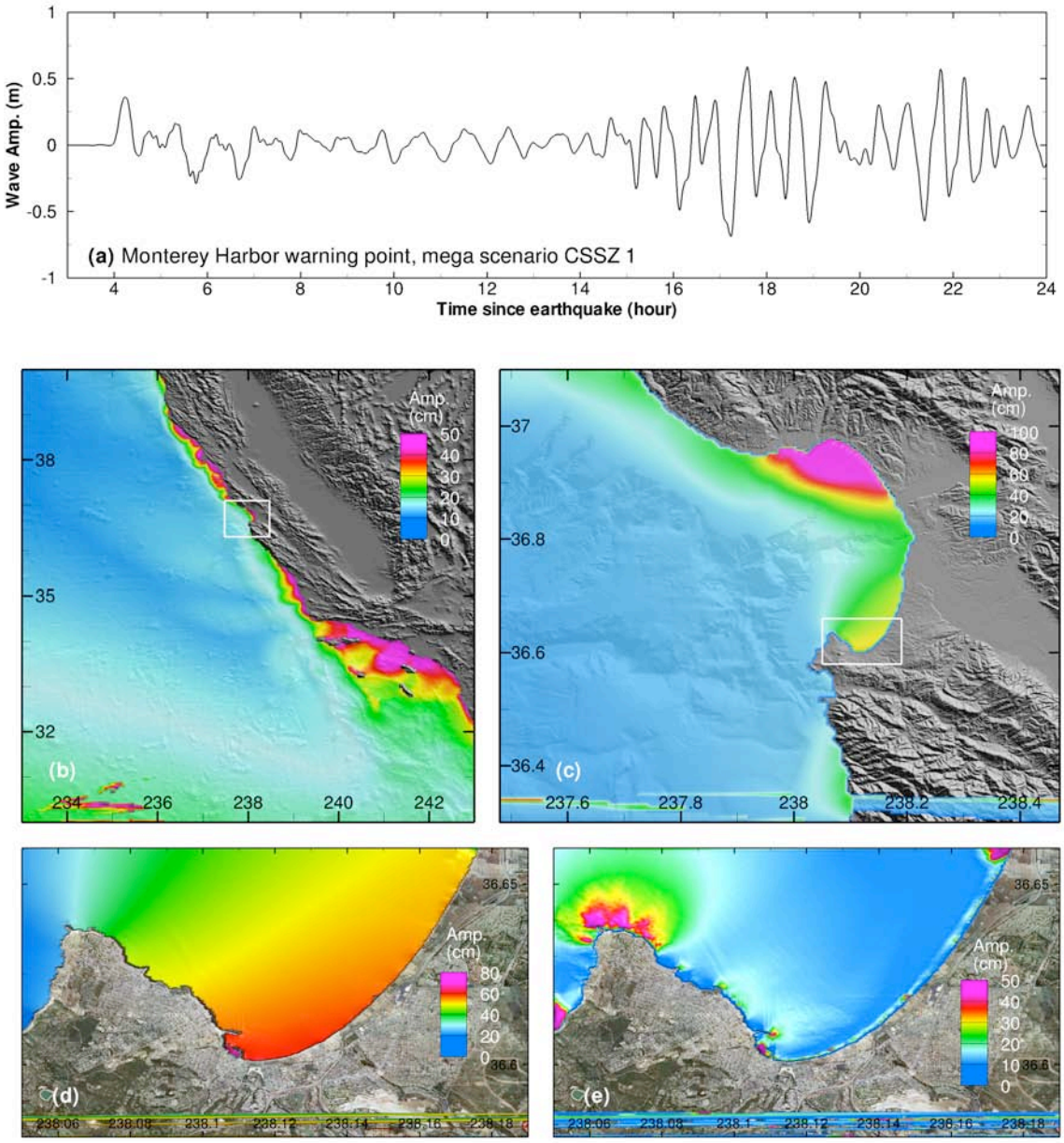

Figure 27. Model stability testing results at Monterey for artificial mega tsunami scenario CSSZ 1. (a) Computed time series at Monterey warning point; (b) Computed maximum wave amplitude in grid A of the forecast model; (c) Computed maximum current speed in grid B of the forecast model; (d) Computed maximum wave amplitude in grid C of the forecast model; (e) Computed current speed in grid C of the forecast model.

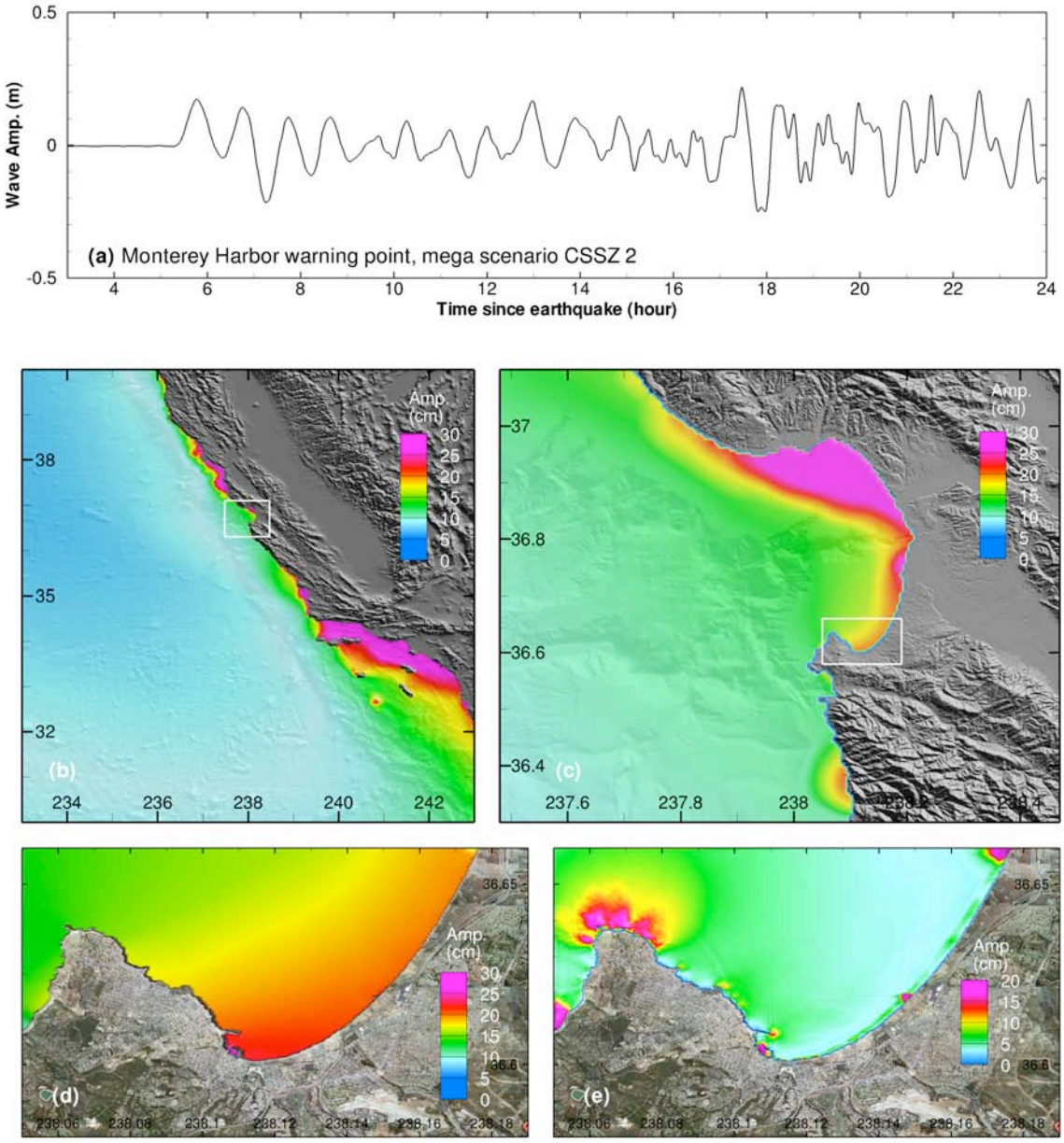

Figure 28. Model stability testing results at Monterey for artificial mega tsunami scenario CSSZ 2. (a) Computed time series at Monterey warning point; (b) Computed maximum wave amplitude in grid A of the forecast model; (c) Computed maximum current speed in grid B of the forecast model; (d) Computed maximum wave amplitude in grid C of the forecast model; (e) Computed current speed in grid C of the forecast model.

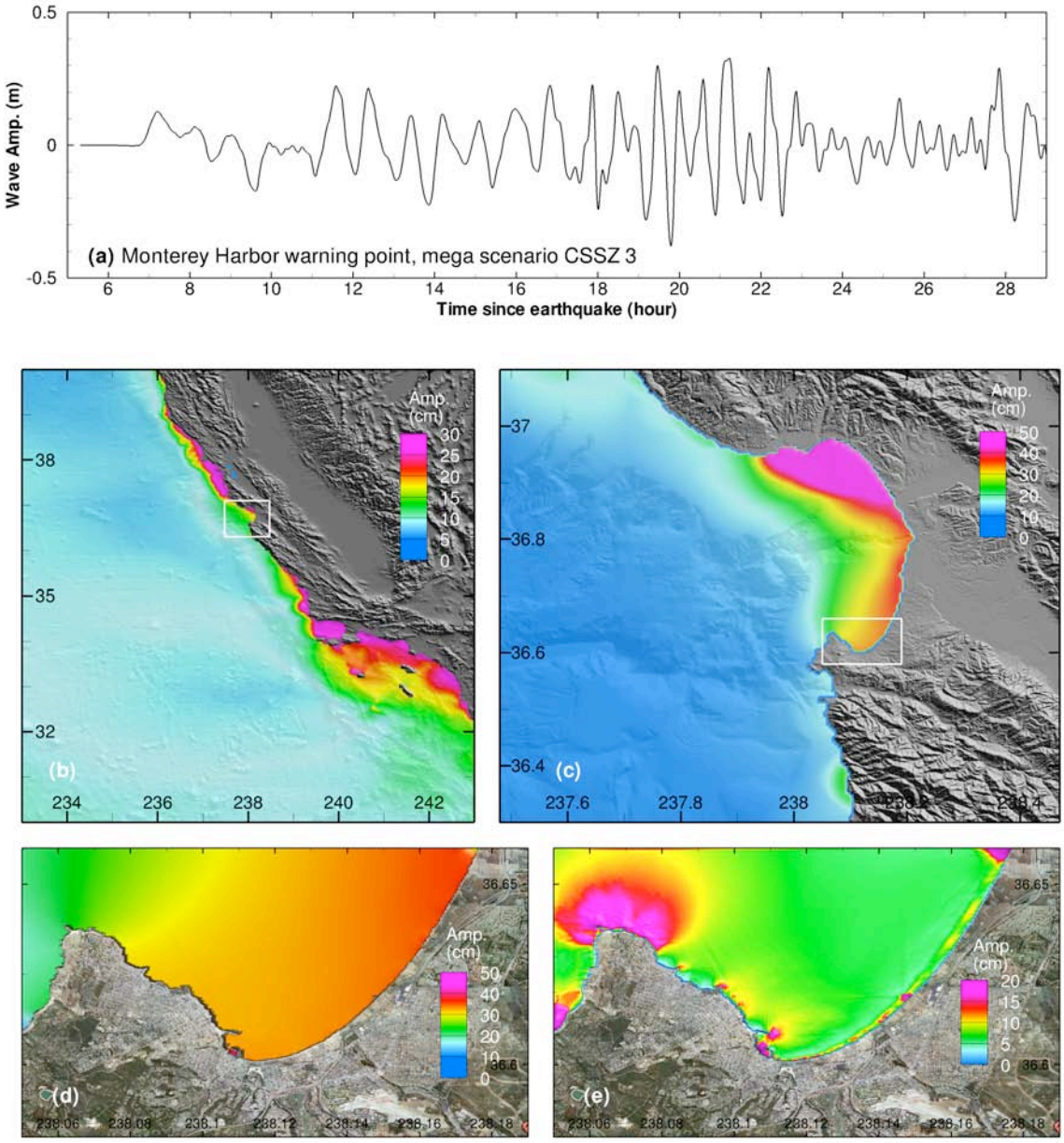

Figure 29. Model stability testing results at Monterey for artificial mega tsunami scenario CSSZ 3. (a) Computed time series at Monterey warning point; (b) Computed maximum wave amplitude in grid A of the forecast model; (c) Computed maximum current speed in grid B of the forecast model; (d) Computed maximum wave amplitude in grid C of the forecast model; (e) Computed current speed in grid C of the forecast model.

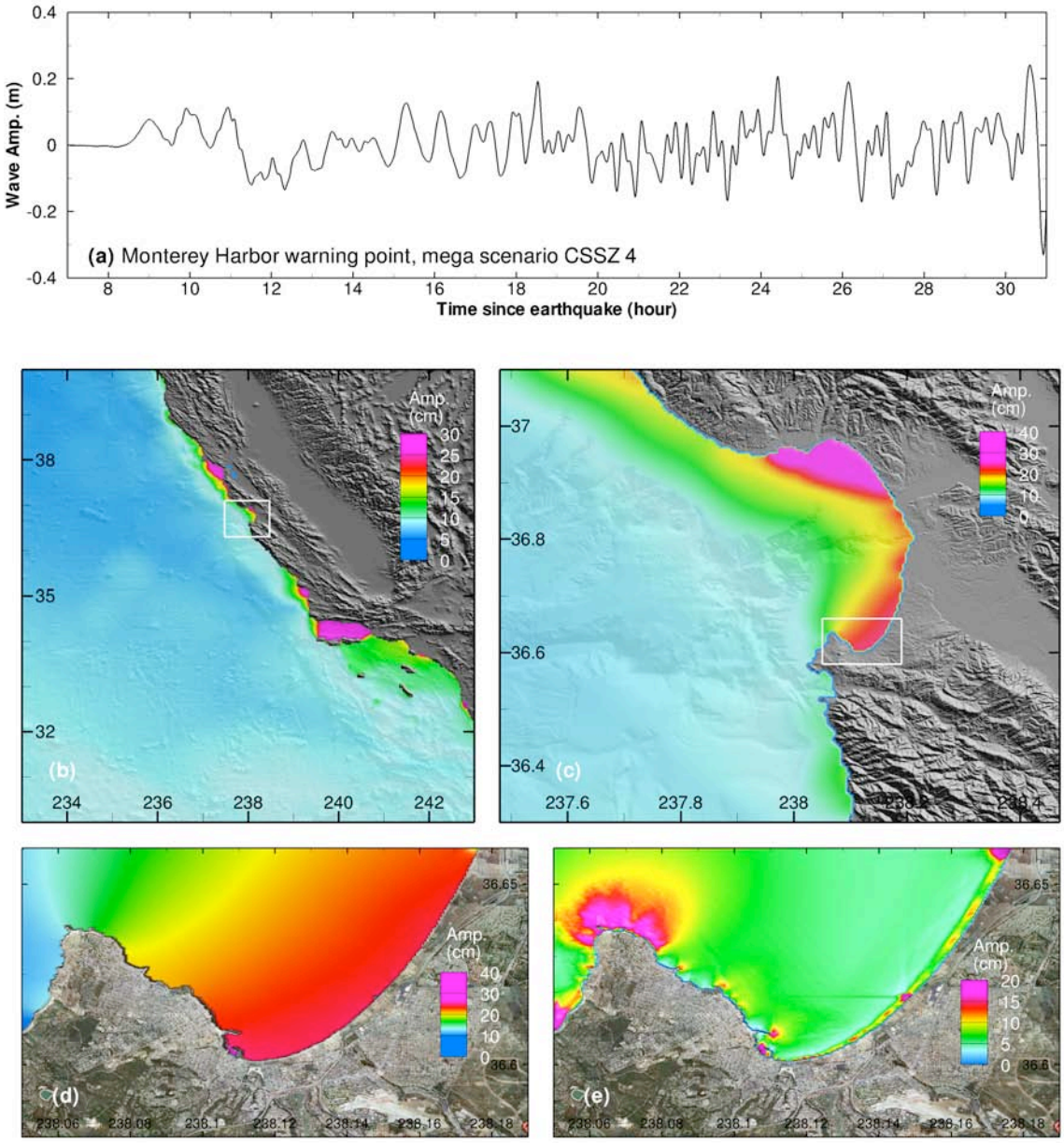

Figure 30. Model stability testing results at Monterey for artificial mega tsunami scenario CSSZ 4. (a) Computed time series at Monterey warning point; (b) Computed maximum wave amplitude in grid A of the forecast model; (c) Computed maximum current speed in grid B of the forecast model; (d) Computed maximum wave amplitude in grid C of the forecast model; (e) Computed current speed in grid C of the forecast model.

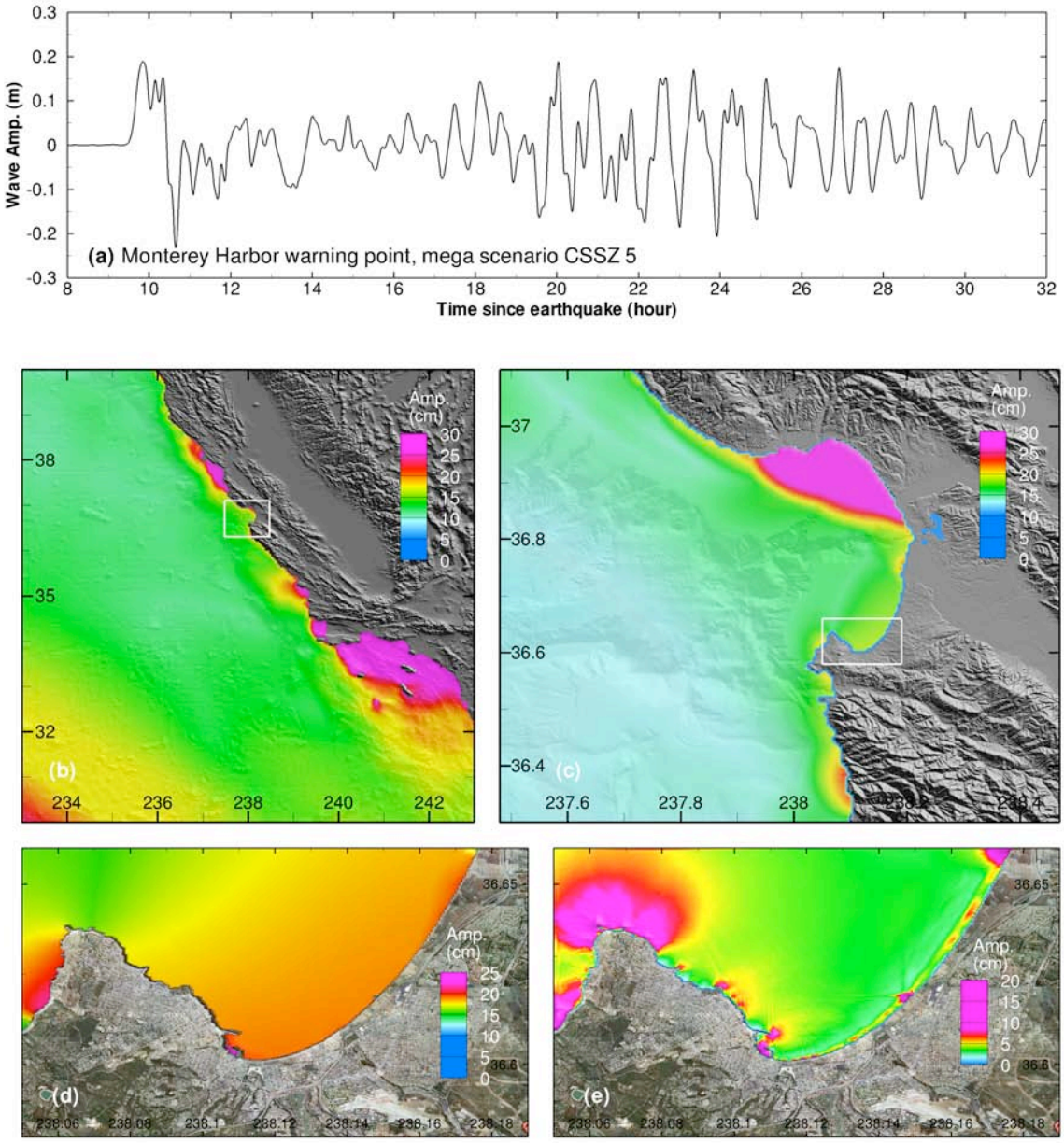

Figure 31. Model stability testing results at Monterey for artificial mega tsunami scenario CSSZ 5. (a) Computed time series at Monterey warning point; (b) Computed maximum wave amplitude in grid A of the forecast model; (c) Computed maximum current speed in grid B of the forecast model; (d) Computed maximum wave amplitude in grid C of the forecast model; (e) Computed current speed in grid C of the forecast model.

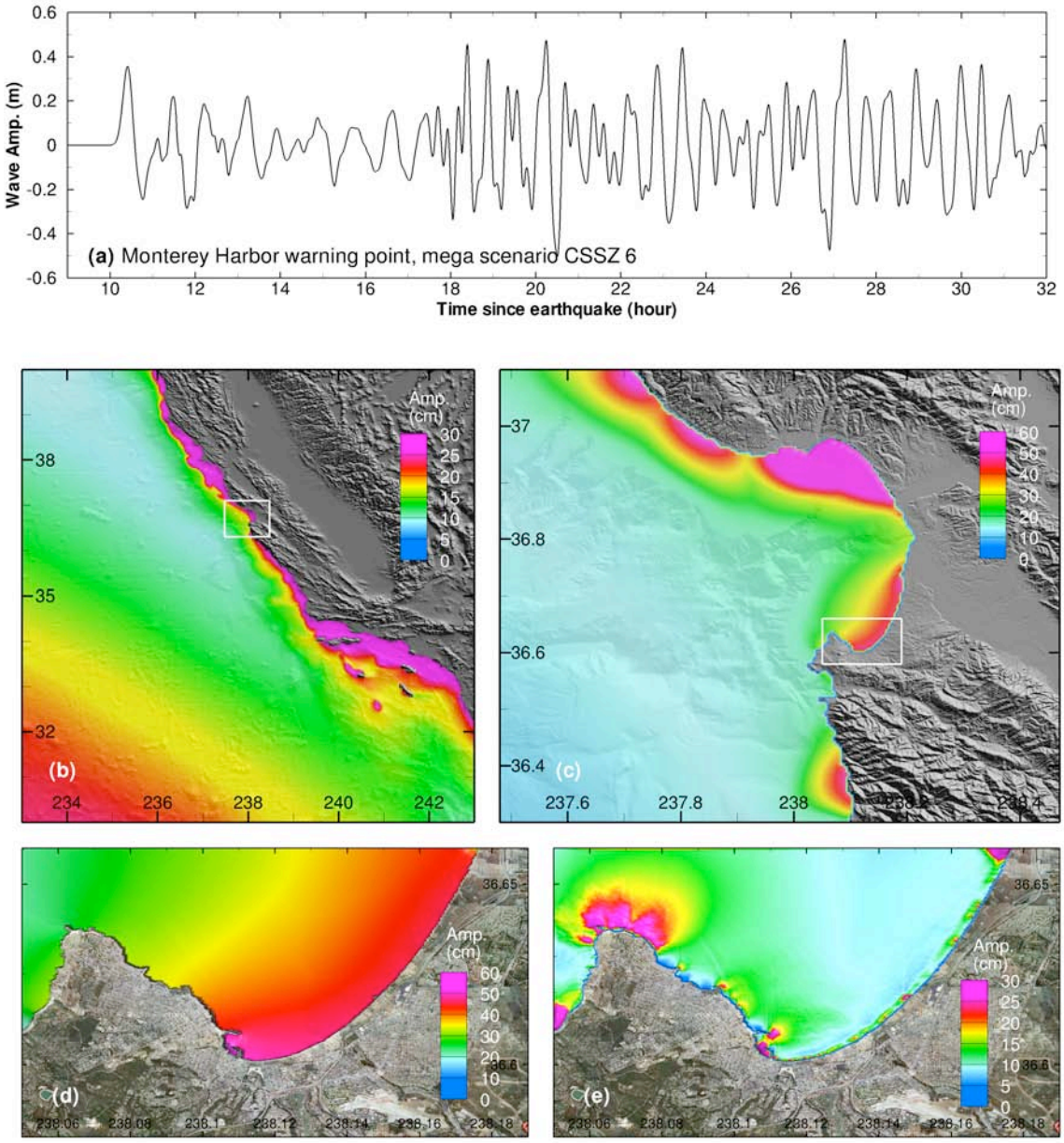

Figure 32. Model stability testing results at Monterey for artificial mega tsunami scenario CSSZ 6. (a) Computed time series at Monterey warning point; (b) Computed maximum wave amplitude in grid A of the forecast model; (c) Computed maximum current speed in grid B of the forecast model; (d) Computed maximum wave amplitude in grid C of the forecast model; (e) Computed current speed in grid C of the forecast model.

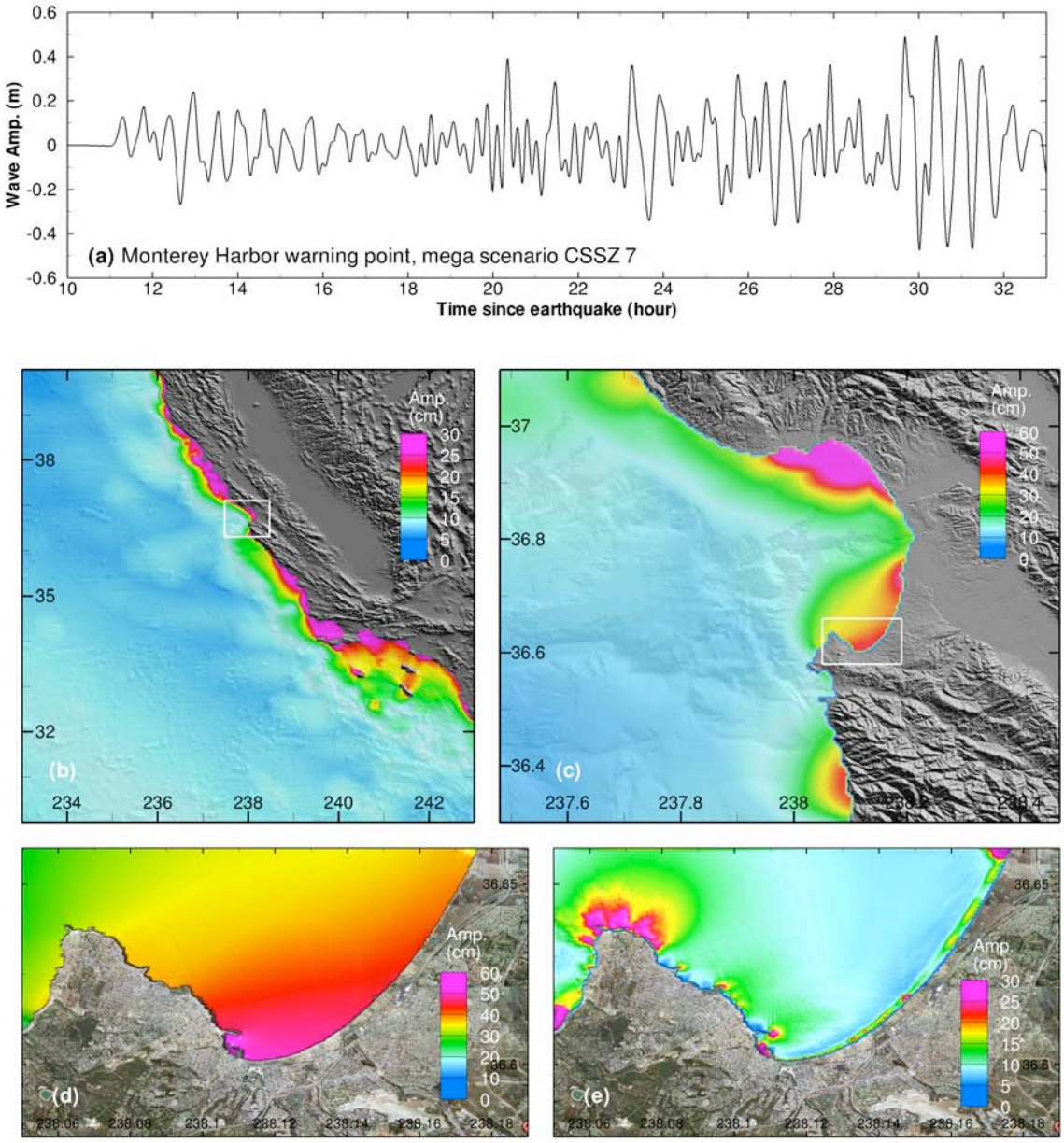

Figure 33. Model stability testing results at Monterey for artificial mega tsunami scenario CSSZ 7. (a) Computed time series at Monterey warning point; (b) Computed maximum wave amplitude in grid A of the forecast model; (c) Computed maximum current speed in grid B of the forecast model; (d) Computed maximum wave amplitude in grid C of the forecast model; (e) Computed current speed in grid C of the forecast model.

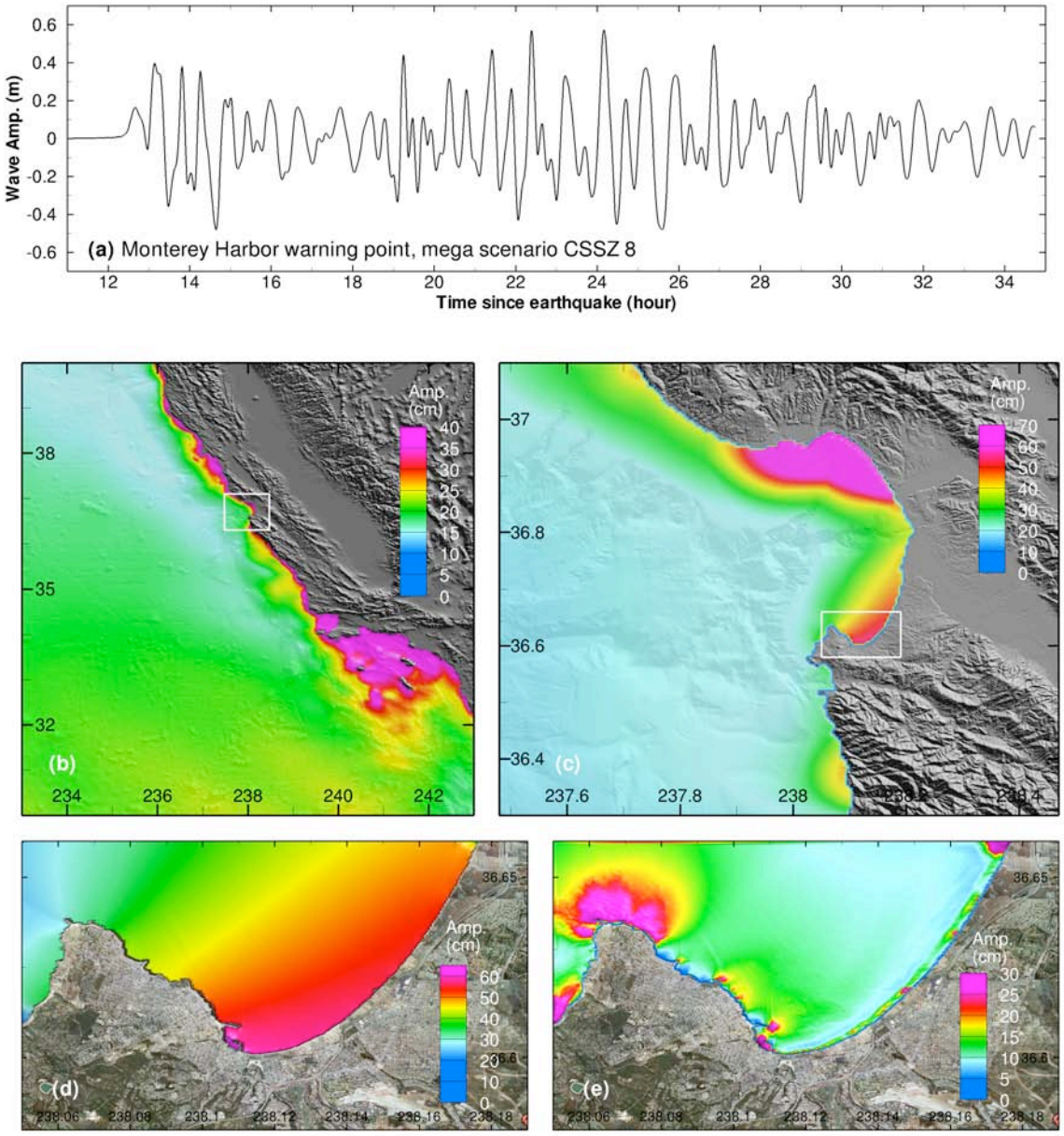

Figure 34. Model stability testing results at Monterey for artificial mega tsunami scenario CSSZ 8. (a) Computed time series at Monterey warning point; (b) Computed maximum wave amplitude in grid A of the forecast model; (c) Computed maximum current speed in grid B of the forecast model; (d) Computed maximum wave amplitude in grid C of the forecast model; (e) Computed current speed in grid C of the forecast model.

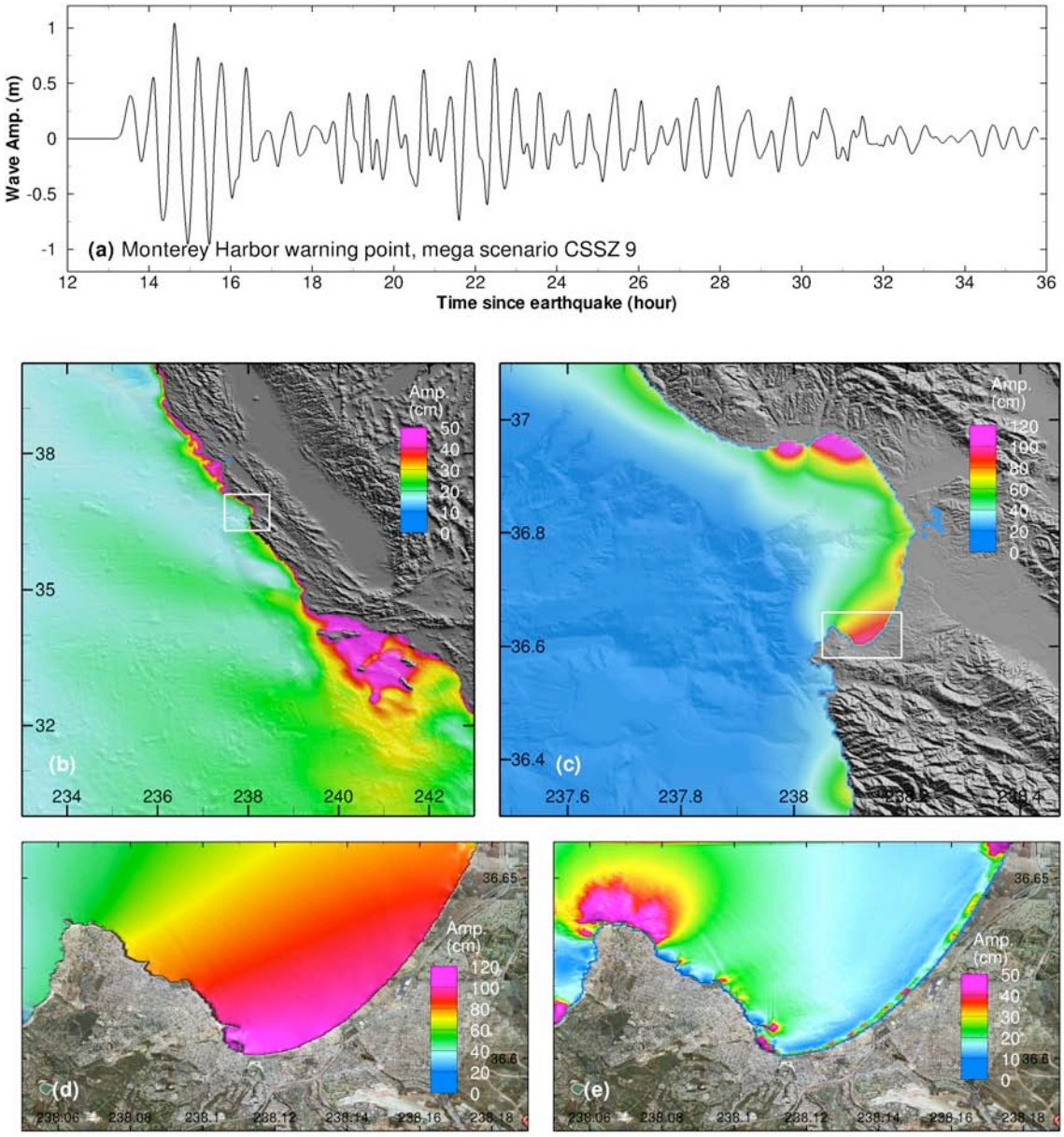

Figure 35. Model stability testing results at Monterey for artificial mega tsunami scenario CSSZ 9. (a) Computed time series at Monterey warning point; (b) Computed maximum wave amplitude in grid A of the forecast model; (c) Computed maximum current speed in grid B of the forecast model; (d) Computed maximum wave amplitude in grid C of the forecast model; (e) Computed current speed in grid C of the forecast model.

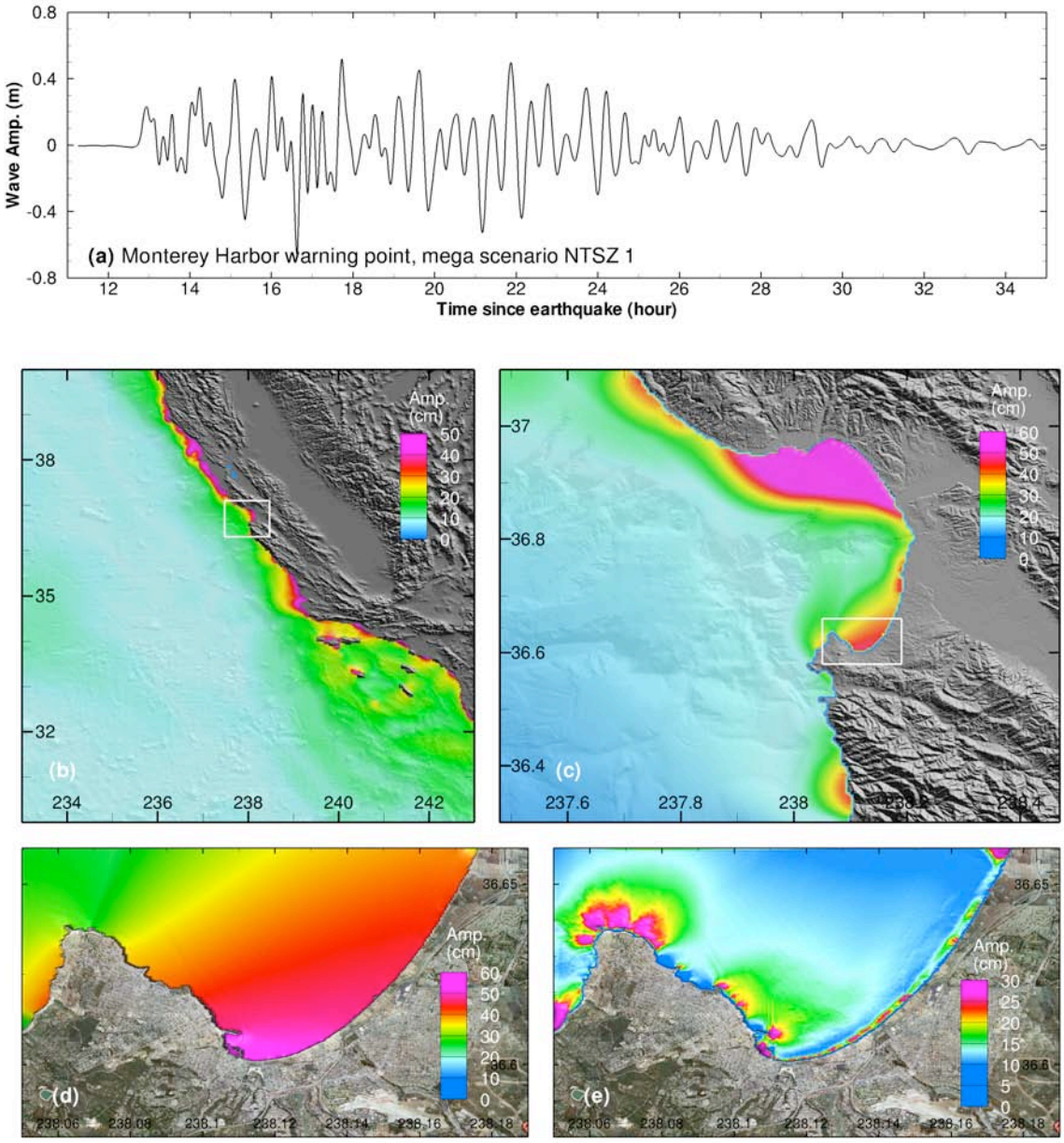

Figure 36. Model stability testing results at Monterey for artificial mega tsunami scenario NTSZ 1. (a) Computed time series at Monterey warning point; (b) Computed maximum wave amplitude in grid A of the forecast model; (c) Computed maximum current speed in grid B of the forecast model; (d) Computed maximum wave amplitude in grid C of the forecast model; (e) Computed current speed in grid C of the forecast model.

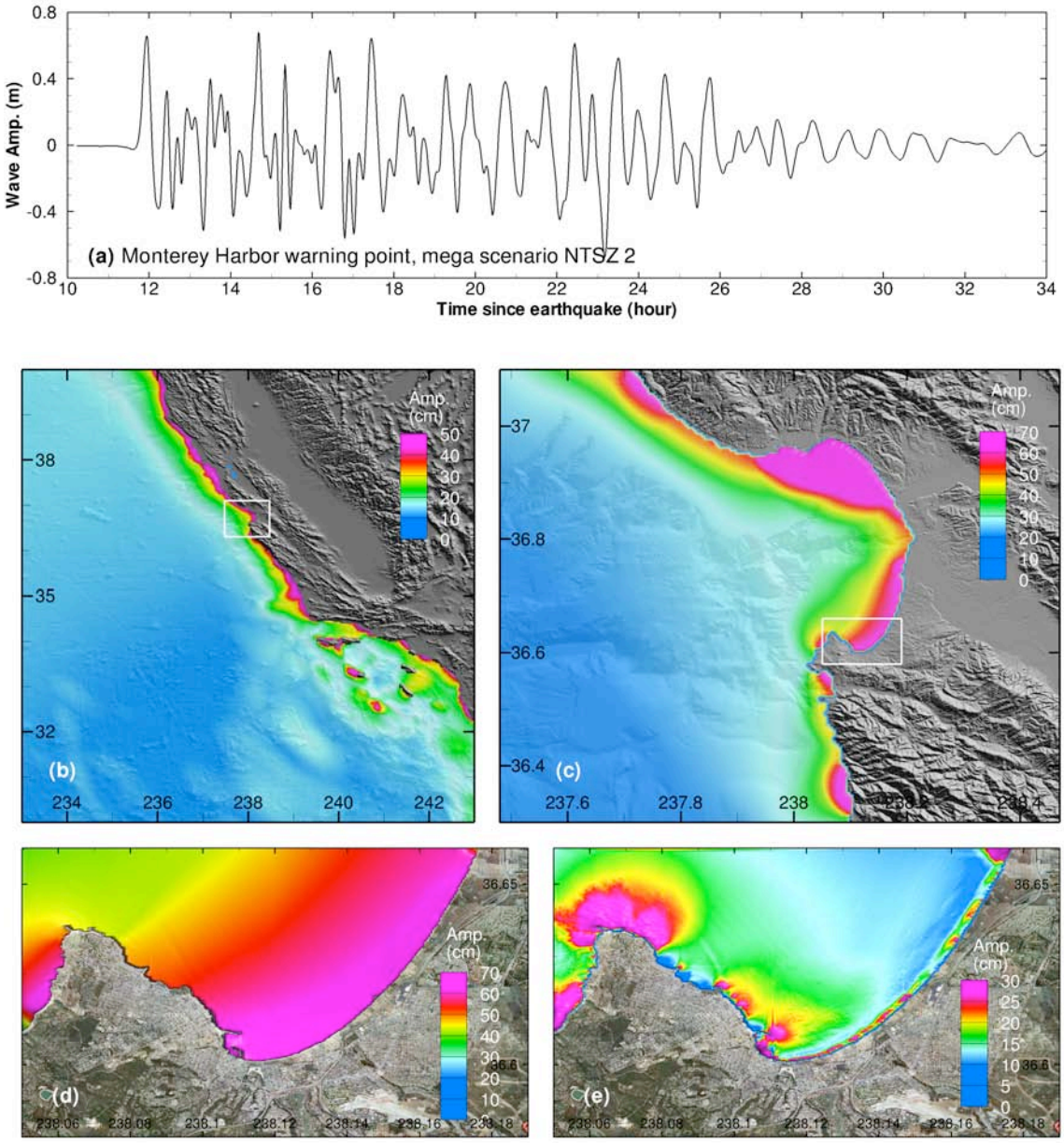

Figure 37. Model stability testing results at Monterey for artificial mega tsunami scenario NTSZ 2. (a) Computed time series at Monterey warning point; (b) Computed maximum wave amplitude in grid A of the forecast model; (c) Computed maximum current speed in grid B of the forecast model; (d) Computed maximum wave amplitude in grid C of the forecast model; (e) Computed current speed in grid C of the forecast model.

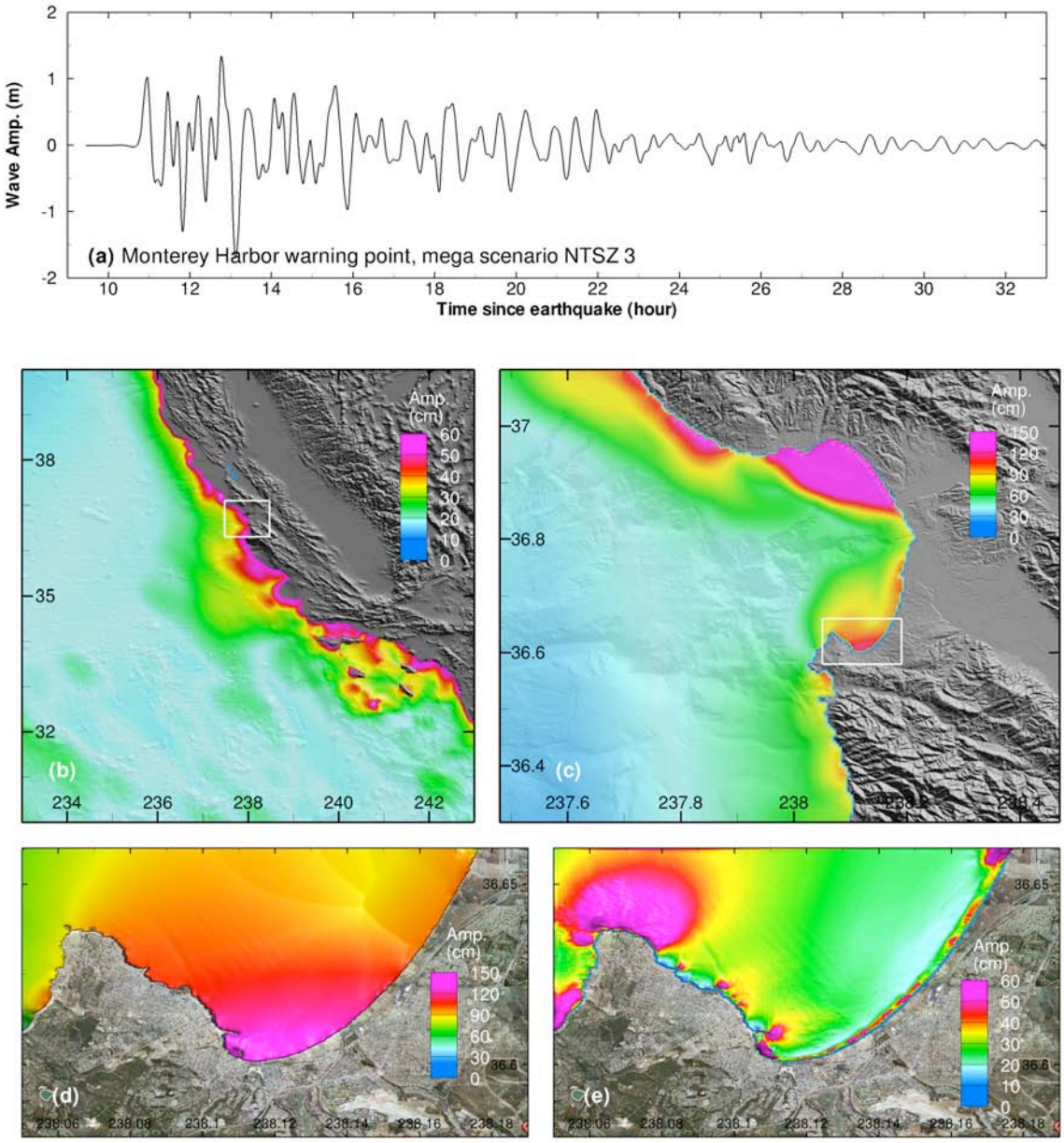

Figure 38. Model stability testing results at Monterey for artificial mega tsunami scenario NTSZ 3. (a) Computed time series at Monterey warning point; (b) Computed maximum wave amplitude in grid A of the forecast model; (c) Computed maximum current speed in grid B of the forecast model; (d) Computed maximum wave amplitude in grid C of the forecast model; (e) Computed current speed in grid C of the forecast model.

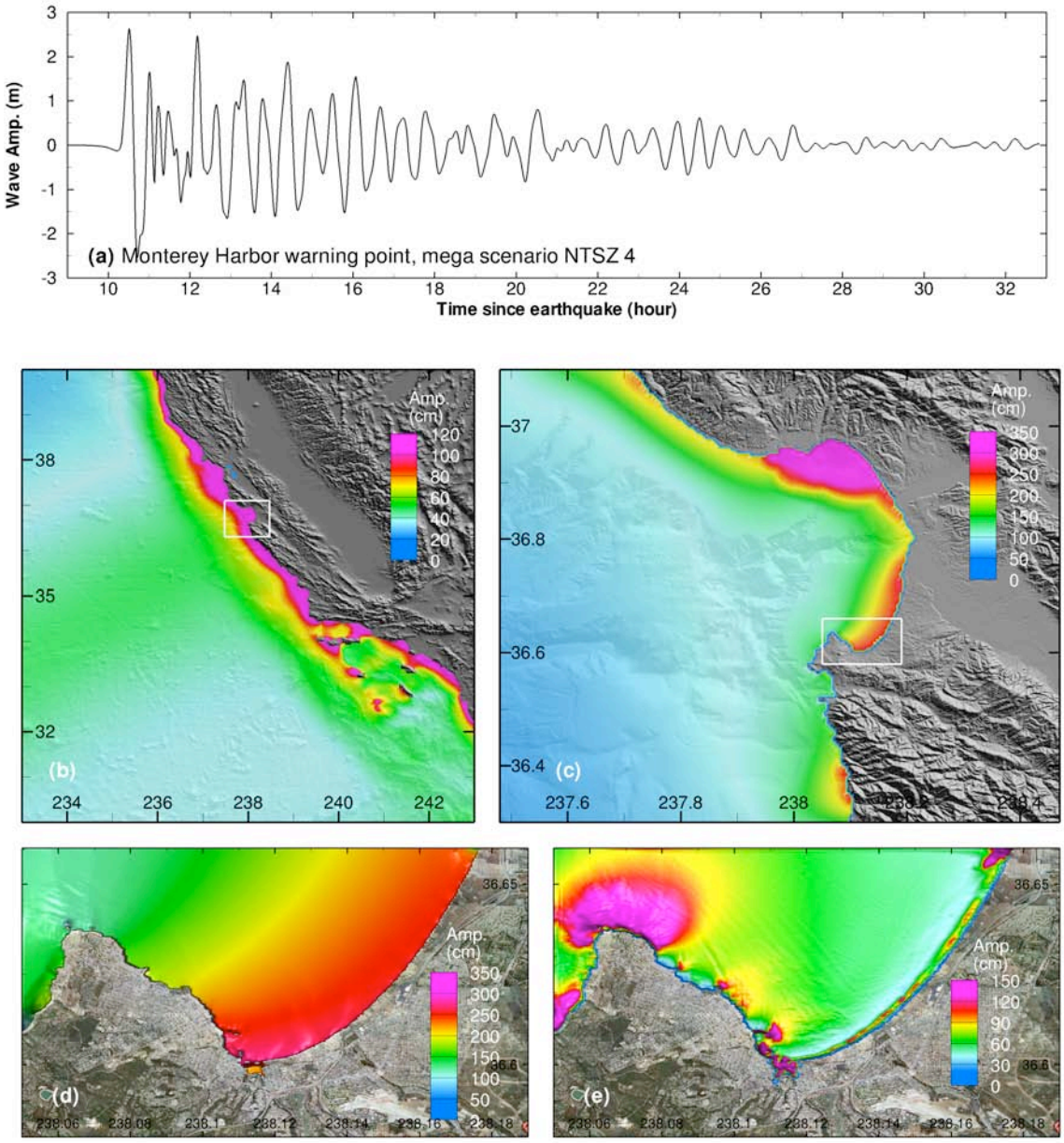

Figure 39. Model stability testing results at Monterey for artificial mega tsunami scenario NTSZ 4. (a) Computed time series at Monterey warning point; (b) Computed maximum wave amplitude in grid A of the forecast model; (c) Computed maximum current speed in grid B of the forecast model; (d) Computed maximum wave amplitude in grid C of the forecast model; (e) Computed current speed in grid C of the forecast model.

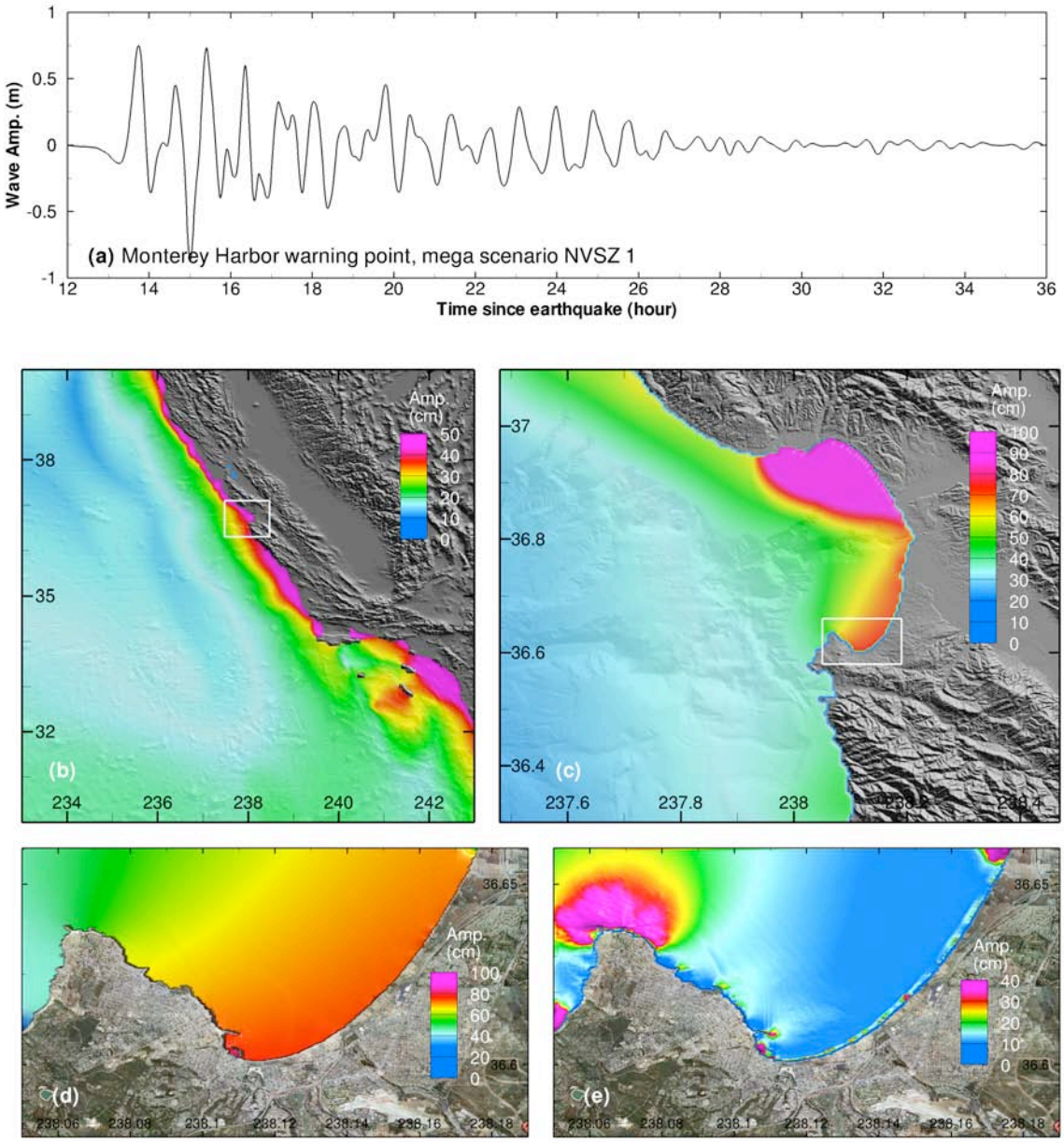

Figure 40. Model stability testing results at Monterey for artificial mega tsunami scenario NVSZ 1. (a) Computed time series at Monterey warning point; (b) Computed maximum wave amplitude in grid A of the forecast model; (c) Computed maximum current speed in grid B of the forecast model; (d) Computed maximum wave amplitude in grid C of the forecast model; (e) Computed current speed in grid C of the forecast model.

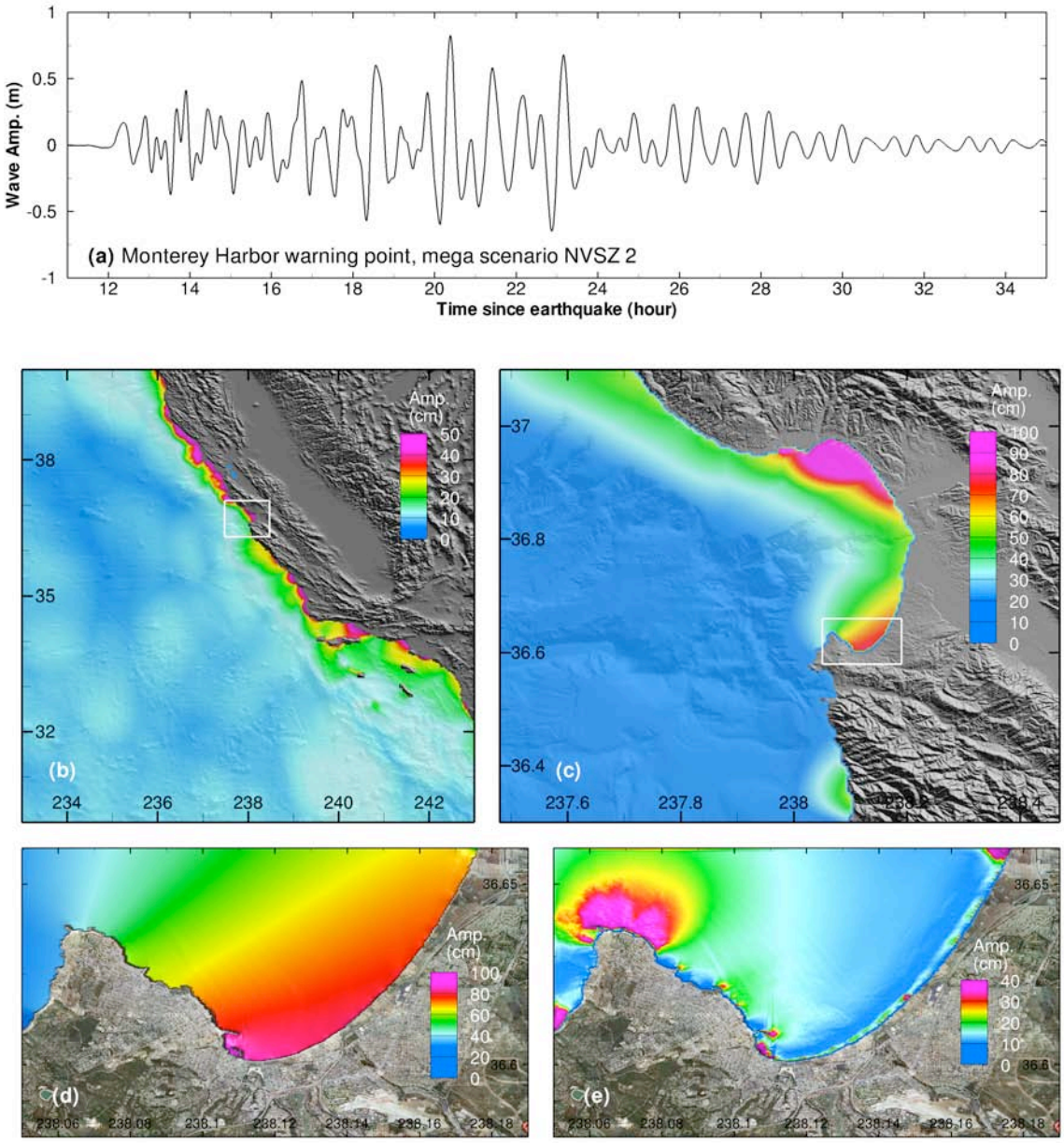

Figure 41. Model stability testing results at Monterey for artificial mega tsunami scenario NVSZ 2. (a) Computed time series at Monterey warning point; (b) Computed maximum wave amplitude in grid A of the forecast model; (c) Computed maximum current speed in grid B of the forecast model; (d) Computed maximum wave amplitude in grid C of the forecast model; (e) Computed current speed in grid C of the forecast model.

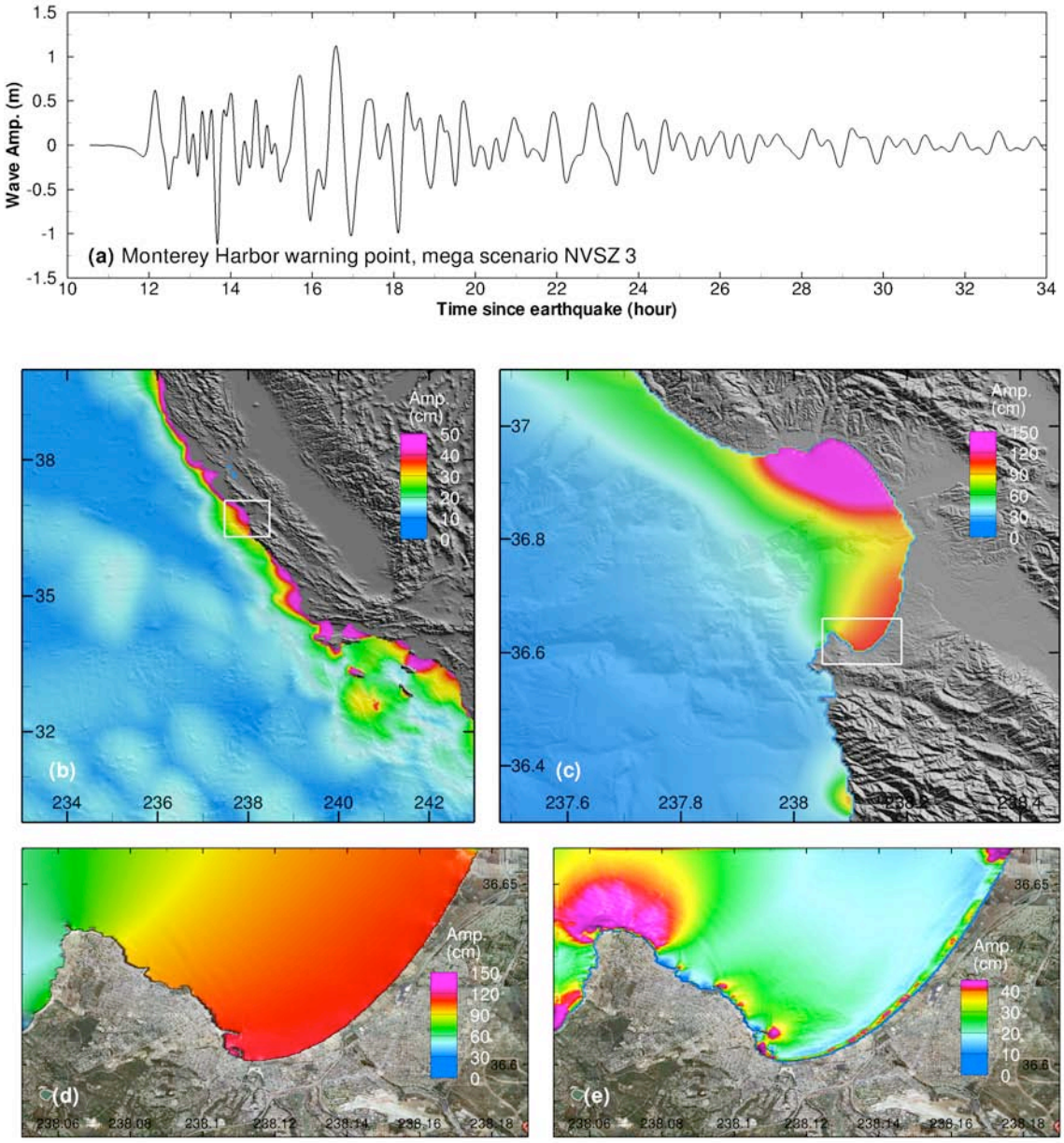

Figure 42. Model stability testing results at Monterey for artificial mega tsunami scenario NVSZ 3. (a) Computed time series at Monterey warning point; (b) Computed maximum wave amplitude in grid A of the forecast model; (c) Computed maximum current speed in grid B of the forecast model; (d) Computed maximum wave amplitude in grid C of the forecast model; (e) Computed current speed in grid C of the forecast model.

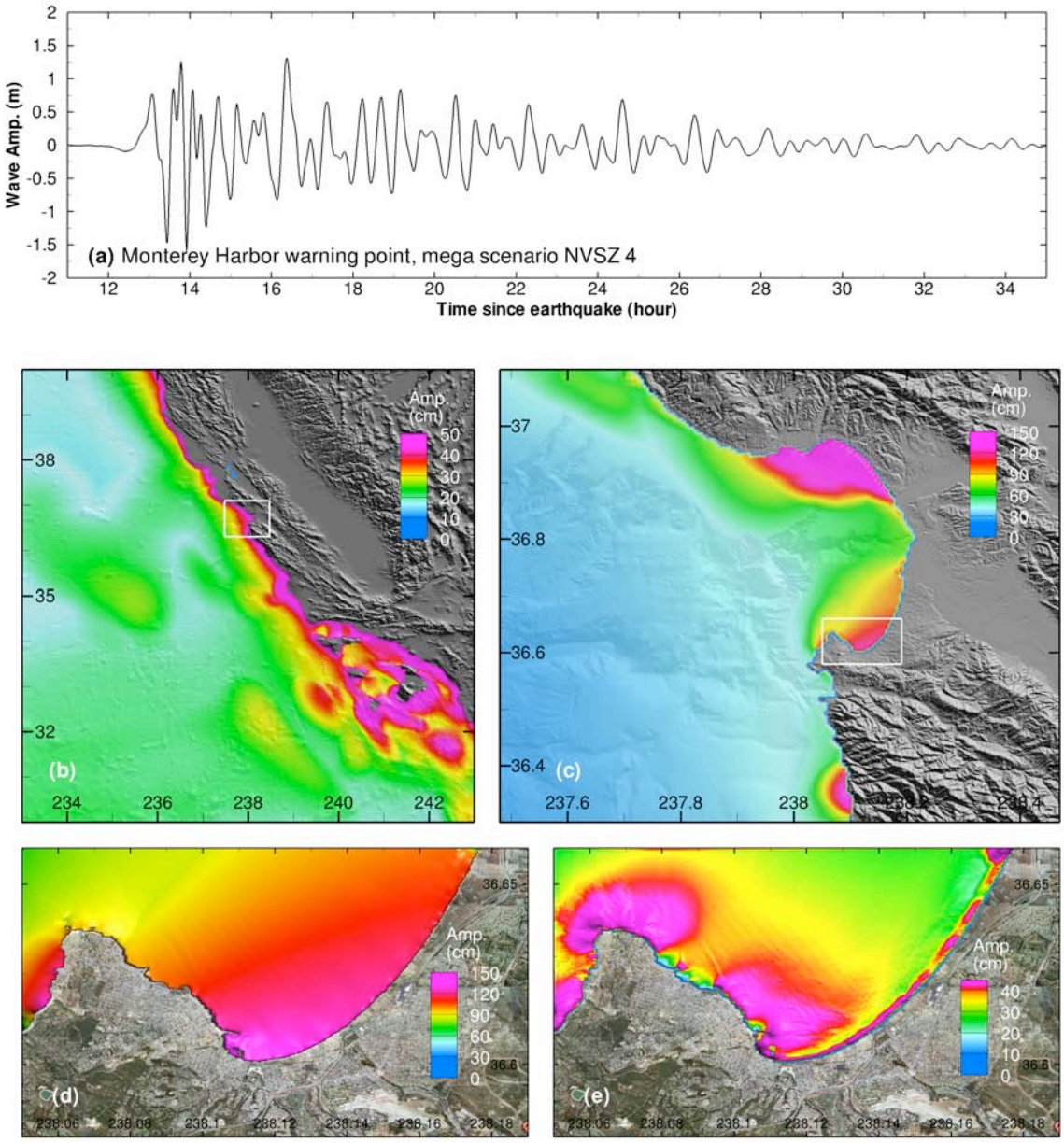

Figure 43. Model stability testing results at Monterey for artificial mega tsunami scenario NVSZ 4. (a) Computed time series at Monterey warning point; (b) Computed maximum wave amplitude in grid A of the forecast model; (c) Computed maximum current speed in grid B of the forecast model; (d) Computed maximum wave amplitude in grid C of the forecast model; (e) Computed current speed in grid C of the forecast model.

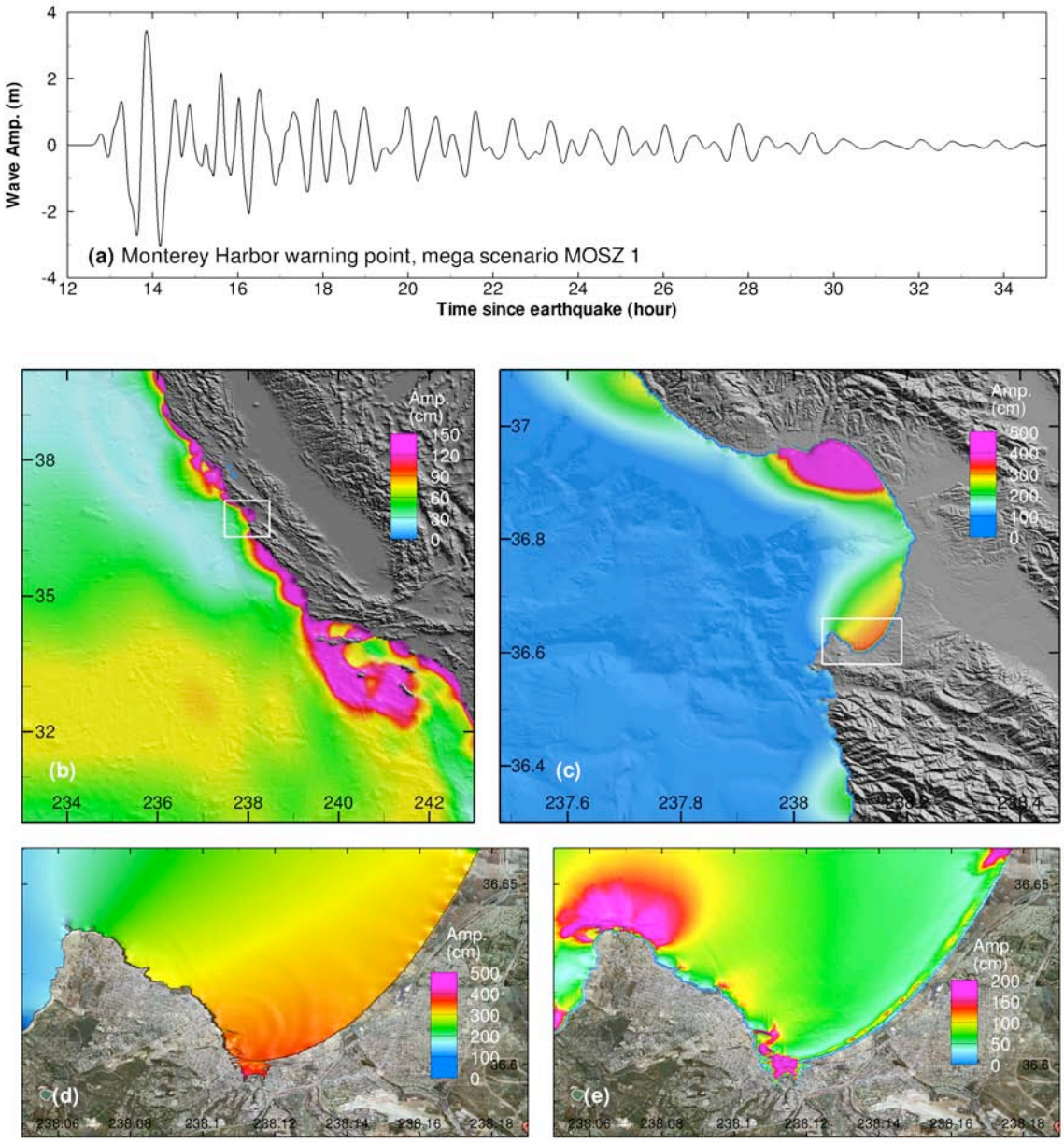

Figure 44. Model stability testing results at Monterey for artificial mega tsunami scenario MOSZ 1. (a) Computed time series at Monterey warning point; (b) Computed maximum wave amplitude in grid A of the forecast model; (c) Computed maximum current speed in grid B of the forecast model; (d) Computed maximum wave amplitude in grid C of the forecast model; (e) Computed current speed in grid C of the forecast model.

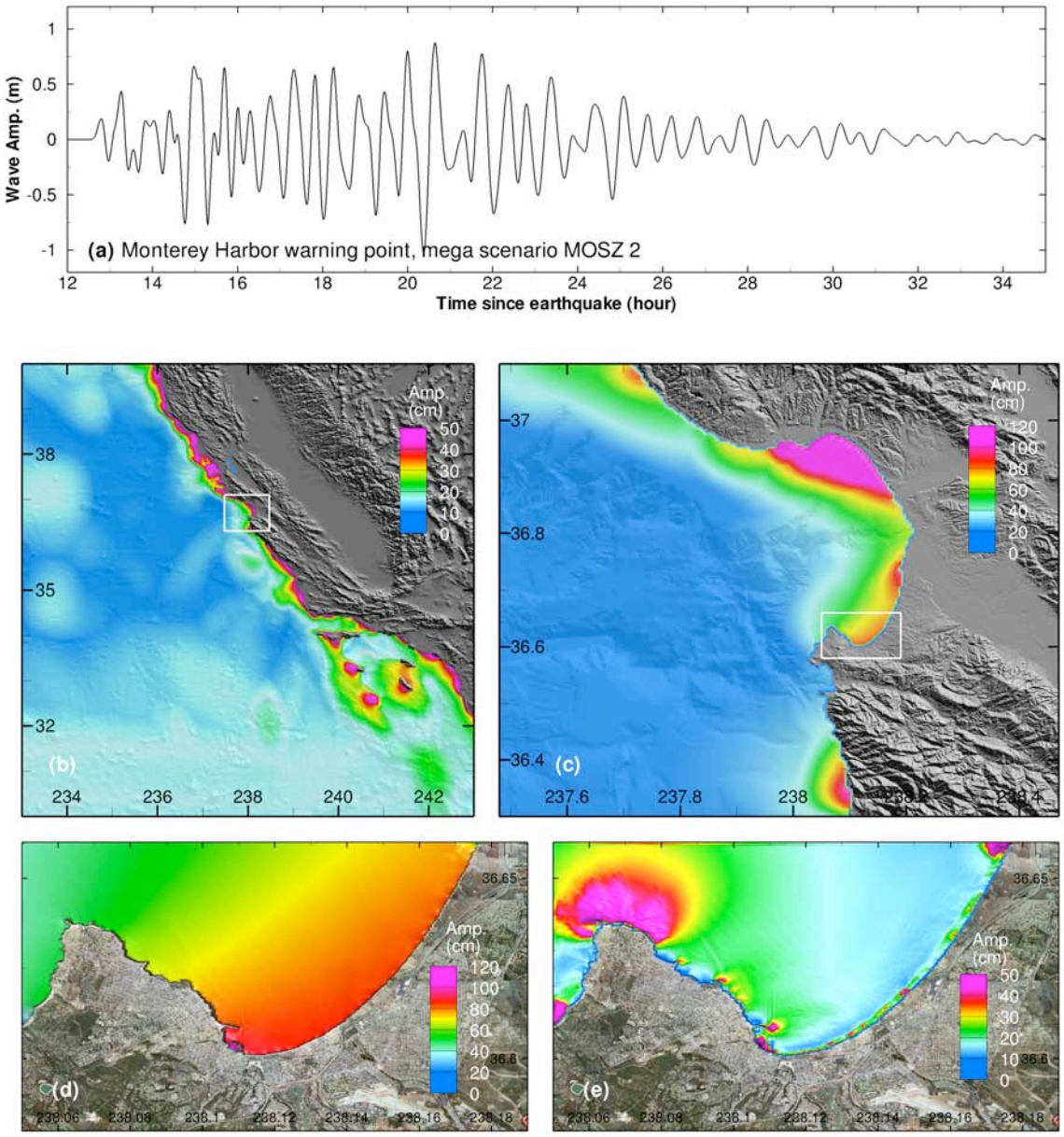

Figure 45. Model stability testing results at Monterey for artificial mega tsunami scenario MOSZ 2. (a) Computed time series at Monterey warning point; (b) Computed maximum wave amplitude in grid A of the forecast model; (c) Computed maximum current speed in grid B of the forecast model; (d) Computed maximum wave amplitude in grid C of the forecast model; (e) Computed current speed in grid C of the forecast model.

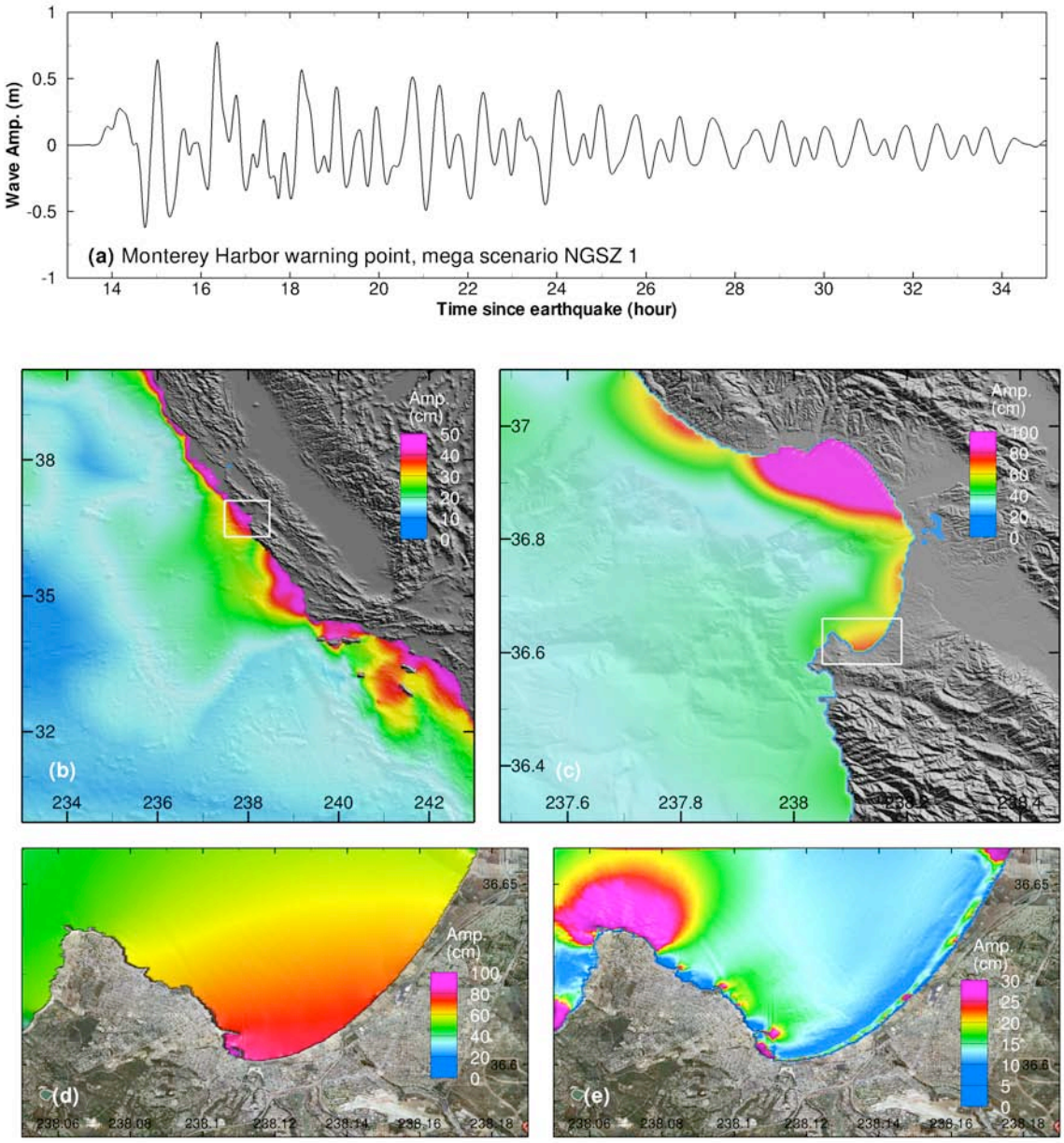

Figure 46. Model stability testing results at Monterey for artificial mega tsunami scenario NGSZ 1. (a) Computed time series at Monterey warning point; (b) Computed maximum wave amplitude in grid A of the forecast model; (c) Computed maximum current speed in grid B of the forecast model; (d) Computed maximum wave amplitude in grid C of the forecast model; (e) Computed current speed in grid C of the forecast model.

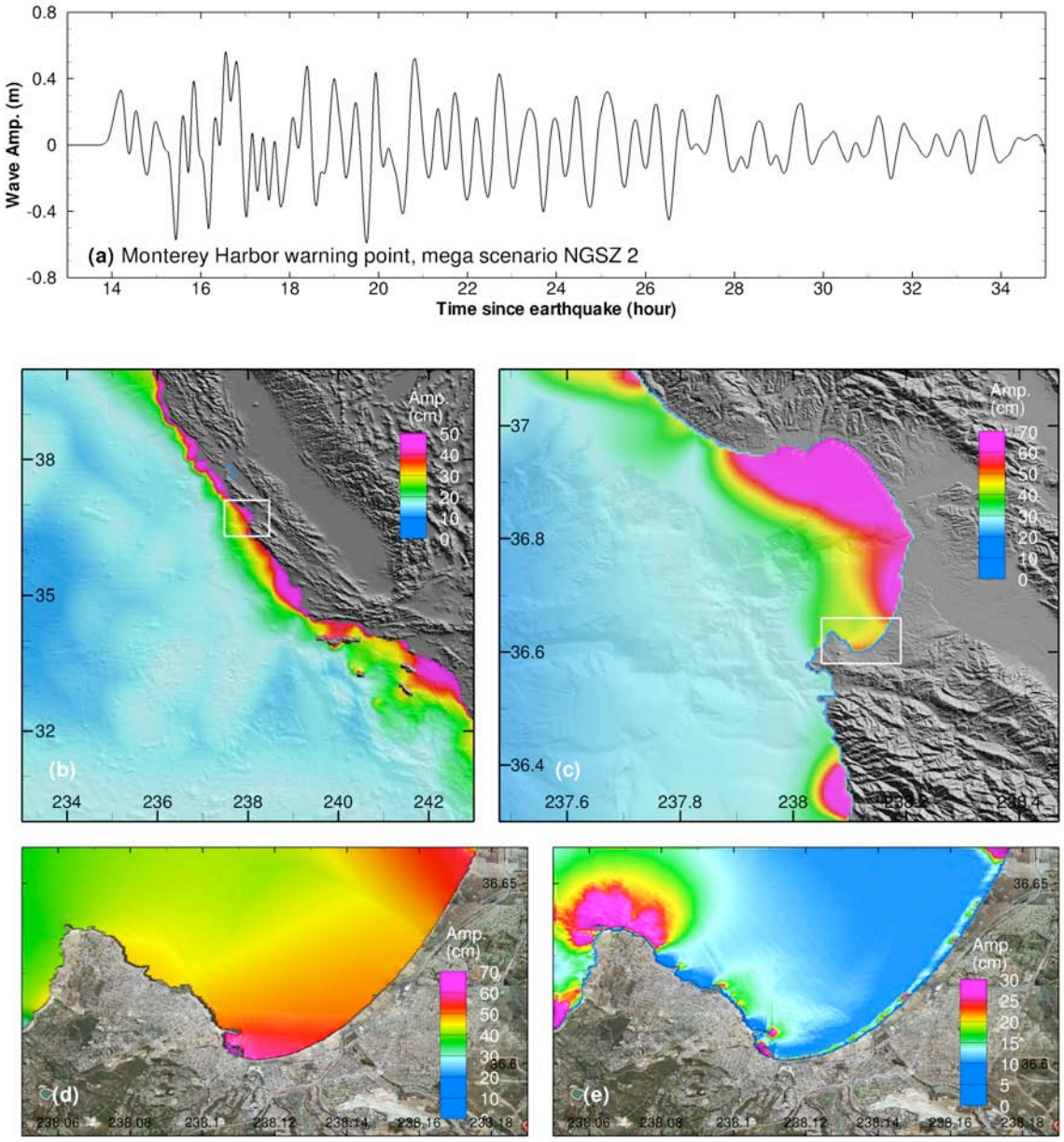

Figure 47. Model stability testing results at Monterey for artificial mega tsunami scenario NGSZ 2. (a) Computed time series at Monterey warning point; (b) Computed maximum wave amplitude in grid A of the forecast model; (c) Computed maximum current speed in grid B of the forecast model; (d) Computed maximum wave amplitude in grid C of the forecast model; (e) Computed current speed in grid C of the forecast model.

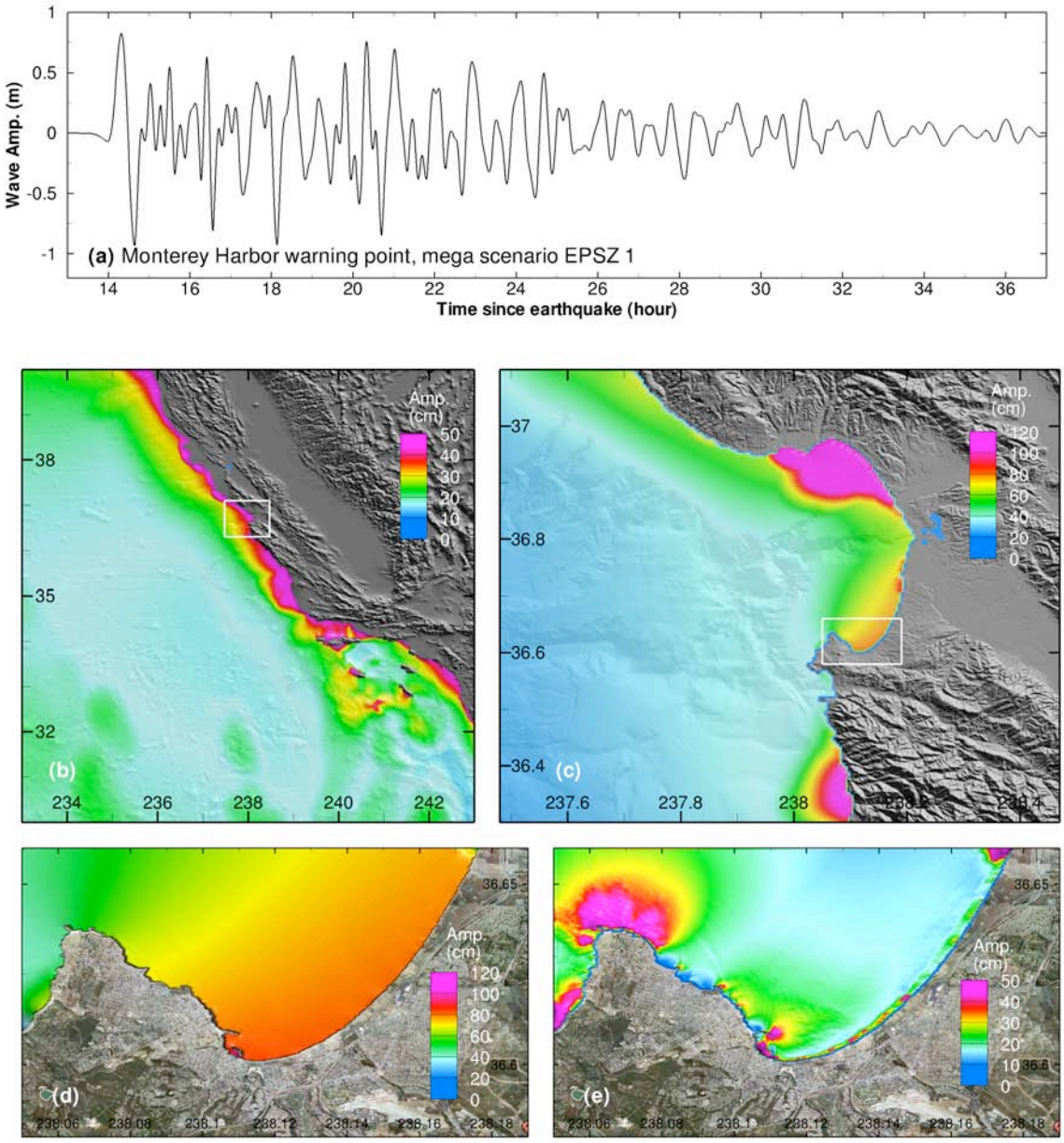

Figure 48. Model stability testing results at Monterey for artificial mega tsunami scenario EPSZ 1. (a) Computed time series at Monterey warning point; (b) Computed maximum wave amplitude in grid A of the forecast model; (c) Computed maximum current speed in grid B of the forecast model; (d) Computed maximum wave amplitude in grid C of the forecast model; (e) Computed current speed in grid C of the forecast model.

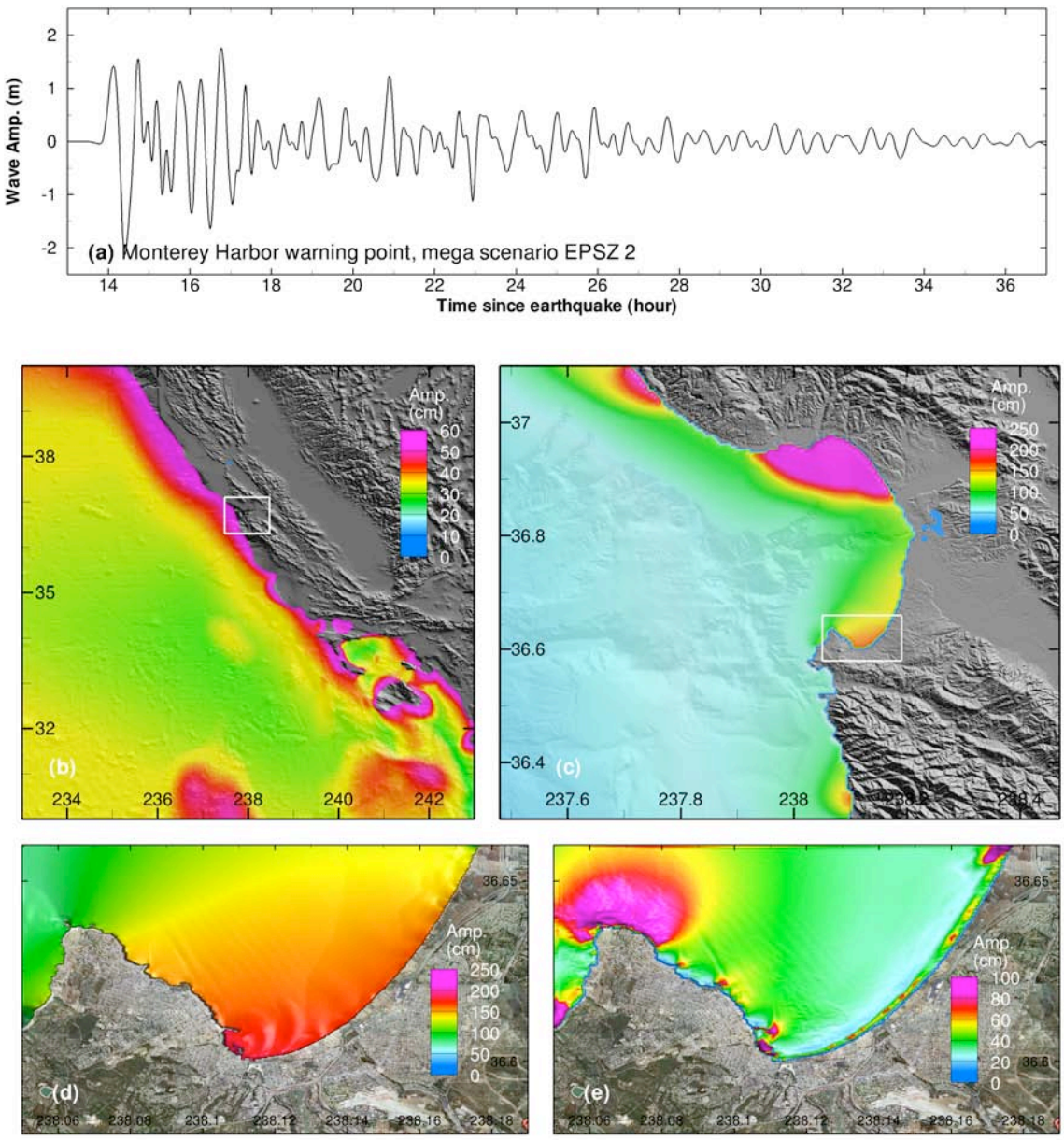

Figure 49. Model stability testing results at Monterey for artificial mega tsunami scenario EPSZ 2. (a) Computed time series at Monterey warning point; (b) Computed maximum wave amplitude in grid A of the forecast model; (c) Computed maximum current speed in grid B of the forecast model; (d) Computed maximum wave amplitude in grid C of the forecast model; (e) Computed current speed in grid C of the forecast model.

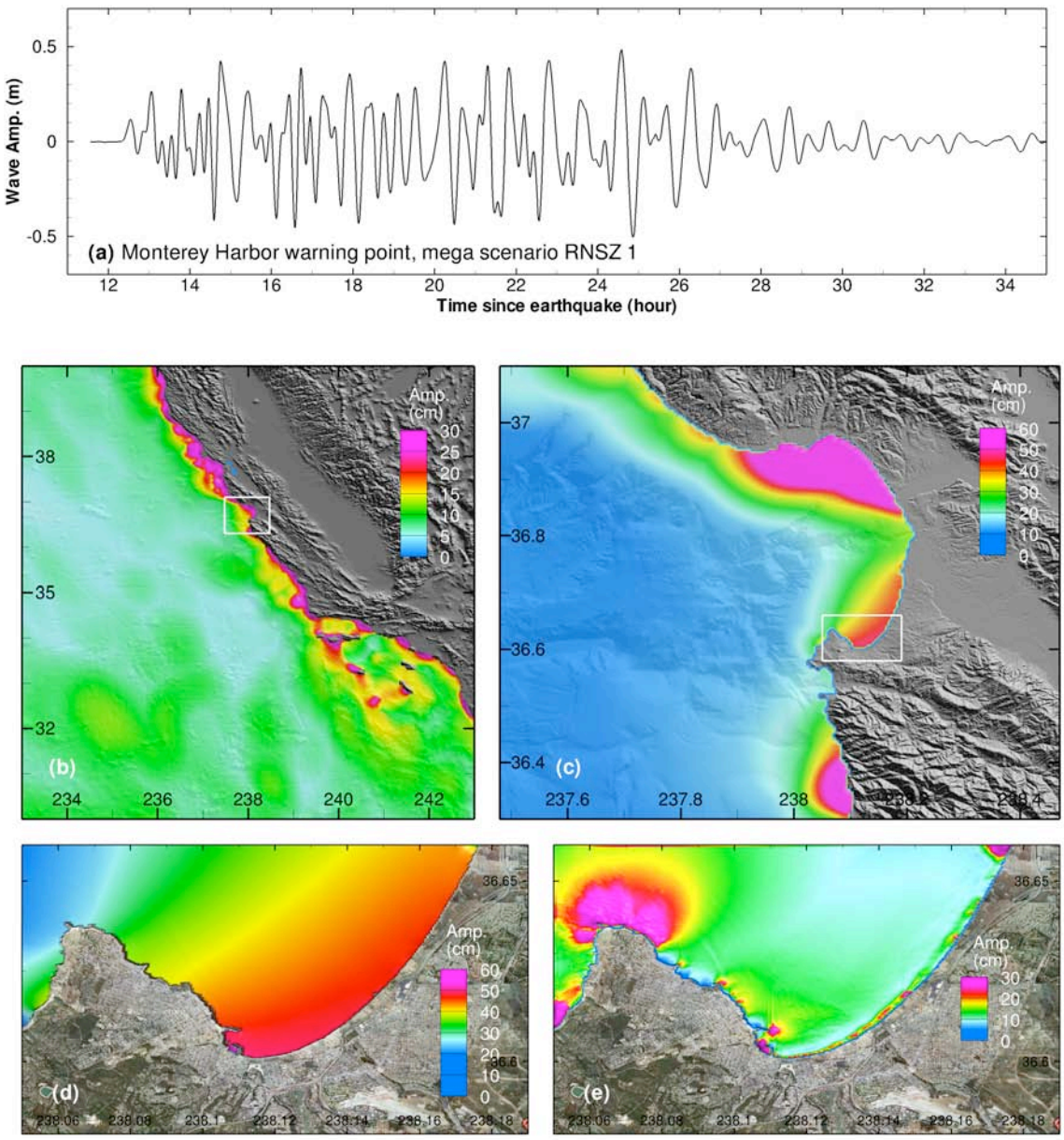

Figure 50. Model stability testing results at Monterey for artificial mega tsunami scenario RNSZ 1. (a) Computed time series at Monterey warning point; (b) Computed maximum wave amplitude in grid A of the forecast model; (c) Computed maximum current speed in grid B of the forecast model; (d) Computed maximum wave amplitude in grid C of the forecast model; (e) Computed current speed in grid C of the forecast model.

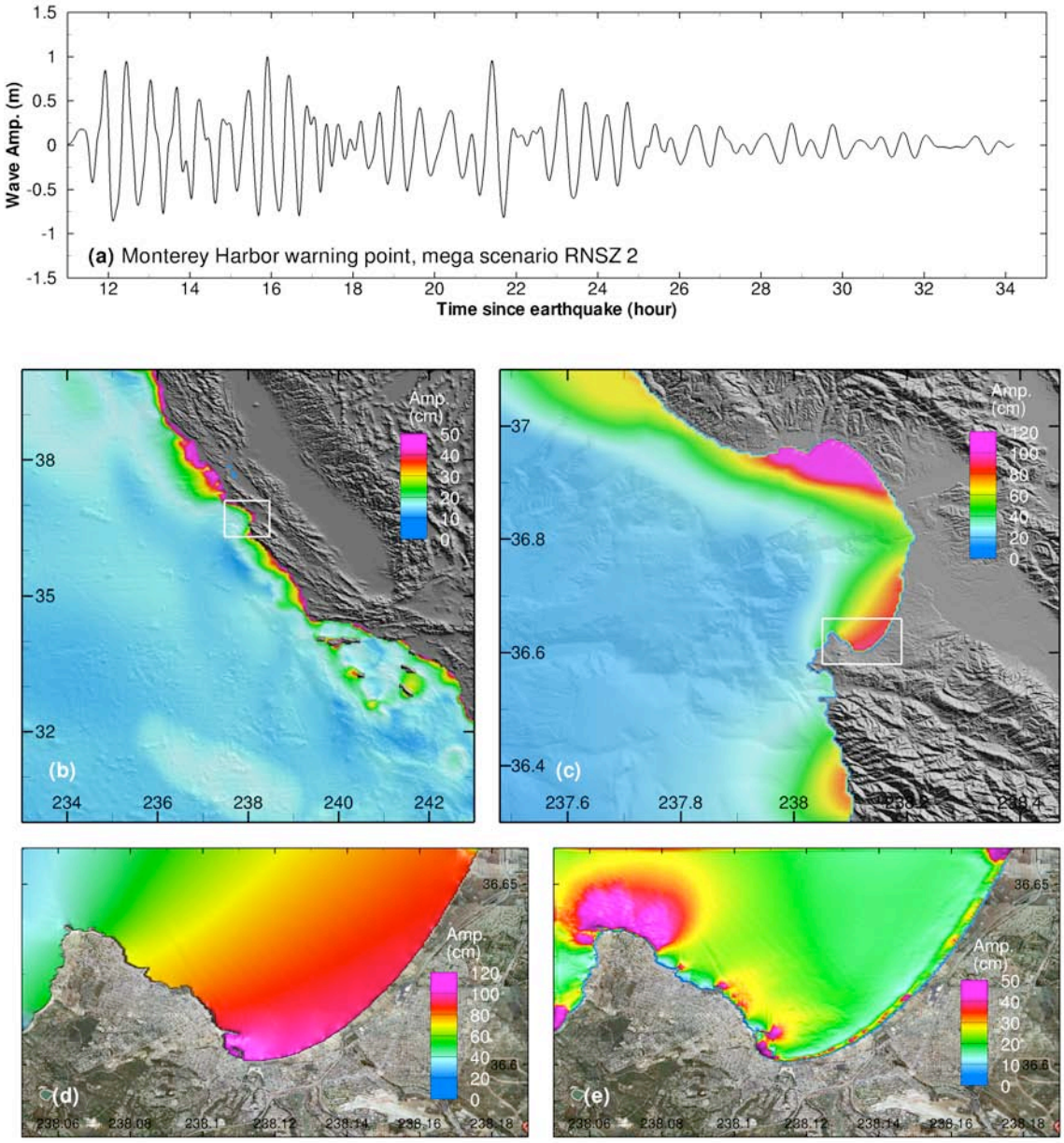

Figure 51. Model stability testing results at Monterey for artificial mega tsunami scenario RNSZ 2. (a) Computed time series at Monterey warning point; (b) Computed maximum wave amplitude in grid A of the forecast model; (c) Computed maximum current speed in grid B of the forecast model; (d) Computed maximum wave amplitude in grid C of the forecast model; (e) Computed current speed in grid C of the forecast model.

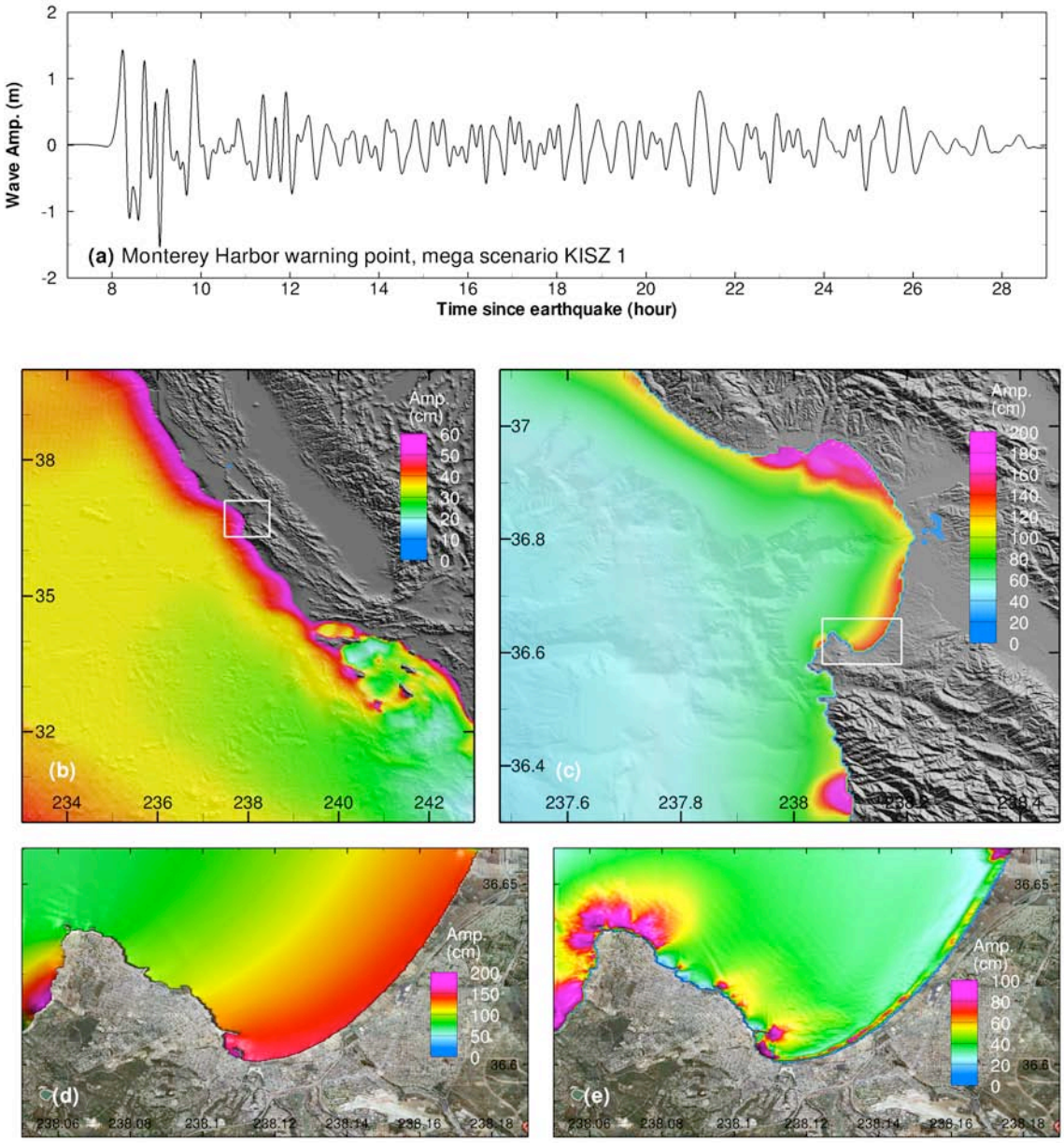

Figure 52. Model stability testing results at Monterey for artificial mega tsunami scenario KISZ 1. (a) Computed time series at Monterey warning point; (b) Computed maximum wave amplitude in grid A of the forecast model; (c) Computed maximum current speed in grid B of the forecast model; (d) Computed maximum wave amplitude in grid C of the forecast model; (e) Computed current speed in grid C of the forecast model.

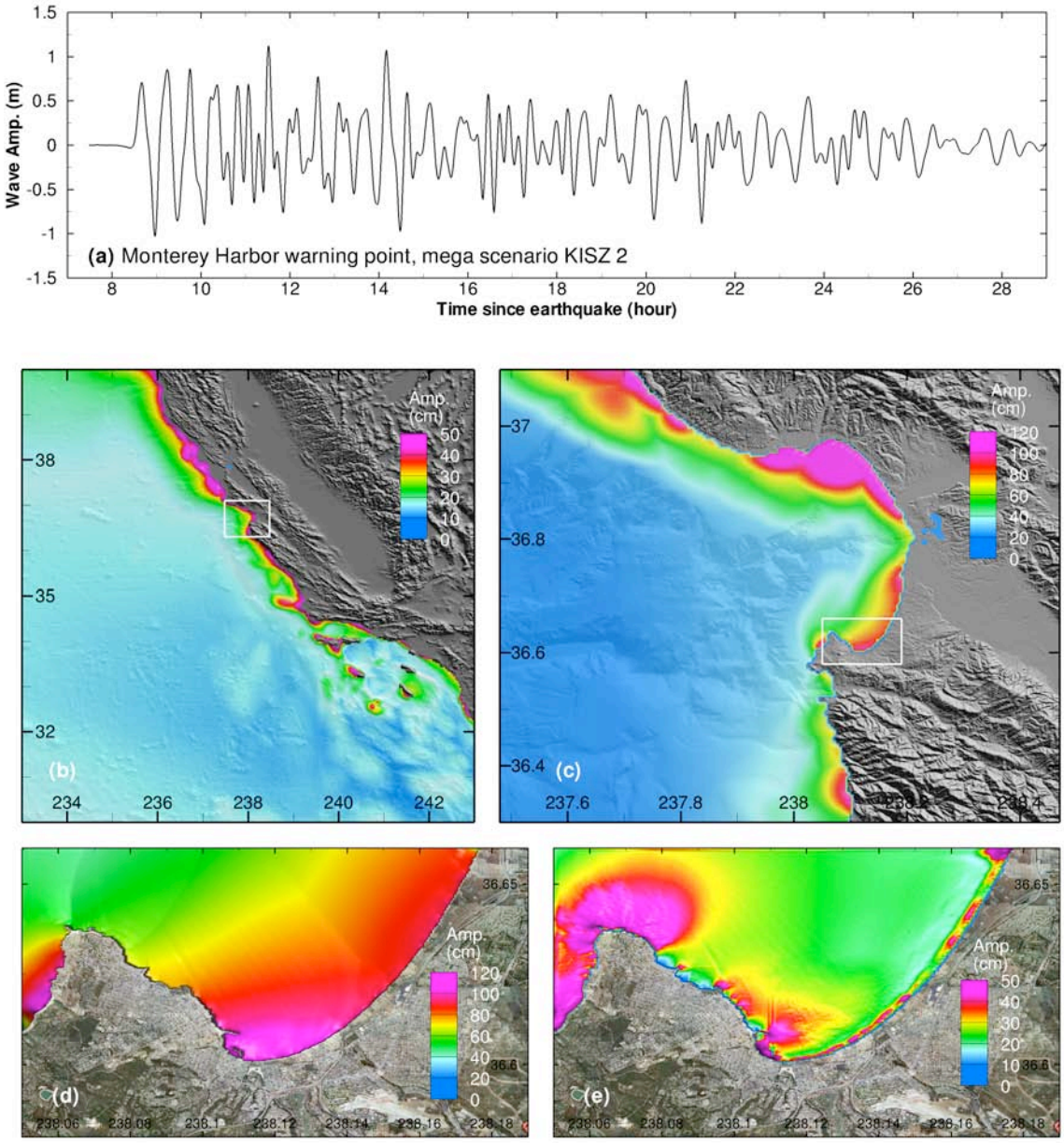

Figure 53. Model stability testing results at Monterey for artificial mega tsunami scenario KISZ 2. (a) Computed time series at Monterey warning point; (b) Computed maximum wave amplitude in grid A of the forecast model; (c) Computed maximum current speed in grid B of the forecast model; (d) Computed maximum wave amplitude in grid C of the forecast model; (e) Computed current speed in grid C of the forecast model.

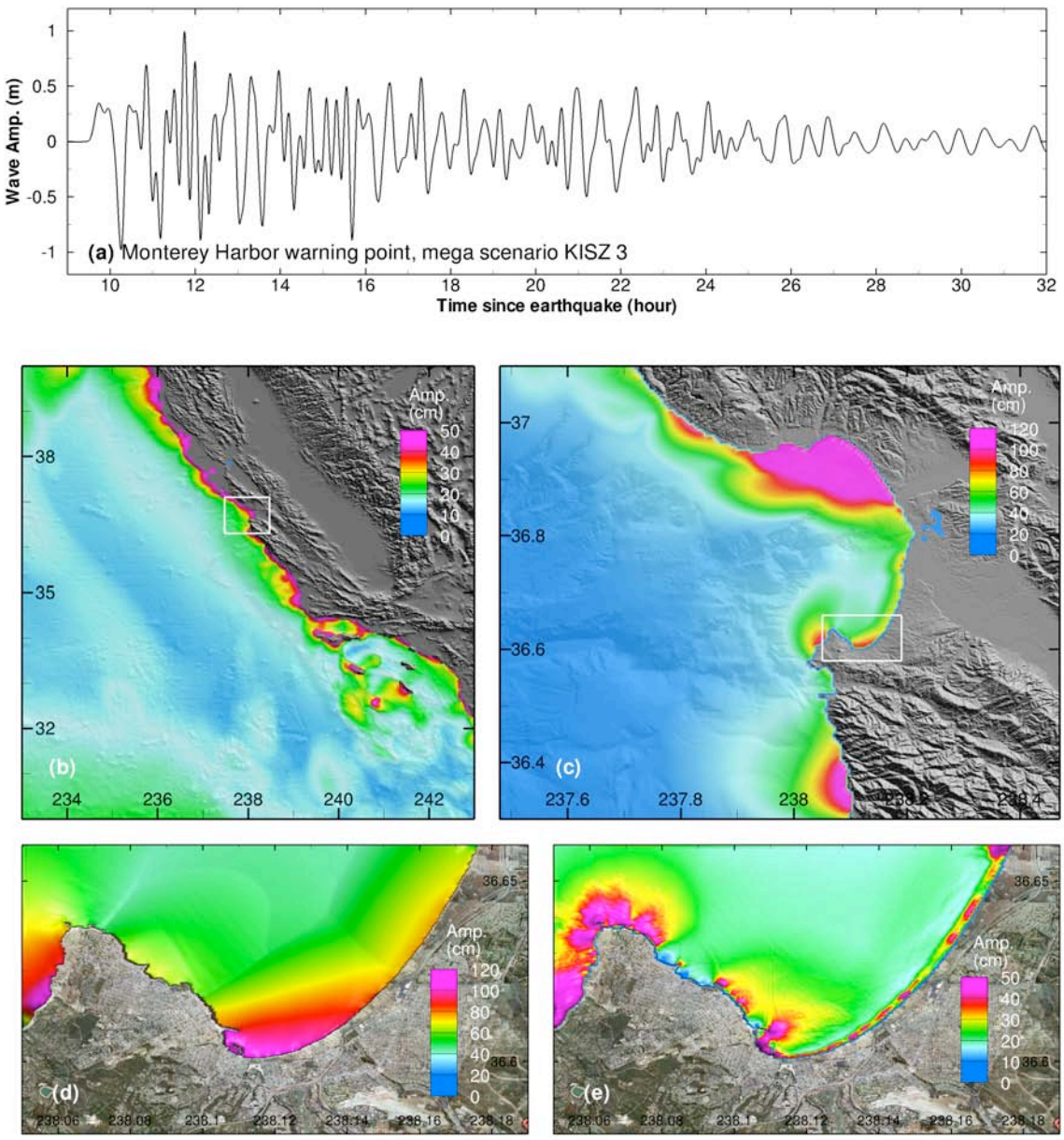

Figure 54. Model stability testing results at Monterey for artificial mega tsunami scenario KISZ 3. (a) Computed time series at Monterey warning point; (b) Computed maximum wave amplitude in grid A of the forecast model; (c) Computed maximum current speed in grid B of the forecast model; (d) Computed maximum wave amplitude in grid C of the forecast model; (e) Computed current speed in grid C of the forecast model.

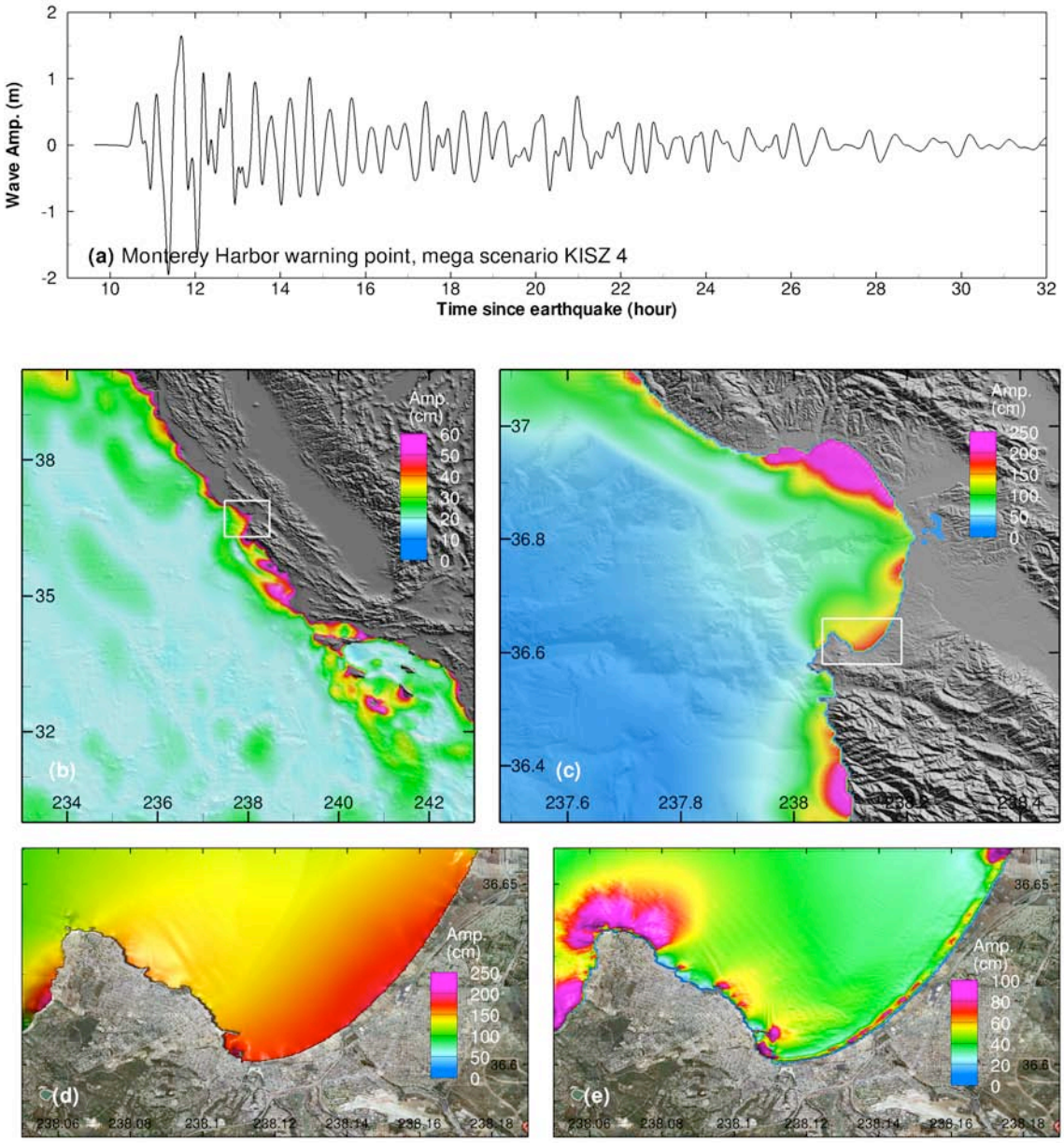

Figure 55. Model stability testing results at Monterey for artificial mega tsunami scenario KISZ 4. (a) Computed time series at Monterey warning point; (b) Computed maximum wave amplitude in grid A of the forecast model; (c) Computed maximum current speed in grid B of the forecast model; (d) Computed maximum wave amplitude in grid C of the forecast model; (e) Computed current speed in grid C of the forecast model.

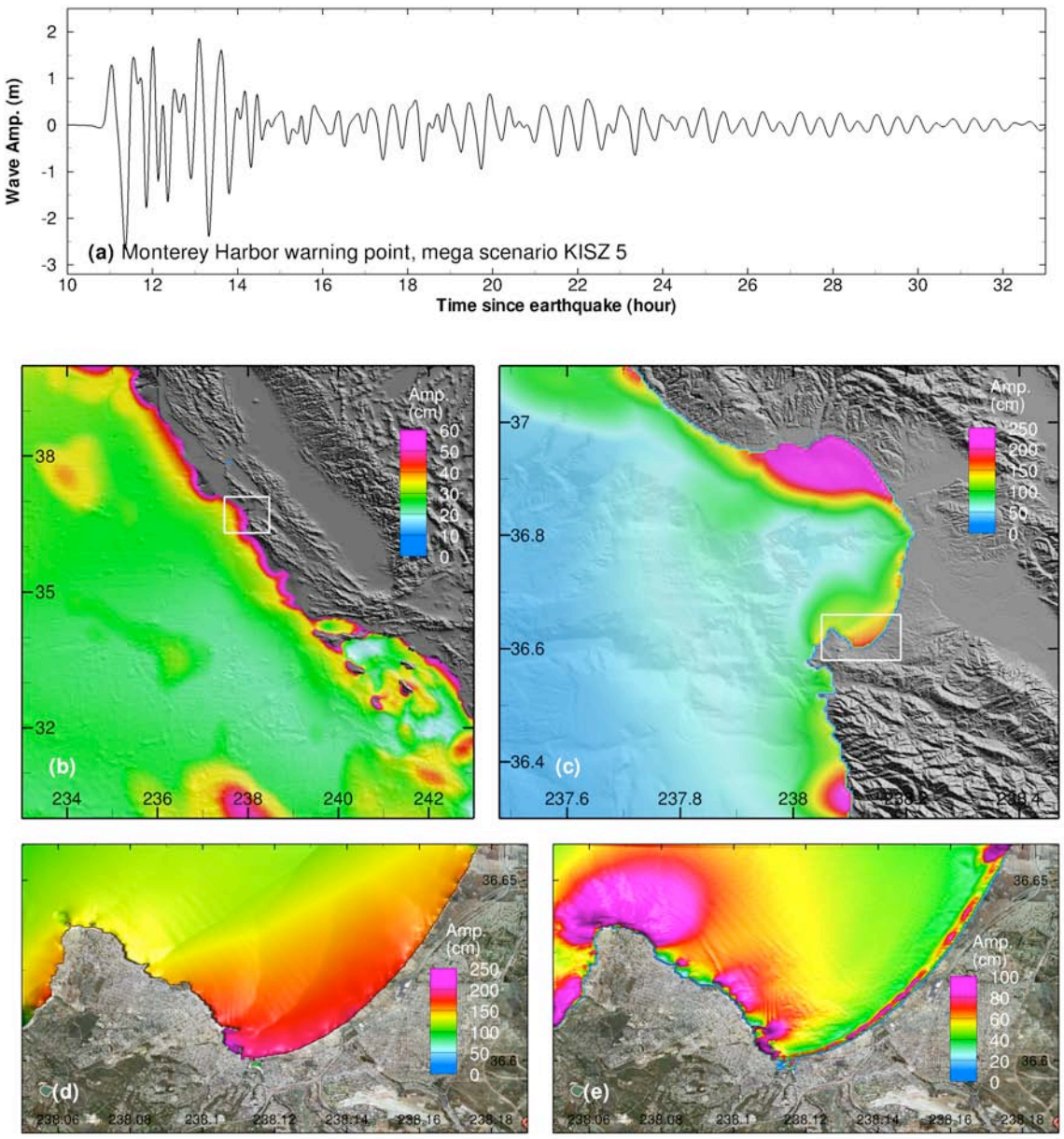

Figure 56. Model stability testing results at Monterey for artificial mega tsunami scenario KISZ 5. (a) Computed time series at Monterey warning point; (b) Computed maximum wave amplitude in grid A of the forecast model; (c) Computed maximum current speed in grid B of the forecast model; (d) Computed maximum wave amplitude in grid C of the forecast model; (e) Computed current speed in grid C of the forecast model.

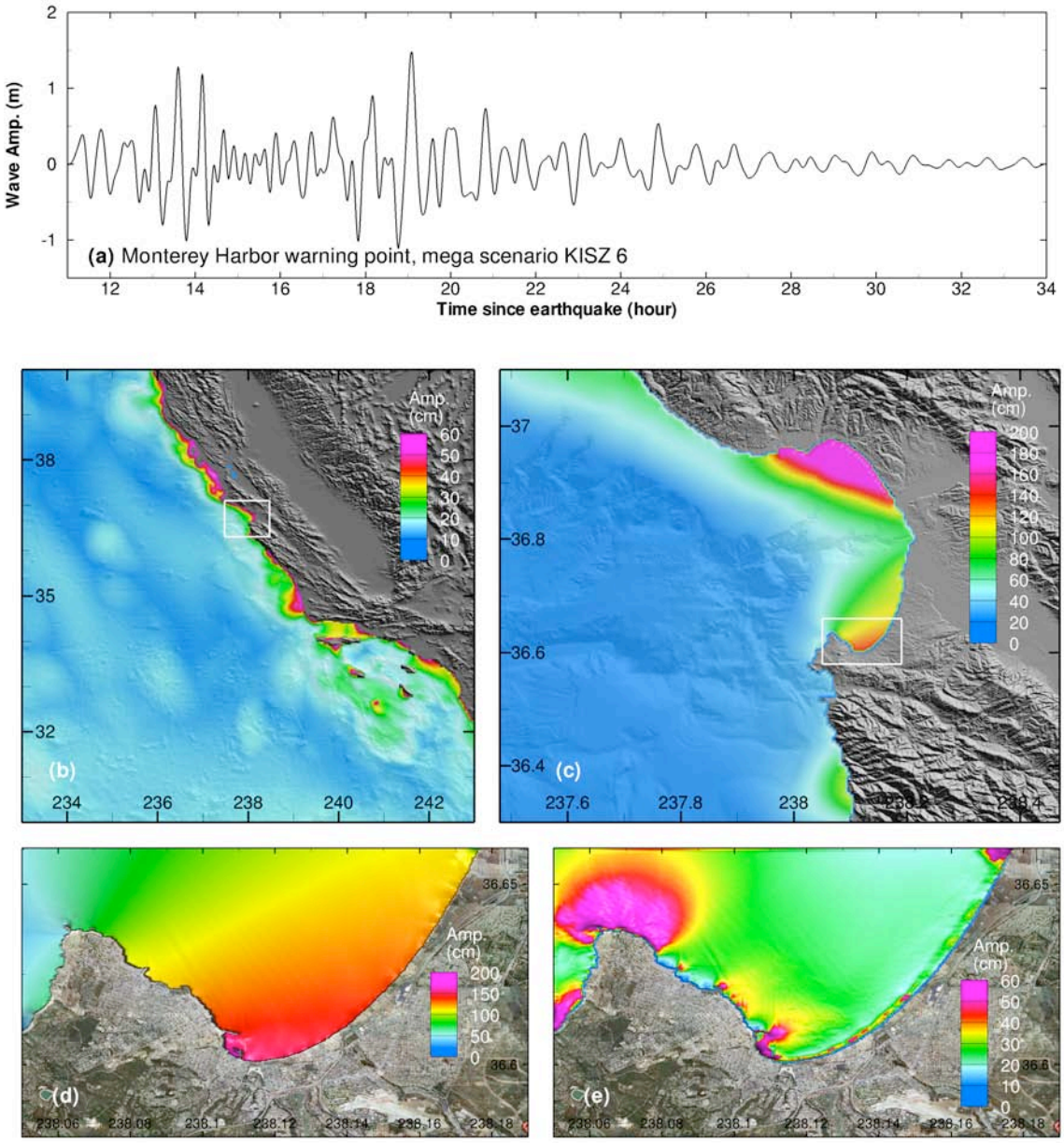

Figure 57. Model stability testing results at Monterey for artificial mega tsunami scenario KISZ 6. (a) Computed time series at Monterey warning point; (b) Computed maximum wave amplitude in grid A of the forecast model; (c) Computed maximum current speed in grid B of the forecast model; (d) Computed maximum wave amplitude in grid C of the forecast model; (e) Computed current speed in grid C of the forecast model.

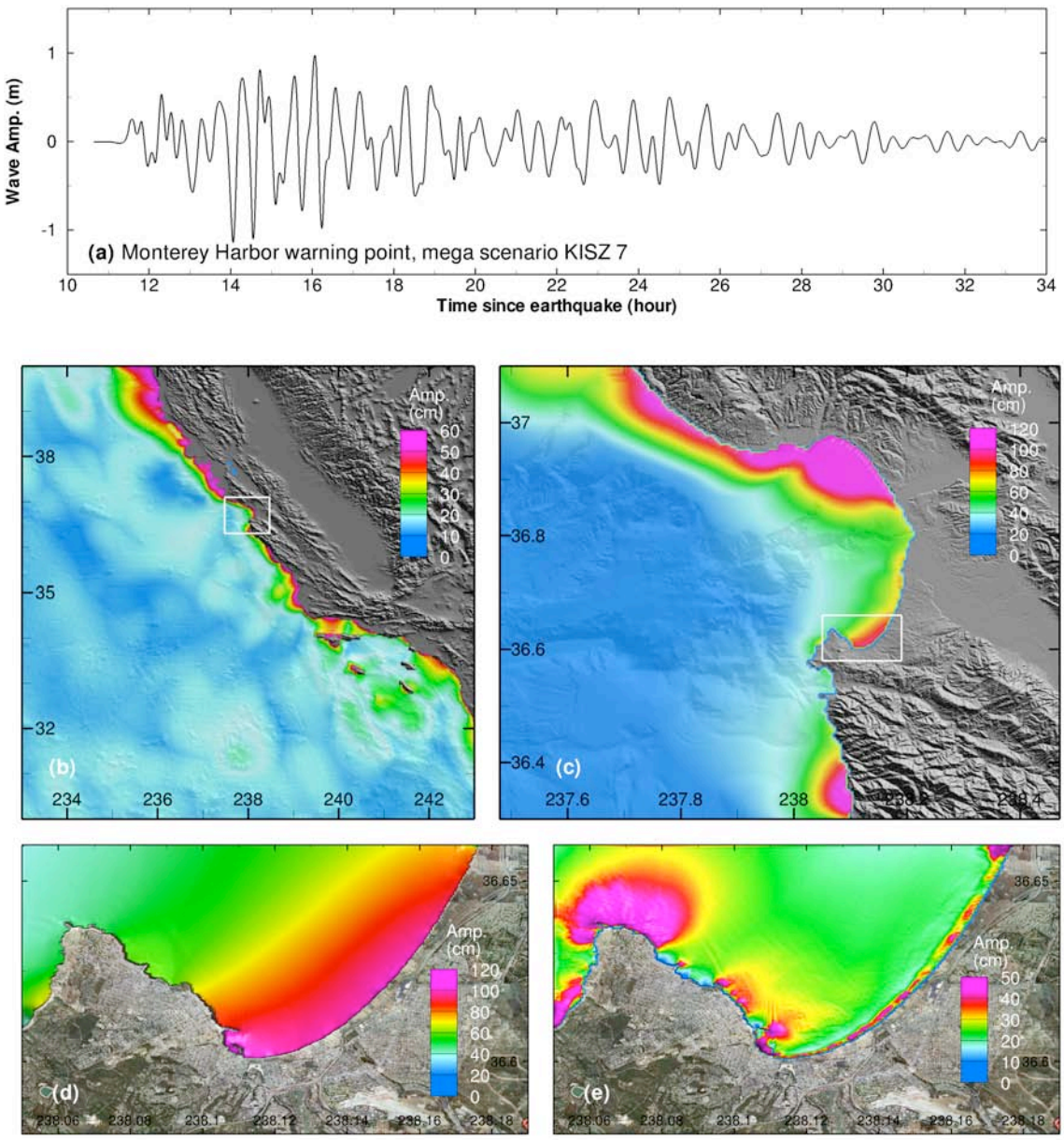

Figure 58. Model stability testing results at Monterey for artificial mega tsunami scenario KISZ 7. (a) Computed time series at Monterey warning point; (b) Computed maximum wave amplitude in grid A of the forecast model; (c) Computed maximum current speed in grid B of the forecast model; (d) Computed maximum wave amplitude in grid C of the forecast model; (e) Computed current speed in grid C of the forecast model.

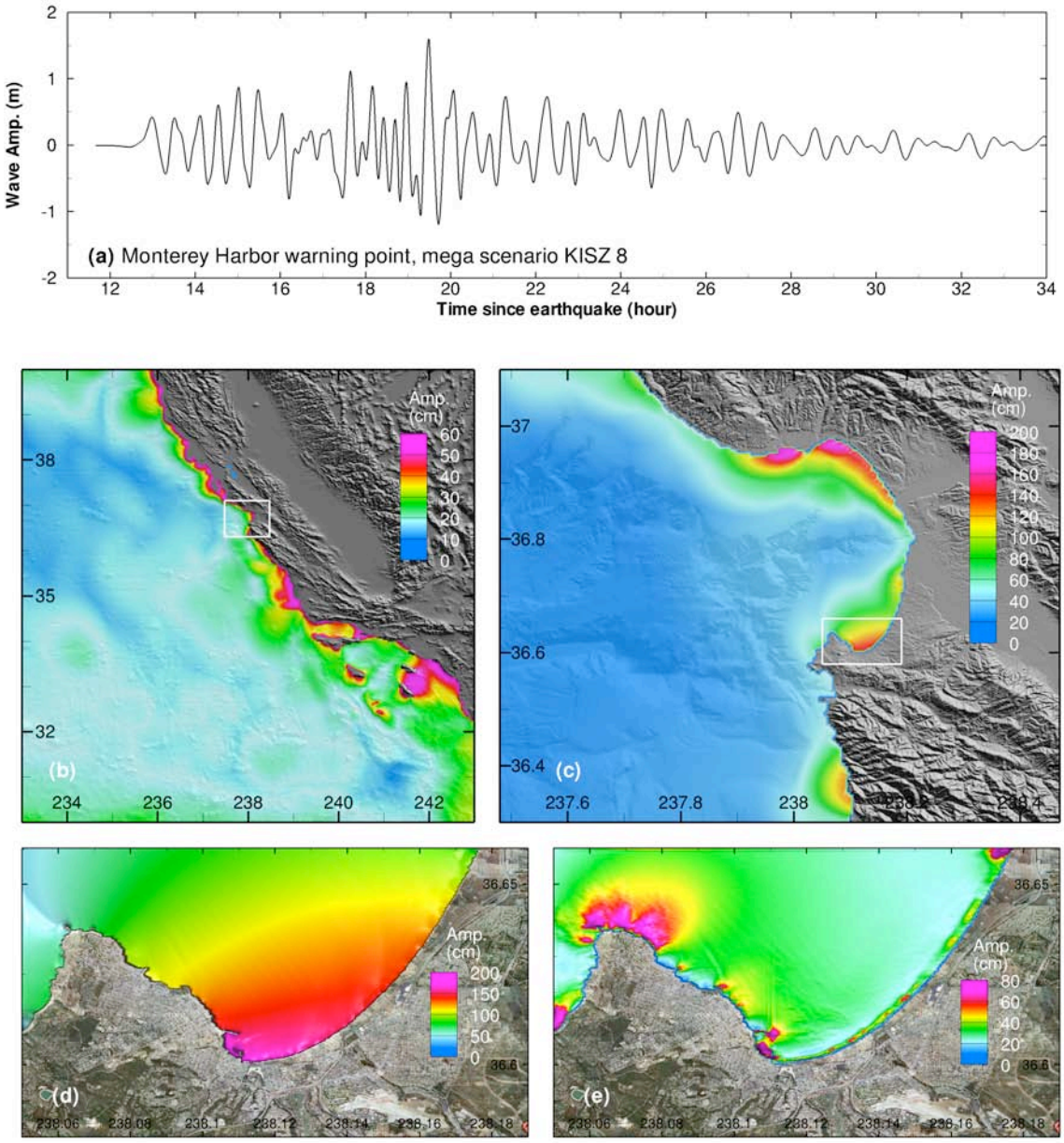

Figure 59. Model stability testing results at Monterey for artificial mega tsunami scenario KISZ 8. (a) Computed time series at Monterey warning point; (b) Computed maximum wave amplitude in grid A of the forecast model; (c) Computed maximum current speed in grid B of the forecast model; (d) Computed maximum wave amplitude in grid C of the forecast model; (e) Computed current speed in grid C of the forecast model.

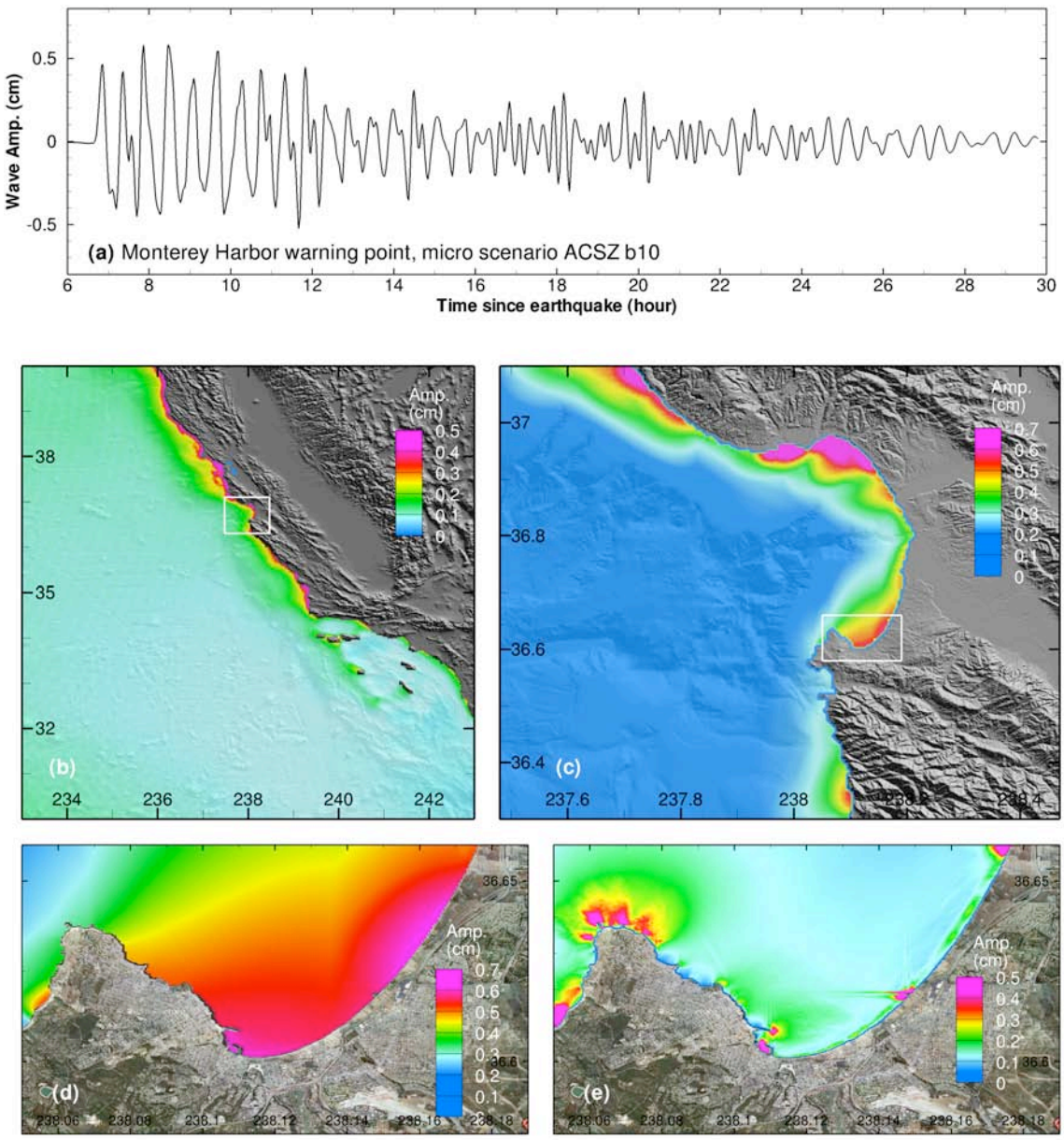

Figure 60. Model stability testing results at Monterey for artificial tsunami scenario ACSZ b10. (a) Computed time series at Monterey warning point; (b) Computed maximum wave amplitude in grid A of the forecast model; (c) Computed maximum current speed in grid B of the forecast model; (d) Computed maximum wave amplitude in grid C of the forecast model; (e) Computed current speed in grid C of the forecast model.

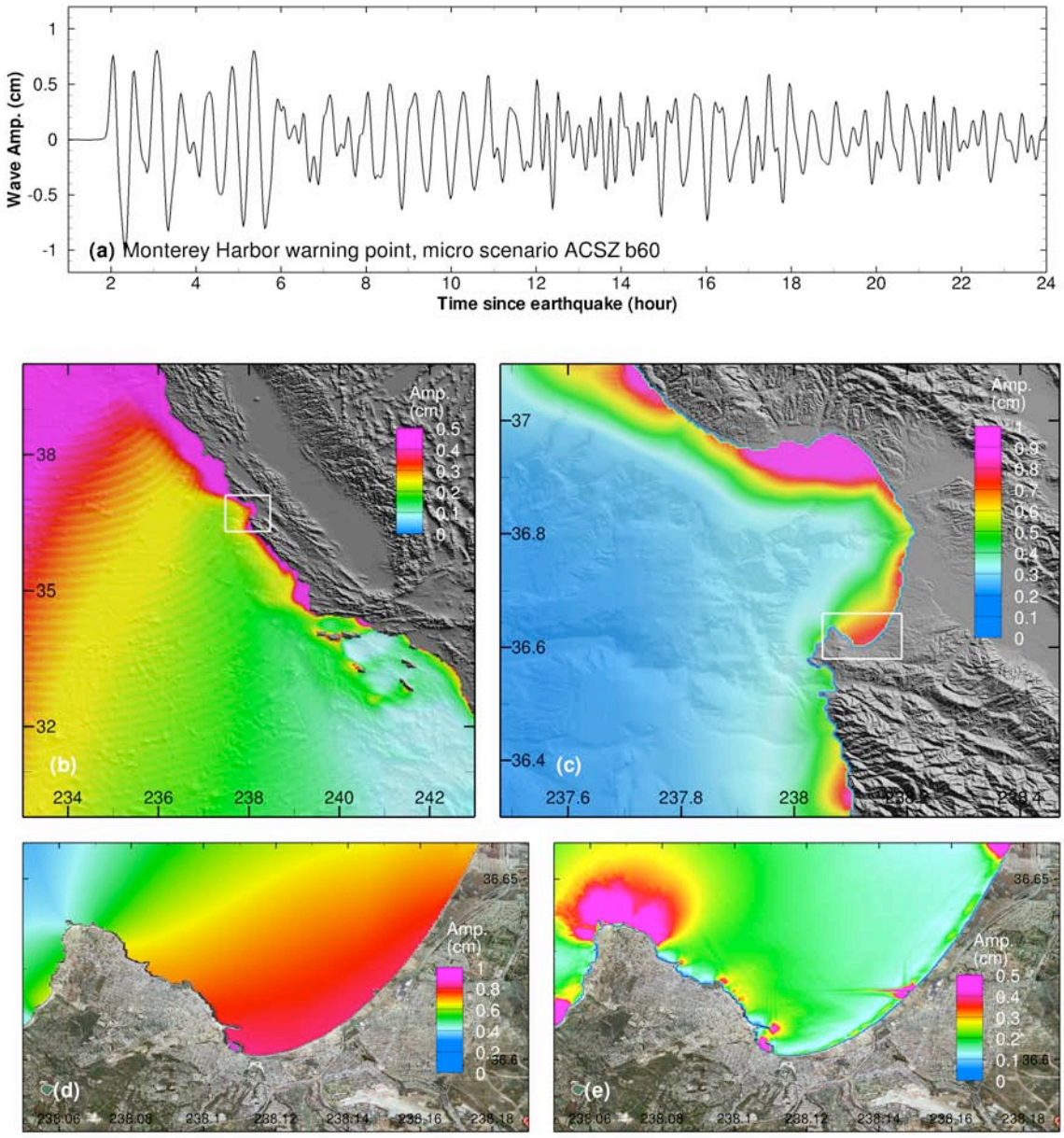

Figure 61. Model stability testing results at Monterey for artificial tsunami scenario ACSZ b60. (a) Computed time series at Monterey warning point; (b) Computed maximum wave amplitude in grid A of the forecast model; (c) Computed maximum current speed in grid B of the forecast model; (d) Computed maximum wave amplitude in grid C of the forecast model; (e) Computed current speed in grid C of the forecast model.

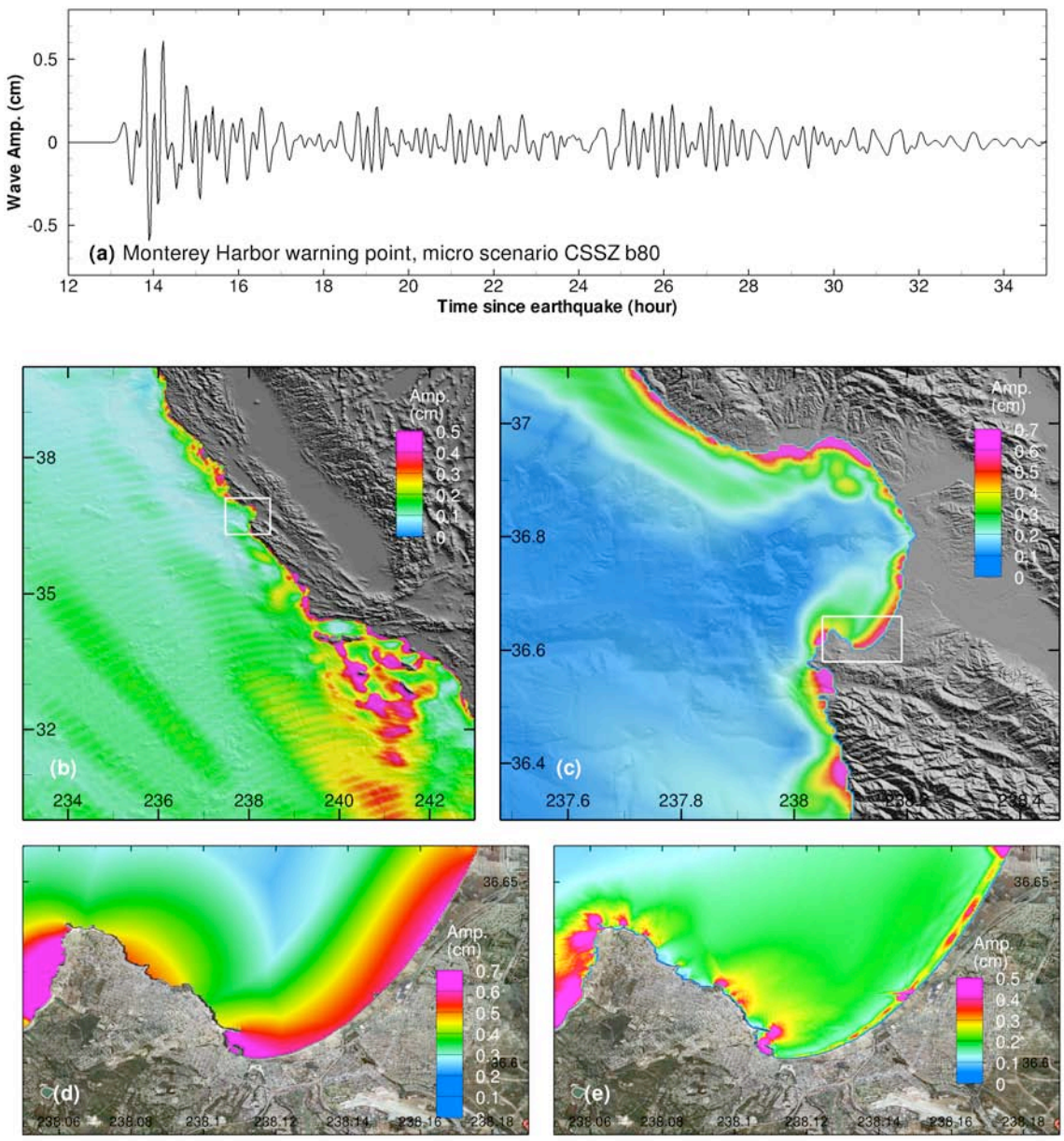

Figure 62. Model stability testing results at Monterey for artificial tsunami scenario CSSZ b80. (a) Computed time series at Monterey warning point; (b) Computed maximum wave amplitude in grid A of the forecast model; (c) Computed maximum current speed in grid B of the forecast model; (d) Computed maximum wave amplitude in grid C of the forecast model; (e) Computed current speed in grid C of the forecast model.

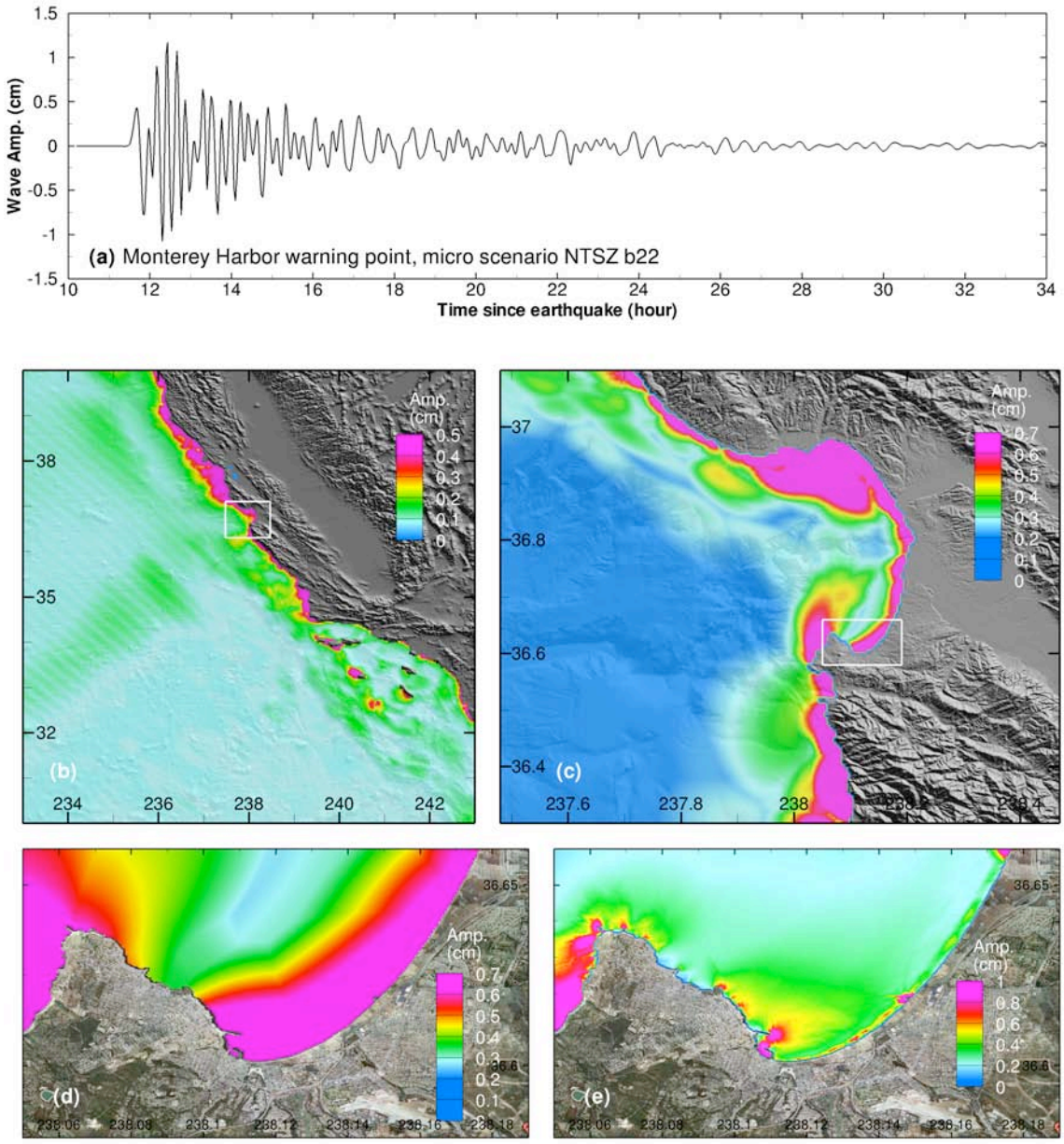

Figure 63. Model stability testing results at Monterey for artificial tsunami scenario NTSZ b22. (a) Computed time series at Monterey warning point; (b) Computed maximum wave amplitude in grid A of the forecast model; (c) Computed maximum current speed in grid B of the forecast model; (d) Computed maximum wave amplitude in grid C of the forecast model; (e) Computed current speed in grid C of the forecast model.

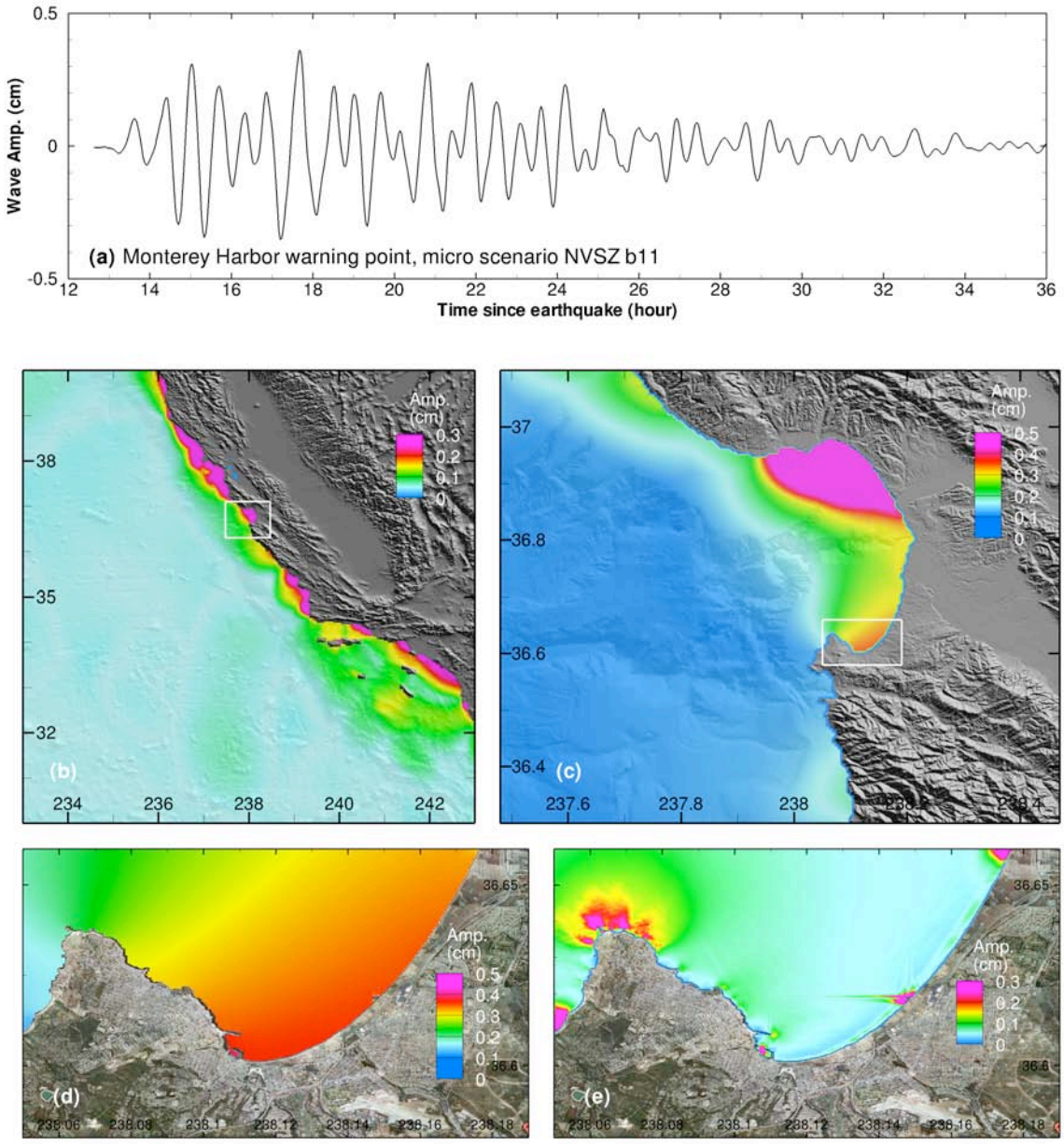

Figure 64. Model stability testing results at Monterey for artificial tsunami scenario NVSZ b11. (a) Computed time series at Monterey warning point; (b) Computed maximum wave amplitude in grid A of the forecast model; (c) Computed maximum current speed in grid B of the forecast model; (d) Computed maximum wave amplitude in grid C of the forecast model; (e) Computed current speed in grid C of the forecast model.

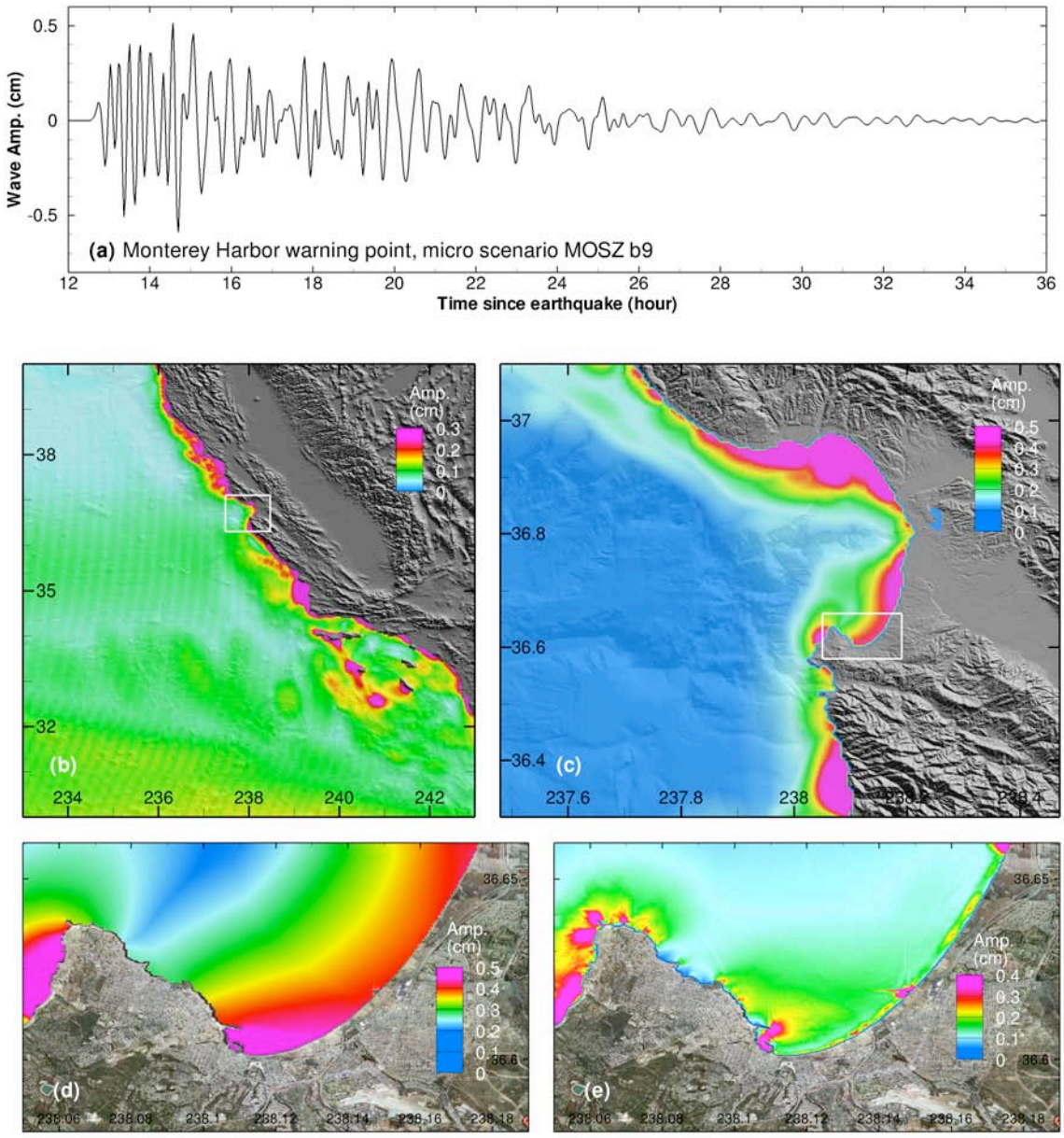

Figure 65. Model stability testing results at Monterey for artificial tsunami scenario MOSZ b9. (a) Computed time series at Monterey warning point; (b) Computed maximum wave amplitude in grid A of the forecast model; (c) Computed maximum current speed in grid B of the forecast model; (d) Computed maximum wave amplitude in grid C of the forecast model; (e) Computed current speed in grid C of the forecast model.

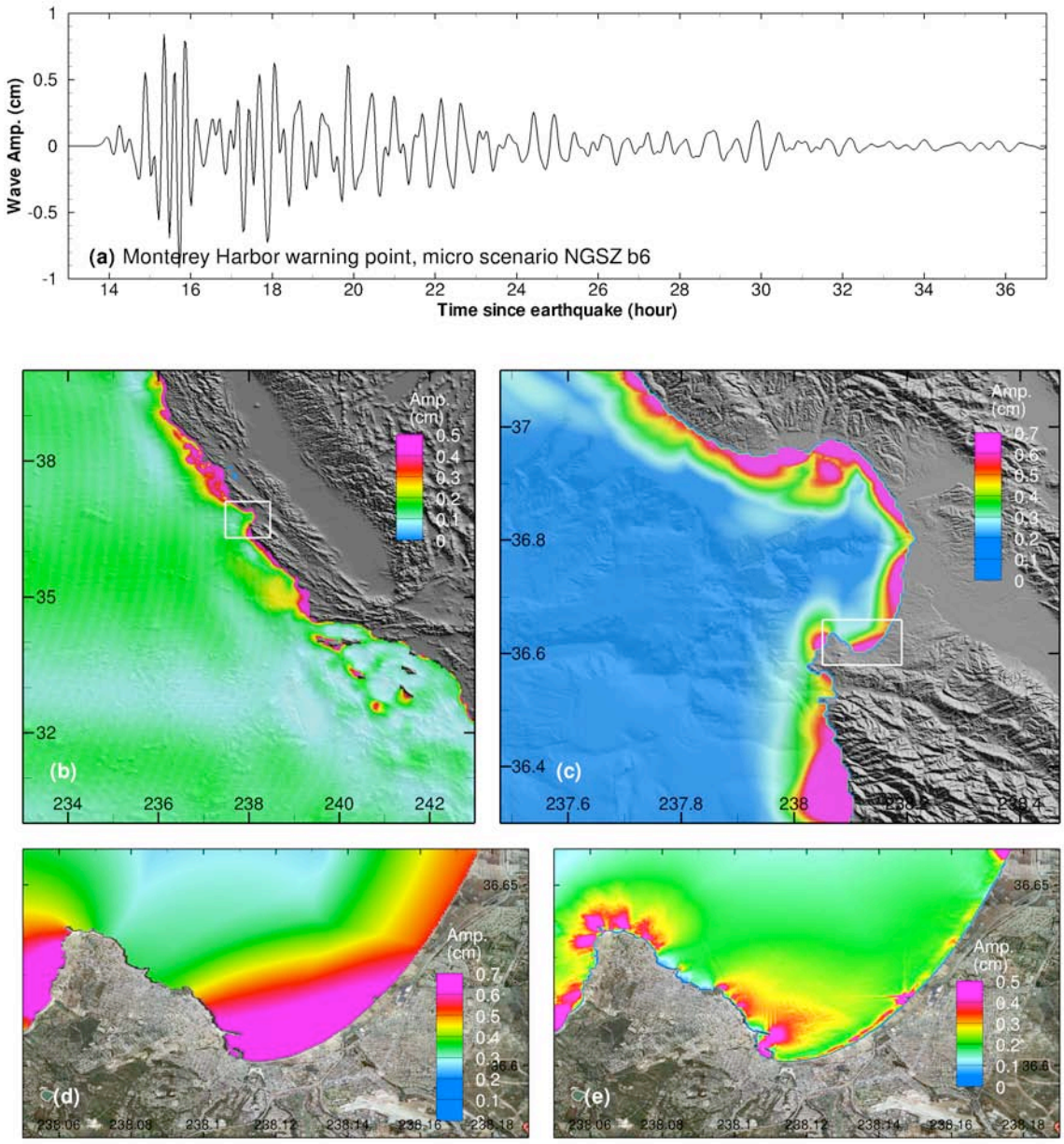

Figure 66. Model stability testing results at Monterey for artificial tsunami scenario NGSZ b6. (a) Computed time series at Monterey warning point; (b) Computed maximum wave amplitude in grid A of the forecast model; (c) Computed maximum current speed in grid B of the forecast model; (d) Computed maximum wave amplitude in grid C of the forecast model; (e) Computed current speed in grid C of the forecast model.

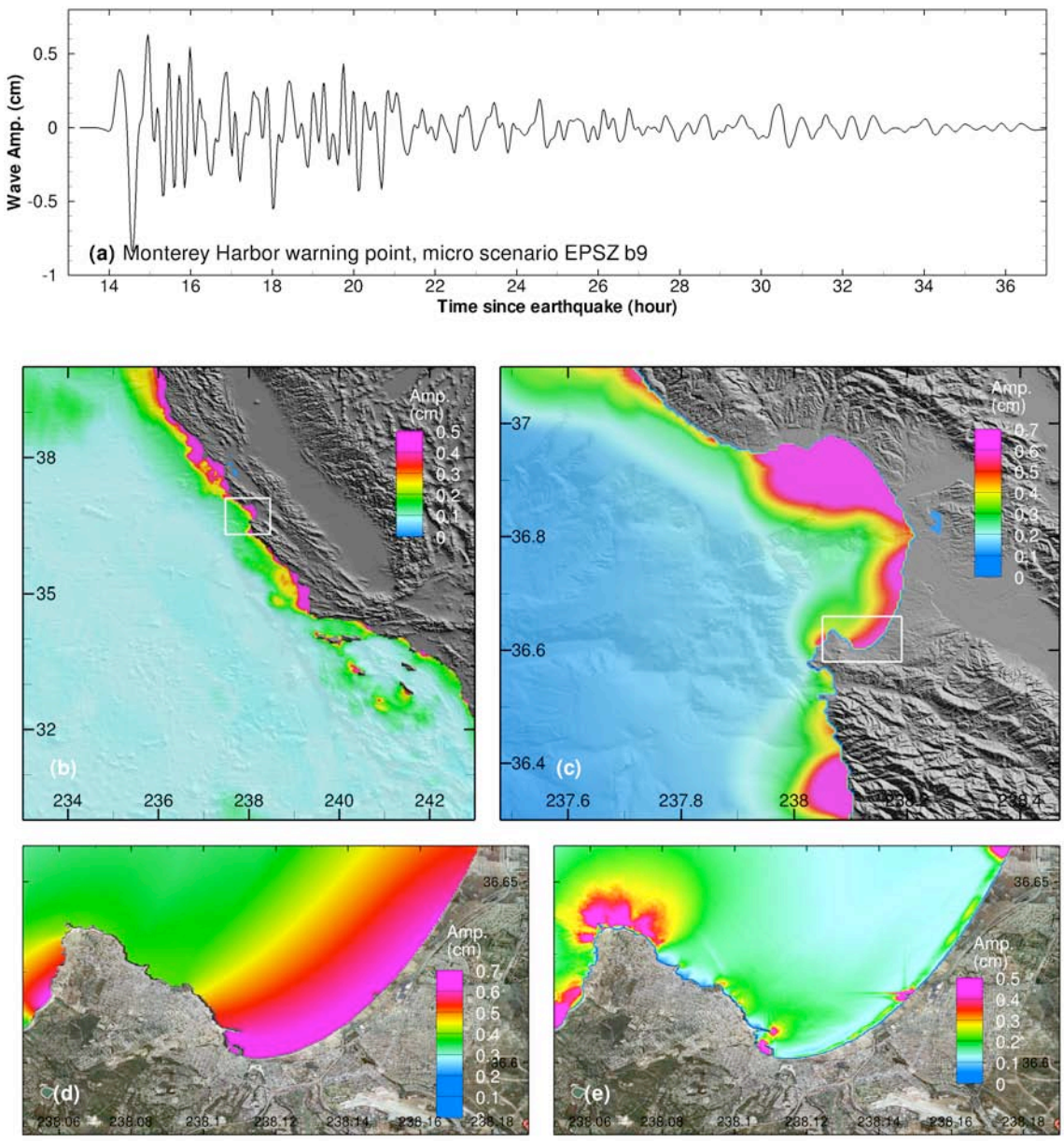

Figure 67. Model stability testing results at Monterey for artificial tsunami scenario EPSZ b9. (a) Computed time series at Monterey warning point; (b) Computed maximum wave amplitude in grid A of the forecast model; (c) Computed maximum current speed in grid B of the forecast model; (d) Computed maximum wave amplitude in grid C of the forecast model; (e) Computed current speed in grid C of the forecast model.

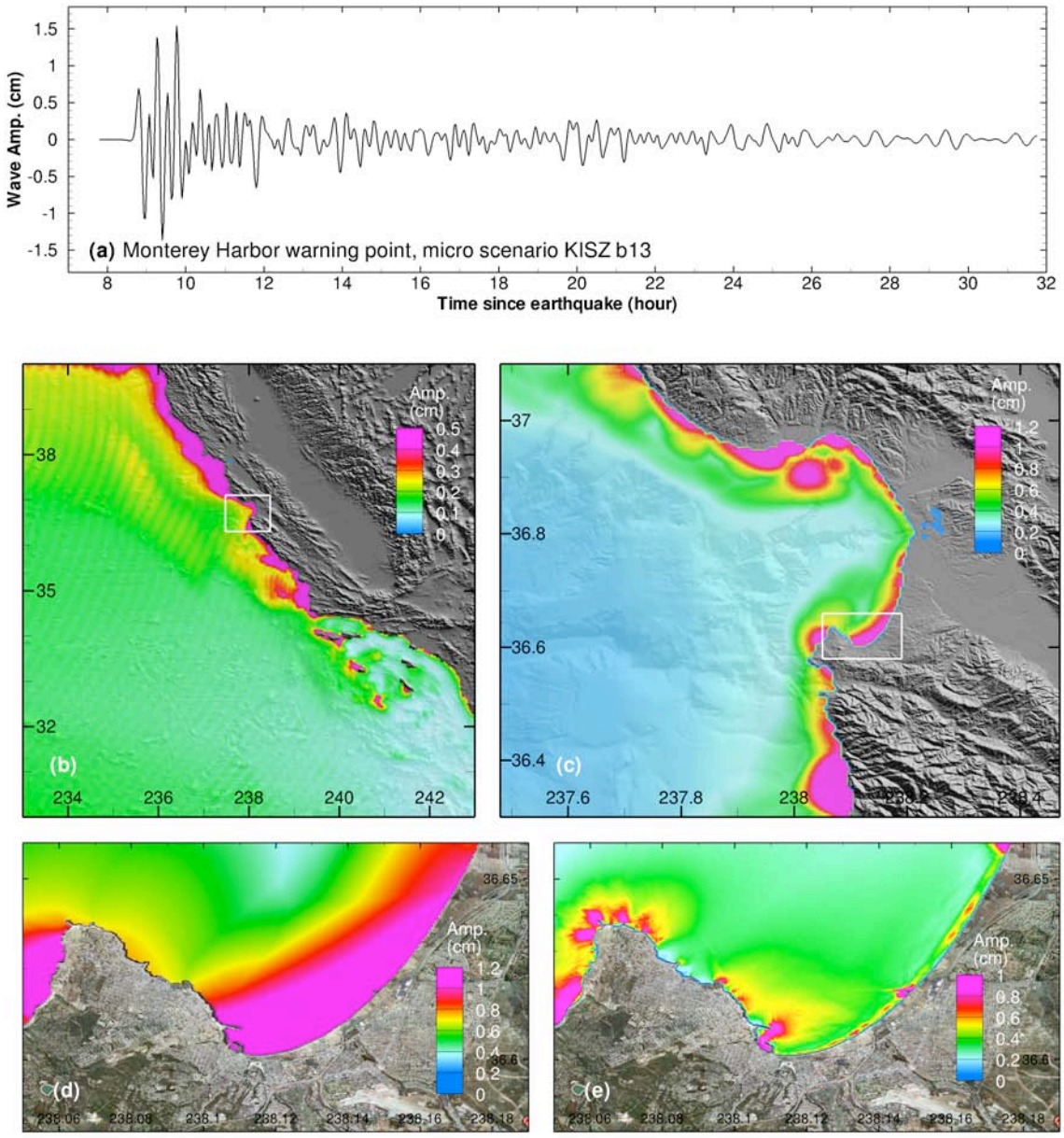

Figure 68. Model stability testing results at Monterey for artificial tsunami scenario KISZ b13. (a) Computed time series at Monterey warning point; (b) Computed maximum wave amplitude in grid A of the forecast model; (c) Computed maximum current speed in grid B of the forecast model; (d) Computed maximum wave amplitude in grid C of the forecast model; (e) Computed current speed in grid C of the forecast model.

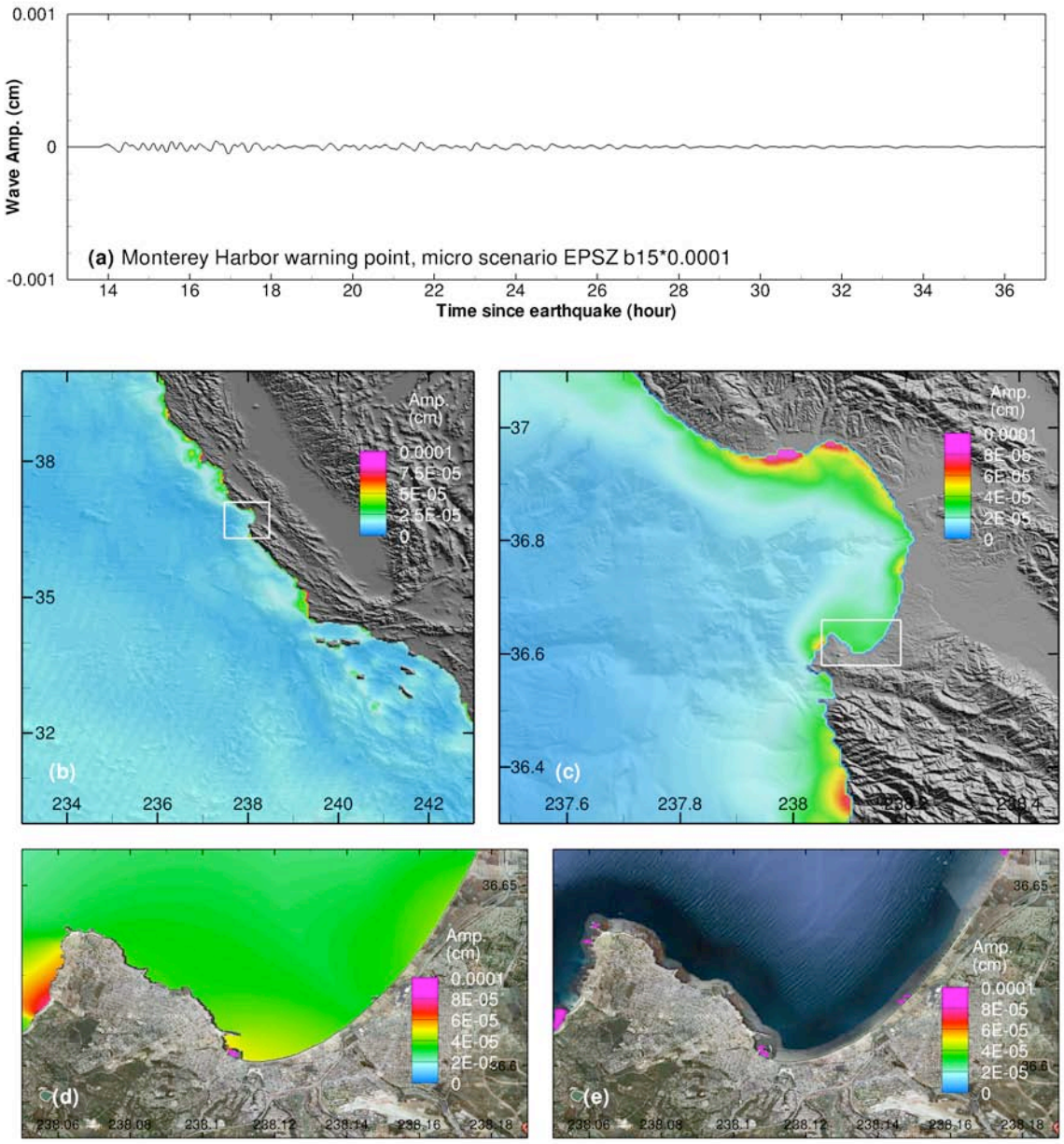

Figure 69. Model stability testing results at Monterey for artificial micro tsunami scenario EPSZ b15. (a) Computed time series at Monterey warning point; (b) Computed maximum wave amplitude in grid A of the forecast model; (c) Computed maximum current speed in grid B of the forecast model; (d) Computed maximum wave amplitude in grid C of the forecast model; (e) Computed current speed in grid C of the forecast model.